

Contact Binary Stars in Survey Data

A *thesis submitted in partial fulfillment of the requirements of a degree of Bachelor of Arts in Physics at Pomona College*



Franklin Marsh
with advisor
Philip I. Choi, Ph.D.
Professor of Astronomy
Pomona College

January 30, 2017

Abstract

Acknowledgments

To Mom and Dad

Contents

1	Introduction - Contact Binaries at the Intersection	6
2	The Contact Binary Star	9
2.1	<i>Discovery</i>	9
2.2	Physical Characteristics	11
2.2.1	The Main-Sequence Star	12
2.2.2	The Main-Sequence Homology Relations	15
2.2.3	ZAMS to TAMS	15
2.2.4	Metallicity	16
2.2.5	The Roche Potential	17
2.2.6	The Geometrical Elements of Contact Binary Systems	20
2.2.7	Thermal Equilibrium Models	22
2.2.8	Surface Brightness	24
2.3	Interior Structure	24
2.3.1	The Criterion for Stellar Convection	26
2.4	The Period-Color Relation	27
2.5	Frequency and Density	30
2.6	Mechanisms of Formation	31
2.7	Evolution in the Contact State	32
2.8	Evolution out of the Contact State	33
2.9	Early-Type Contact Binaries	35
2.10	Magnetic Activity	36
3	Observations	38
3.1	Images of Contact Binaries	38
3.2	Photometry of Contact Binaries	40
3.3	Spectra of Contact Binaries	41
3.4	X-ray and Ultraviolet Data on Contact Binaries	42
4	Analysis Techniques	43
4.1	Physical Light-Curve Modeling	43
4.2	Nomographic Light-Curve Solutions	44
4.3	O-C Analysis	44

5 Working with Survey Data	46
5.1 Modern Sources of Survey Data	49
5.1.1 The Kepler Spacecraft	49
5.1.2 The Sloan Digital Sky Survey	49
5.1.3 The SuperWASP Survey	49
6 Paper I: Characterization of 9,380 Contact Binaries from the CRTS Variable Sources Catalogue	50
7 Paper II: Geometrical Parameters	65
7.1 Light-curve Features	65
8 Paper III: Optical and UV Variability	69
9 The Future	69
9.1 Coronal Rotation with GALEX	70
9.2 Period Changes with Evryscope	70
9.3 H α Fluxes in PTF	70
9.4 Future Surveys	71
10 Conclusion	71

1 Introduction - Contact Binaries at the Intersection

The contact binary star is placed at the intersection of some of the largest questions in modern astronomy. In this introduction, we will see how contact binaries connect to a range of issues in modern astrophysics.

Modern observational techniques have allowed for the detection of transients (light sources that appear for a brief time and then disappear) in vast quantities. The supernova is a common example of a transient. By observing hundreds of supernovae, astronomers discovered that not all supernovae are the same - some are brighter than others, some last longer than others. They have also discovered transients that are not supernovae. In recent years, astronomers have been gaining information about transients that are much brighter than novae, but dimmer than supernovae. They named this class “Intermediate Luminosity Red Transients” (ILRT). Until recently, there was not a viable physical model for these transients. In late 2008, an ILRT emerged in the constellation of Scorpius. When astronomers looked in archival data - they found a contact binary in the spot where the nova had occurred. The leading theory is that the merger of the two components of a contact binary system causes these Intermediate Luminosity Red Transients.

While contact binaries systems are very different than the sun, they are important tools for testing the solar-stellar connection: the idea that the sun is similar to other stars and that we can learn about other stars by observing the sun, and vice-versa. While the sun takes almost a month to rotate, almost all contact binaries complete a full orbit in less than a day. Contact binaries have much greater angular momenta than single stars of the same spectral type. Contact binaries have strong magnetic fields (as much as 1000 times stronger than the sun’s), because they are moving about their rotational axis much more quickly. We will see that each component of a solar type contact binary exhibits a similar structure to the sun: a radiative inner layer surrounded by a convective envelope. For this reason, contact binaries exhibit the same magnetic phenomena (such as starspots, and flares) as the sun does - except these phenomena on contact binaries are much more dramatic, owing to their stronger magnetic fields. The dramatic magnetic phenomena in contact binaries is observable from large distances. From the earth, we can monitor the magnetic activity of thousands of contact binary stars. This is the subject of much of the original work in this thesis.

With the recent direct observation of gravitational waves by LIGO, there has been renewed interest in gravitational wave sources. The source of the first gravitational wave detection was two intermediate mass ($20 - 30M_{\odot}$) black holes, which was an unexpected result. Astronomers were uncertain about how two intermediate mass back holes could get close enough to each other to merge. The short-lived, massive contact binary stars offer a

solution to this problem. The vast majority of contact binary stars have components with similar masses to the sun. However, a few consist of two very massive O or B type stars. When a O or B type star ends its life, it undergoes a supernova explosion, resulting in a black hole. Additionally, some astronomers believe that a massive star can collapse directly to a black hole, without first undergoing a supernova. Each of the two stellar components in a O or B type contact binary is massive enough to form its own black hole at the end of its life. In this way, O and B type contact binaries provide a mechanism for producing two intermediate black holes in a close orbit.

As we will learn, contact binaries are a well-defined class with strict relationships between parameters like mass, luminosity, temperature, and orbital period. This means that by measuring a few parameters, many others can be accurately predicted. There are theoretically and empirically defined relationships between a contact binary's period, temperature, and luminosity. This means, by measuring a contact binary's orbital period (which can be done easily and precisely) astronomers can predict the contact binary's absolute luminosity (which is difficult to measure with traditional methods). For this reason, contact binaries are important *standard candles*. Contact binaries are much more common than Cepheid Variables, or RR Lyrae variables. They can be used to trace the structure of the milky way galaxy, and accurately determine distances to other galaxies.

In these ways, the contact binary stands at the intersection of time-domain, solar, gravitational wave, and stellar astronomy. But the study of contact binaries also stand at another important intersection: the intersection of “old” and “new” observational techniques.

We roughly can split observational astronomy into two modes, which I will call:

1. “Survey Mode”: Look out and see what there is to see, without a particular target in mind.
2. “Target Mode”: Observe very specific set of objects in a way tailored to learn about known phenomena.

In the 20th century, much of the science of astronomy operated in “target mode”. The science of astronomy was “data poor”. The limiting factor of discovery was observations from large telescopes of the day. If a scientist had new, proprietary data, science would come out of it. At the turn of the 21st century (enabled by advances in data storage, processing and robotics, and as a direct result of Moore’s law) observational astronomical science began to shift modes.

Old telescopes were being remodeled, old gears, motors and lenses were being replaced with robotic systems, enabling their autonomous operation. New telescopes were being constructed with the express purpose of deeply surveying the sky - with minimal human intervention. No longer inhibited by human operators, telescopes could image the sky continuously - dawn to dusk. Data poured from these telescopes like water from a firehose. Since

the 1990s, the new images filled massive stacks of servers: for the first time, astronomers were “data rich”.

The monstrous stream of data that was provided by these new systems had to be filtered. The most productive scientist was no longer the scientist with access to the best data, it became the scientist with the best techniques for filtering, stacking, folding, combining, or otherwise analyzing the data. Astronomers started shifting back to “Survey Mode”.

Asteroids were discovered by the thousands. The rate of supernova discovery accelerated from one every few years to approximately *one every night*. The number of known eclipsing binaries ballooned from just over a thousand, to tens of thousands. The number of galaxies with known distances was increased dramatically by the Sloan Digital Sky Survey. This progress is accelerating: within the decade, at least three major sky surveys of unprecedented depth and cadence will come online.

In the 21st century, we can study thousands of contact binary systems at once, using data from all-sky surveys. This approach presents huge advantages over taking painstaking observations of single contact binary systems. Due to the sheer number of systems studied, conclusions about contact binary behavior can be supported by robust statistics. However, there are also weaknesses to this approach. Many of the techniques that have been developed for extracting physical information out of observational data do not work well with survey data, because survey data tends to be of lower quality. We are forced to develop new techniques, and ask different questions.

In §2 I provide a brief history of the discovery of the first contact binary star, and outline major leaps of understanding in the field. In §3, I discuss the types of observations that can be used to learn about contact systems. In §4, I describe some ways that astronomers use models to convert raw observational data into measurements of physical parameters. We are introduced to survey data in §5. I then present original research that I have undertaken with Dr. Tom Prince, Dr. Ashish Mahabal, Dr. Eric Bellm, and Dr. Andrew Drake at the California Institute of Technology. In §9, I provide three projects that a student can undertake right now to continue the study of contact binary stars.

In this thesis, my main objectives are:

1. To provide an introduction to the field of Contact Binary study.
2. To provide an example of how we can adapt techniques developed during the age of “data-poor” astronomy to “data-rich” astronomy.
3. To provide a roadmap that a future student can use to continue this work.

2 The Contact Binary Star

2.1 Discovery

Q: *How was the first contact binary star discovered?*

To understand the history of the study of contact binaries, we must start at the source: the advent of a precise way of measuring the brightness of a celestial object.

In 1861, J.K.F. Zöllner, developed the first practical photometer. In Zöllner's photometer, the image of a real star as focused by a 5" objective lens was compared with the light of an artificial star, produced by a bunsen-like gas burner, in the same field of view [Stauber-mann, 2000]. The brightness of this artificial star could be adjusted by changing the relative orientation of two prisms, until it matched that of the real star. By recording the relative angle of the prisms when the brightness of the artificial and real star were equal, a photometric measurement could be obtained. In the 1860s, Zöllner supplied 22 photometers to the great observatories throughout the western world. One of these photometers arrived at the Potsdam Observatory, 15 miles southwest of Berlin's city center [Krisciunas, 2001].

Karl Hermann Gustav Müller , and Paul Friedrich Ferdinand Kempf collaborated on observations for the Potsdam *Photometrische Durchmusterung des Nördlichen Himmels* (Photometric Catalogue of the Northern Heavens), one of the three great photometric catalogues of the late nineteenth century [Bolt et al., 2007]. When it was finished, it contained the brightnesses and colors of roughly 14,000 stars down to visual magnitude 7.5 - a monumental undertaking.

While Kempf and Müller were making the initial observations for Part III of their *Durchmusterung*, they discovered that two measurements of an otherwise inconspicuous star (the first made in 1899, the second made in 1901) differed by an amount that was greater than was expected. In their survey, each star that showed the potential for variability was observed at a later date to verify the nature of variability.

At the Potsdam Observatory on January 14th, 1903, the sun set at 4:20pm. An hour and a half later, (at 5:56pm) Kempf and Müller began constructing a complete light-curve of $BD + 56^{\circ}.1400$, which would later be named W Ursae Majoris. They observed until 10:30PM. Follow-up observations three nights later allowed for the construction of the first light-curve of a contact binary star (Figure 2).



Figure 1: Fig. 4 from Staubermann [2000], showing a modern reproduction of a Zöllner photometer. Note the tube: the refractor telescope.

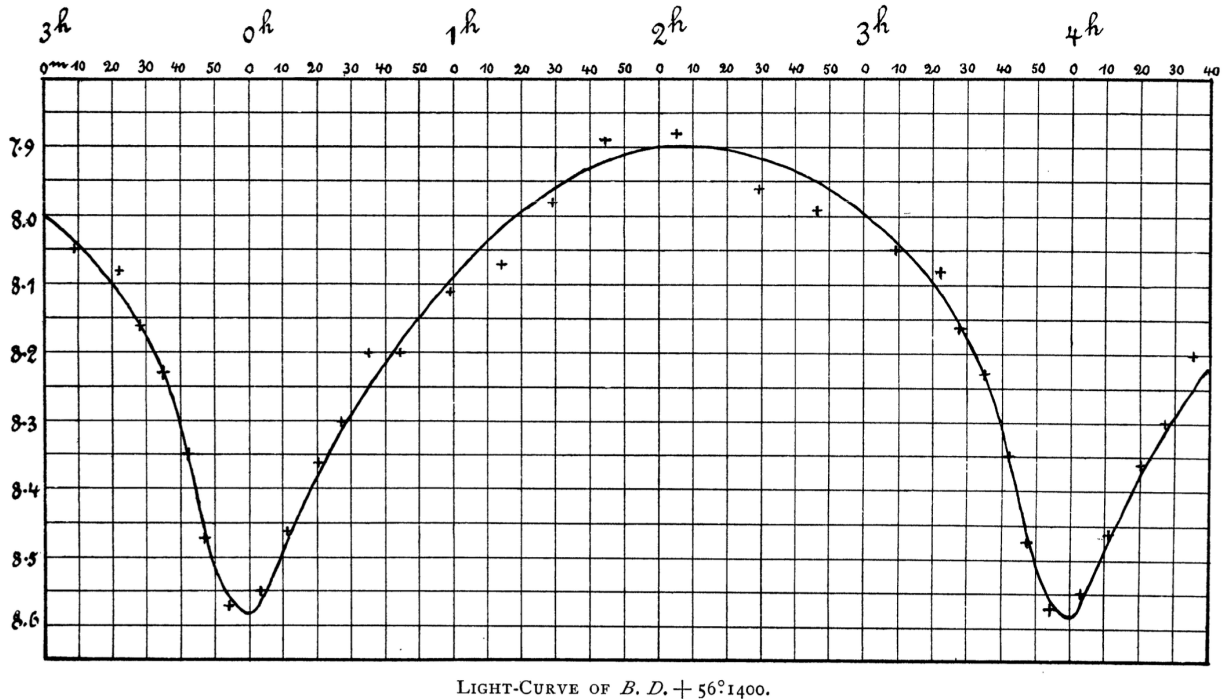


Figure 2: The first light-curve of a contact binary star. Note that the solid curve is interpolated by eye and drawn carefully in pen. Figure 1 from Müller and Kempf [1903].

The shape of the light-curve was unlike anything that Müller and Kempf had seen before, and they struggle to think of a physical system that can produce such a light curve, rejecting many hypotheses, before speculating:

“We may finally consider the hypothesis that the light-variation is produced by two celestial bodies almost equal in size and luminosity whose surfaces are at a slight distance from each other, and which at times almost centrally occult each other in their revolution... On this hypothesis we have only one difficulty, and the not inconsiderable one, as to whether such a system is mechanically possible and can remain stable for any length of time.”

This passage marks the beginning of the study of contact binary stars. In this thesis (written 114 years after the initial discovery), we will journey to the forefront of contact binary research.

2.2 Physical Characteristics

In this section, we will gain a physical understanding of contact binary systems. Contact binary stars are made up of two main-sequence stars. In §2.2.1 we will understand what main-sequence stars are like on the inside, how energy is generated in the cores of main-sequence stars, and how this energy is transported to their surfaces.

Once we have got a firm grasp of the properties of main-sequence stars, we will bring two of them together to form a contact binary. In §2.2.5, we learn that we must change the potential that the stellar matter exists in from the point potential to the Roche potential. Also, the components of contact binary stars can transfer mass and energy, from one to the other. We must take this into account when building our model.

In §??, we will learn how common contact binary stars as compared to single main-sequence stars. We will also learn how common they are in the Milky Way galaxy.

In §??, we will learn how contact binaries are formed. We will be introduced to the concepts of angular momentum loss (AML), and Kozai-Lidov cycles. In §??, we will learn how contact binaries evolve during their lifetimes. We will see how this evolution can drive changes in the observable properties of contact binary systems.

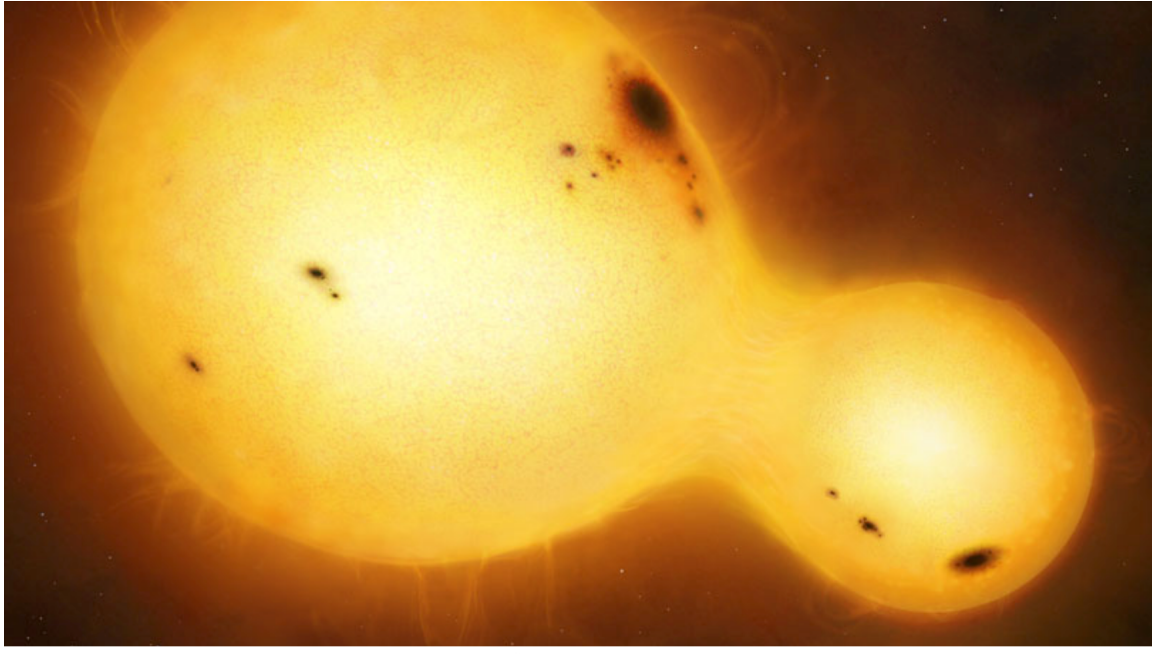


Figure 3: Model for a contact binary system. The hatched areas denote convection zones, and the vertical dashed line is the axis of rotation. Figure 1 from Lucy [1968a].

2.2.1 The Main-Sequence Star

In order to understand the internal structure of contact binaries, we must first understand the structure of their two components: main-sequence stars. The main sequence was an empirically derived group: When astronomers started recording the luminosity and color of large numbers of stars, they observed that most stars obeyed a relationship between

luminosity and color. This relationship can be visualized in an *Hertzsprung-Russell Diagram* (or H-R Diagram), like Figure 4. They called the main cluster of points on this diagram the “Main Sequence”. The most familiar example of a main sequence star is our Sun. When a star is fusing hydrogen into helium at its core, we say that it is on the main sequence.

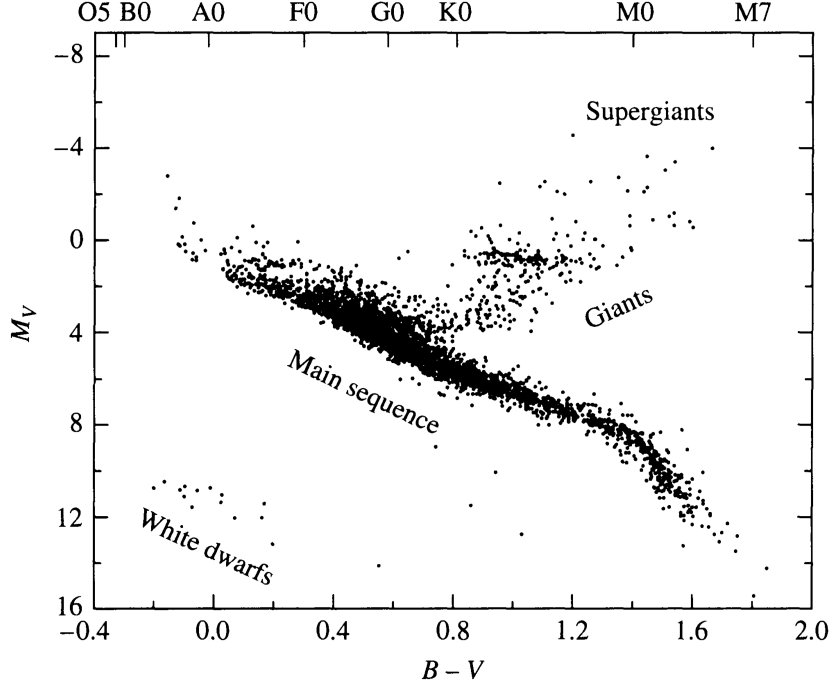


Figure 4: An observer’s Hertsprung-Russel (H-R) diagram. The data are from the Hipparcos catalog. Figure 8.13 from Carroll and Ostlie [2006].

Astronomers have an excellent understanding of the observables (like mass, luminosity, or temperature) of main-sequence stars. Models of main-sequence stars that rely on basic time-independent equations of stellar structure have been successful.

The time-independent equations of stellar structure are a set of relationships between the properties of main sequence stars. They tell how pressure (P), enclosed mass (M_r), enclosed luminosity (L_r), and temperature (T) change as a function of radius r . You will notice that that all of the following equations are actually derivatives. When we supply the appropriate boundary condition (eg. “the temperature T at 1 solar radius is 5800K”), the equations allow for the complete solution of the run of temperature, pressure, and mass through the star.

$$\frac{dP}{dr} = -G \frac{M_r \rho}{r^2} \quad (2.1)$$

$$\frac{dM_r}{dr} = 4\pi r^2 \rho \quad (2.2)$$

$$\frac{dL_r}{dr} = 4\pi r^2 \rho \epsilon \quad (2.3)$$

$$\frac{dT}{dr} = -\frac{3}{4ac} \frac{\bar{\kappa}\rho}{T^3} \frac{L_r}{4\pi r^2} \quad (2.4)$$

Energy is generated at the core of low-mass main sequence stars via the Proton-Proton Chain, or *pp-chain*. The pp-chain has three branches, each producing helium out of Hydrogen (H), Helium (He) and Beryllium (Be).

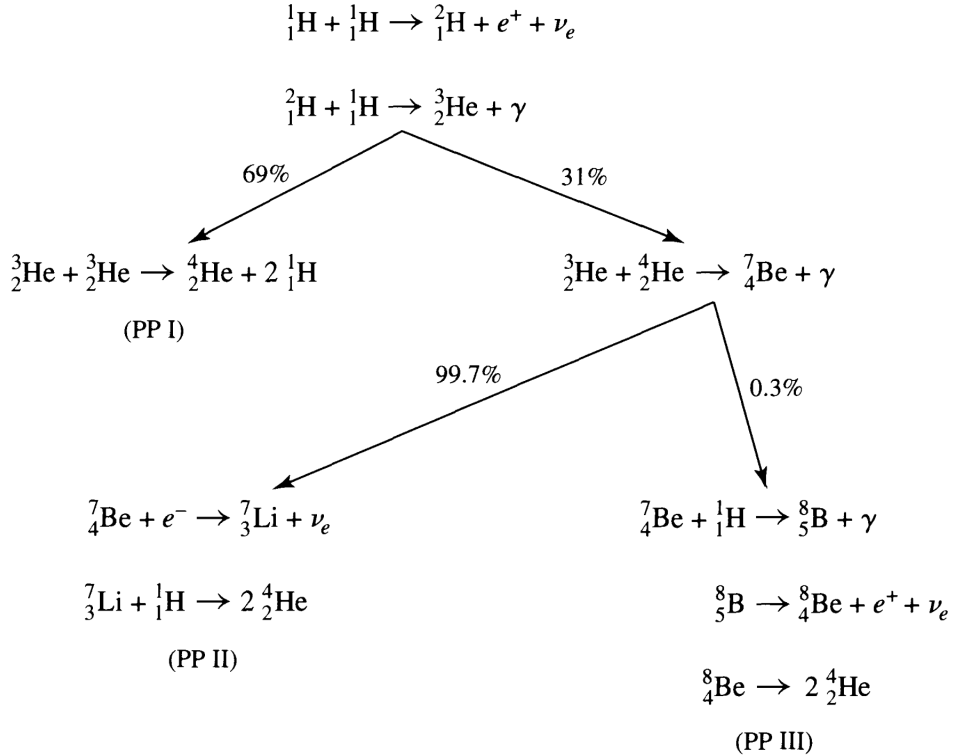


Figure 5: A diagram of pp chain reactions. Percentages by the arrows indicate the branching ratios, revealing that the PP I and PP II chains occur much more frequently than the PP III chain. Figure 10.8 from Carroll and Ostlie [2006].

At temperatures near the temperature of the solar core, the efficiency of the pp-chain ϵ is proportional to T^4 , so hotter stars can get more energy out of the pp-chain. For stars with higher core temperatures than the sun, another reaction (the CNO-cycle) becomes much more efficient than the pp-chain. Through the conversion of mass to energy via the pp-chain, low-mass main-sequence stars shine. For the rest of this thesis, we can treat the core of the main-sequence star as a “black-box” which pumps energy into the outer layers of the star..

2.2.2 The Main-Sequence Homology Relations

The Main-Sequence Homology Relations (sometimes called the Main-Sequence Scaling Relations) are relationships between the Luminosity L , Mass M , Radius R , and temperature T of Zero-age main-sequence (ZAMS) stars. These relationships exist because main sequence stars with the same reaction mechanism at their cores (e.g. the pp-chain) are homologous. Two stars that both produce the vast majority of their energy through the pp-chain and obey the same equations of stellar structure, have homologous structures, i.e. the smaller star is just a “scaled-down” version of the larger star.

We can calculate these homology relations using models based on the time-independent equations of stellar structure. Researchers have used models to derive the following relationships for stars with $M < 1.66M_{\odot}$:

$$\frac{L_{\text{ZAMS}}}{L_{\odot}} \approx 1.03 \left(\frac{M}{M_{\odot}} \right)^{3.42} \quad (2.5)$$

$$\frac{R_{\text{ZAMS}}}{R_{\odot}} \approx 0.89 \left(\frac{M}{M_{\odot}} \right)^{0.89} \quad (2.6)$$

$$\frac{T_{\text{ZAMS}}}{T_{\odot}} \approx 1.07 \left(\frac{M}{M_{\odot}} \right)^{0.41} \quad (2.7)$$

Of the three observables (L, R, T), luminosity L has the strongest dependence on mass M . The homology relationships are broken into two (Low mass) and (High mass) because of the differing primary reaction mechanisms at the cores of stars of different masses. The homology relationships are great for providing reasonable approximations of stellar parameters.

For example, if I told you that “The mass of Tau Ceti is about $0.78 M_{\odot}$ ”, and asked you to calculate the luminosity of Tau Ceti, you would perform the following calculation:

$$\left(\frac{M_{\text{tau ceti}}}{M_{\odot}} \right) = 0.78 \quad \left(\frac{L_{\text{tau ceti}}}{L_{\odot}} \right) = \left(\frac{M_{\text{tau ceti}}}{M_{\odot}} \right)^{5.5} = 0.78^{5.5} \approx 9 \times 10^{-6} L_{\odot} \quad (2.8)$$

2.2.3 ZAMS to TAMS

The observable characteristics of main sequence stars change slightly throughout their time on the main sequence. When a protostar starts fusing hydrogen into helium, we say that it has reached *ZAMS*, which stands for Zero-Age Main-Sequence. When the hydrogen in the core of the main-sequence star is depleted, it must burn other elements to remain stable. When the core of the star uses the last of its hydrogen, we say that the star has reached *TAMS*, which stands for Terminal-Age Main-Sequence.

In the context of contact binaries, it is important to discuss the changes that occur to a star as it progresses through its main-sequence life. At ZAMS, the main-sequence star is

the most compact. As it gets older, its radius and luminosity increase, and its temperature decreases. We can calculate the magnitude of these changes using analytical fits to stellar models. The analytical fits from Demircan and Kahraman [1991] that we will use have been derived for main-sequence stars with $M < 1.66M_{\odot}$. The vast majority of the components of contact binaries have $M < 1.66M_{\odot}$, for which the following relations are valid:

$$R_{ZAMS} \approx 0.89M^{0.89} \quad R_{TAMS} \approx 2.00M^{0.75} \quad L_{ZAMS} \approx 1.03M^{3.42} \quad L_{TAMS} \approx 2.54M^{3.41} \quad (2.9)$$

Where M is the mass of the star in solar units.

$$\frac{R_{TAMS}}{R_{ZAMS}} = \frac{2.25}{M^{0.14}} \quad \frac{L_{TAMS}}{L_{ZAMS}} = \frac{2.46}{M^{0.01}} \quad (2.10)$$

Using the Stephen-Boltzmann equation for the radiation of a sphere, we can solve for the fractional temperature change $\frac{T_{TAMS}}{T_{ZAMS}}$:

$$L = 4\pi R^2 \sigma_b T^4 \rightarrow \frac{T_A}{T_B} = \left(\frac{L_A}{L_B}\right)^{\frac{1}{4}} \left(\frac{R_A}{R_B}\right)^{\frac{1}{2}} \quad (2.11)$$

Using equations 2.10 and 2.11, we can compute a table comparing ZAMS stars to TAMS stars, for a variety of masses.

Table 1: Comparison of Stellar Observables from ZAMS to TAMS

Stellar Mass	$\frac{R_{TAMS}}{R_{ZAMS}}$	$\frac{L_{TAMS}}{L_{ZAMS}}$	$\frac{T_{TAMS}}{T_{ZAMS}}$
$1.5M_{\odot}$	2.10	2.45	0.86
$1.0M_{\odot}$	2.25	2.46	0.84
$0.5M_{\odot}$	2.48	2.48	0.79
$0.2M_{\odot}$	2.81	2.50	0.75

We can see that at TAMS, a low-mass main-sequence star's radius and luminosity have increased by a factor of over 2 , while the surface temperature drops to 75% - 86% of the ZAMS value. The changes in luminosity and radius that occur during the main-sequence have strong implications for the stability of contact binary systems.

2.2.4 Metallicity

By far, the parameter that has the largest effect on the stellar observables is the mass. However the chemical composition of a star can also influence its observables. Astronomers

will use a simplified system consisting of three numbers $[X, Y, Z]$ to refer to the chemical composition of a star:

$$X = \text{Hydrogen Abundance} \quad Y = \text{Helium Abundance} \quad Z = \text{Abundance of everything else}$$

$$X + Y + Z = 1 \quad (2.12)$$

When astronomers refer to “Metallicity”, they are often referring to Z : the fraction of the mass of the star that is not hydrogen or helium. For our own sun, $Z = 0.02$, which is referred to as the *solar metallicity*.

Metallicity influences the observables of main-sequence stars through affecting the opacity κ of the stellar material. In general, stars with a higher metallicity z also have a higher opacity κ . The increased opacity increases the effect of radiation pressure on the outer layers of stars, causing stars with higher metallicities to also have a larger radius.

2.2.5 The Roche Potential

In the equations of stellar structure, there is a hidden assumption. These time-independent equations of stellar structure assume that the stellar matter exists in the potential of a point mass:

$$\Psi_{\text{point}} = \frac{GM}{r} \quad (2.13)$$

However, a contact binary system cannot be modeled as a point mass. A contact binary most definitely contains *two* masses, because it contains two stellar components. We can approximate these stellar components as two point masses, separated by a distance a . Despite this necessary point-mass approximation, the Roche model can be used to calculate the structure of binary stars [Kippenhahn and Thomas, 1970]. The Roche model assumes synchronous rotation, circular orbits and two point masses. Its coordinate system is based in the rotating frame [Kopal, 1959].

Mochnacki [1984] has computed the Roche potential in Cartesian (x,y,z) coordinates, useful for performing numerical integrations. They write:

“In Cartesian coordinates, with the origin at the center of mass of the primary, the x -axis aligned with the centers of mass, and the z -axis parallel to the rotation axis, the potential at a point (x, y, z) co-rotating with binary system is given by: ”

$$\Psi_{\text{roche}}(x, y, z) = -\frac{G(M_1 + M_2)}{2a} C \quad (2.14)$$

where

$$C(x, y, z) = \frac{2}{1+q} \frac{1}{(x^2 + y^2 + z^2)^{\frac{1}{2}}} + \frac{2q}{1+q} \frac{1}{1+q[(x-1)^2 + y^2 + z^2]^{\frac{1}{2}}} + (x - \frac{q}{1+q})^2 + y^2 \quad (2.15)$$

$q = \frac{m_2}{m_1}$, (x, y, z) are in units of a , the separation between the two point masses.

The Roche potential has points where $\nabla\Psi = 0$, called Lagrange Points (see Figure ??).

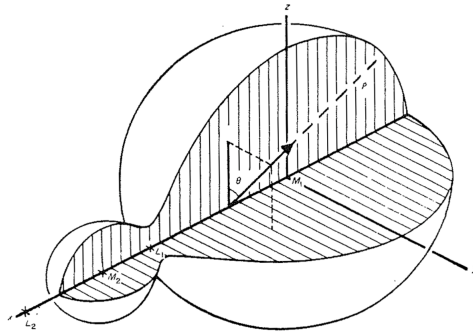


Figure 6: The coordinate system used in equations 2.14 and 2.15 to describe the potential Ψ of a contact binary system. Figure 1 from Mochnacki and Doughty [1972]

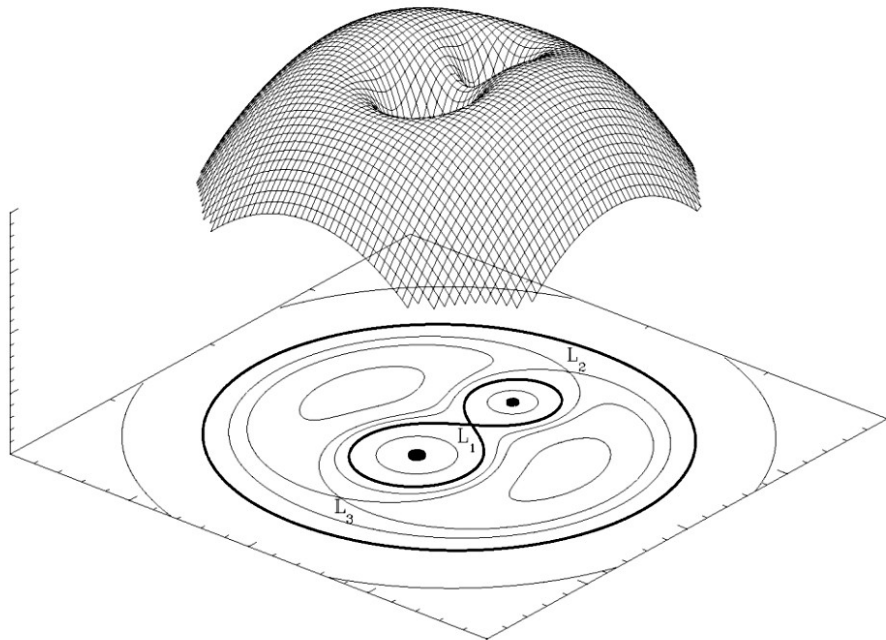


Figure 7: A composite 3D and contour plot of the Roche potential. The Roche lobe is the dark equipotential curve shaped like the ∞ symbol. Three out of the five Lagrange points are labelled L_1, L_2, L_3 . [Sluys, 2006]

Now that we understand the shape of the Roche potential, we can learn how the Roche potential is used to classify eclipsing binary stars, in a scheme primarily developed by the work of Kopal [1959].

In this scheme, eclipsing binaries are classified according to the location of the two photospheres relative to certain Roche equipotentials. In Figure 8, we see three types of eclipsing binaries. In Detached systems, the photosphere of each component is well within the Roche lobe (the equipotential curve shaped like ∞). In a Semi-detached configuration, the photosphere of one component completely fills its Roche lobe (touching the L_1 point, while the photosphere of the other component remains well within its Roche lobe. In Overcontact systems, both components *overfill* the Roche lobe, and a bridge of stellar material connects the two components, covering the L_1 point [Terrell, 2001].

Now we know how Detached, Semi-Detached, and Overcontact binaries are classified - but wait: Where are the *Contact Binaries*? In this section, we have been referring to contact binaries as “Overcontact Binaries”. But why did we have to make the name change?

Since the first half of the 20th century, most astronomers believe that the term “contact” means that the photospheres of the two components are touching physically. This is incorrect, according to the original classification scheme of Kopal [1959]. He intended contact to mean that the photospheres of the stars were in contact with their Roche Lobes, (the inner Jacobi Equipotential). Though the term “contact” binary is technically incorrect, it is the most common usage in the literature, and is now the accepted name for these kinds of stars. For an excellent review of this naming issue, see Wilson [2001]. For a review of the classification scheme, see p. 109 of Kallrath and Milone [2009].

The Roche lobe, (as we have been calling it) is also referred to as the *Inner Jacobi Equipotential*. There also exists an *Outer Jacobi Equipotential*. In Figure 8, the Outer Jacobi Equipotential is the outer-most curve that is drawn. It passes through the L_2 point. The Inner Jacobi Equipotential is the curve that we have been referring to as the “Roche Lobe”. It is the curve shaped like the ∞ symbol.

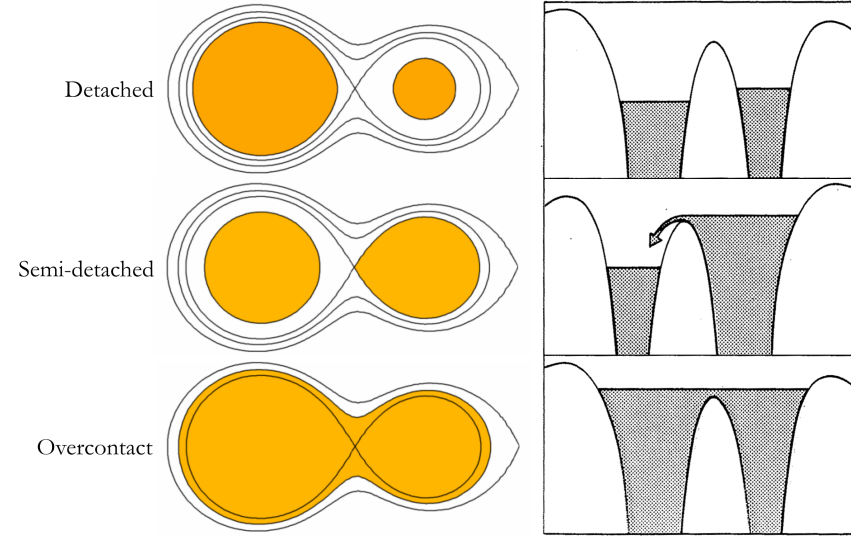


Figure 8: Types of eclipsing binary systems based on Roche geometry. In the bottom panel, (labelled “overcontact”), the photosphere of the star (shaded in orange), lies between the inner and outer Jacobi equipotentials. Figures 2,3, and 4 from Terrell [2001], and Figure 1.4 from Pringle and Wade [1985]

We can use the Cartesian Roche potential (Equations 2.14 and 2.15) to calculate the relative volume within the Roche lobe (Inner Jacobi Equipotential) of the two components. We can measure the size of a Roche lobe by using an average radius r , which is defined so that $\frac{4}{3}\pi r^3$ is equal to the volume within the Roche lobe.

Paczynski [1971]

$$\frac{r_1}{A} = \frac{2}{3^{\frac{4}{3}}} \left(\frac{M_1}{M_1 + M_2} \right)^{\frac{1}{3}} \quad (2.16)$$

Analytical approximations for the effective radius r_L of a Roche Lobe. Eggleton [1983]

2.2.6 The Geometrical Elements of Contact Binary Systems

In the previous section, we have learned how to differentiate contact binary systems from the other types of eclipsing binary stars. In this section, we will learn how to describe specific contact binaries in terms of their geometrical elements. When we refer to the geometry of the contact binary system, we are really referring to the geometry of its photosphere. The vast majority of what we know of contact binary systems comes from their visible light-curves, which is why there is the convention of treating the photosphere as the “boundary” of the system. Astronomers have developed a set of geometrical elements that can describe the location of the photosphere with respect to the inner and outer Jacobi equipotentials.

The first geometrical element of note is the mass ratio $q = \frac{M_1}{M_2}$ of the contact binary. The

mass ratio is an important geometrical element in that it influences the shape of the Roche potential. We can see the effect of the mass-ratio term in equation 2.15. The Roche potential for a system with a mass ratio of unity (one) is perfectly symmetrical about the L_1 point. The Roche potential for a system with a mass ratio that is far from unity is not symmetrical about the L_1 point: the more massive component has an inner Jacobi equipotential that encloses more area.

The second geometrical element is the Roche lobe fill-out factor (also called the degree of contact), f . This is the element that is used to describe the location of the photosphere with respect to the Inner and Outer Jacobi equipotentials.

The fill-out factor has a variety of definitions, but the most common is:

$$f = \frac{C_1 - C}{(C_1 - C_2) + 1} \quad (2.17)$$

When the photosphere of a contact binary is exactly filling the inner Jacobi equipotential, eqn. 2.17 gives $f = 0$. When the photosphere of a contact binary fills the outer Jacobi equipotential, eqn. 2.17 gives $f = 1$. In Fig. 9, we see the diameter of the “neck” region (containing the L_1 point), is a sizable fraction (0.1 to 0.3) of the separation of the centers of mass of the star for $f > 0.2$.

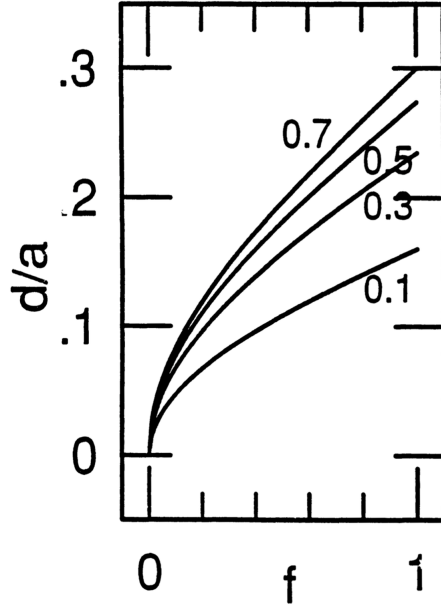


Figure 9: The widths of the “neck” between stars, d , as a function of the degree of contact, f , for a few values of the mass-ratio, q . The width of the neck is expressed in units of the separation between components, a . Fig. 5 from Rucinski [1993a].

The final element that is commonly reported is i , or the inclination of the contact binary’s

orbit with respect to the line of sight of the observer. This element is not intrinsic to the contact binary system, so it actually does not provide any information about the physics of the contact binary system. This element is reported because together with f and q , it completely defines the shape of the observed contact binary light-curve. The light-curve of a contact binary with given values of f and q will exhibit the largest amplitude when the inclination $i = 90^\circ$, corresponding to a complete eclipse. When $i = 0$, the two components do not eclipse at all and the light-curve has amplitude 0. Inclinations between 0 and 90 correspond to partial eclipses, and the amplitude of the resulting light-curves increases monotonically with inclination (see Fig. 10).

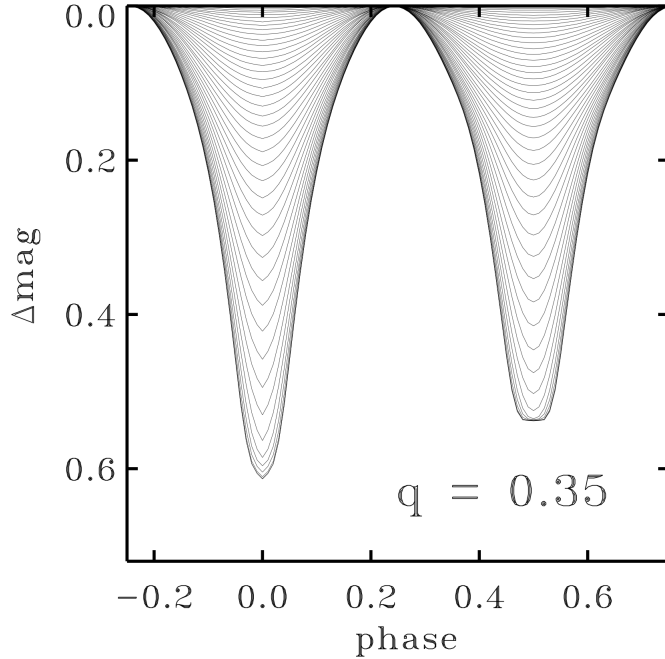


Figure 10: The light-curve of a contact binary star with $q = 0.35$, $f = 0.25$. Orbital inclination i is varied in 2° steps. Fig 1. from Rucinski [2001].

We will see how the shape of the contact binary light-curve can be used to estimate the system geometry as described by $[f, q, i]$ in §4.1 and §4.2.

2.2.7 Thermal Equilibrium Models

This class of models that we will explore in this section was first developed in the late 1960's. The great triumph of the thermal-equilibrium model is that it adequately explained the observed shape of the contact binary light-curve.

Under the condition of hydrostatic equilibrium, the gradient in the pressure P is equal to the negative of the density $-\rho$ times the gradient in the potential $\nabla\Psi$.

$$\nabla P = -\rho \nabla \Psi \quad (2.18)$$

$$\nabla \rho = \frac{dP(\Psi)}{d\Psi} = \rho(\Psi) \quad (2.19)$$

If we assume a homogenous composition on equipotential surfaces, then all state variables (pressure, density, temperature, surface gravity) are functions of Ψ alone. Since the temperature T is constant across the surface, we can say that the shared photosphere is in thermal equilibrium. According to observations of contact binaries, this is true: the temperature of the shared photosphere does not vary by much across its surface.

This is troubling in the light of the Main-Sequence Homology Relations discussed in ???. Recall that, for a single main-sequence star:

$$T \propto M^{1.3} \text{(Low mass),} \quad T \propto M^{0.4} \text{(High mass)} \quad (2.20)$$

A typical mass ratio $q = \frac{m_1}{m_2}$ for a contact binary star is 0.5. For a contact binary with a low mass,

$$\frac{T_1}{T_2} = \left(\frac{M_1}{M_2} \right)^{1.3} \quad (2.21)$$

However, observations indicate that the two components of a contact binary system (almost always) do *not* have equal-mass. This means that, in order to achieve hydrostatic equilibrium, energy must be exchanged between the two components of the contact binary. In fact, up to a third of the energy generated by the primary is transferred to the secondary [Mochnacki, 1981].

We can construct two model main sequence stars, with masses M_1 and M_2 . Main sequence stars will obey main-sequence scaling relationships, which are well defined laws the describe how stellar radii, density, and temperature vary with stellar mass [Kippenhahn et al., 1990]. The mass - radius relationship is particularly important when constructing contact models.

$$\left(\frac{R}{R_\odot} \right) = \left(\frac{M}{M_\odot} \right)^\alpha \quad (2.22)$$

$$\left(\frac{R_1}{R_2} \right) = \left(\frac{M_1}{M_2} \right)^{0.46} \quad (2.23)$$

Because of the mass - luminosity relationship of main sequence stars, there is a mass ratio - luminosity ratio relationship for the components of contact binaries:

$$\left(\frac{L_1}{L_2} \right) = \left(\frac{M_1}{M_2} \right)^{0.9} \quad (2.24)$$

Advection is a transport mechanism of a substance, or property (e.g. temperature, density) by a fluid due to the fluid's bulk motion.

[Shu et al., 1976] contact discontinuity model

[Lubow and Shu, 1977]

Gazeas and Stępień [2008] have shown that orbital parameters of contact binary systems obey certain relationships.

$$P = 0.1159 * a^{\frac{3}{2}} M^{\frac{1}{2}} \quad (2.25)$$

Where P is the orbital period in days, $M = M_1 + M_2$ is the total mass of the binary system, and a is the semi major axis of the system in meters.

We can also calculate the orbital angular momentum H_{orb}

$$H_{\text{orb}} = 1.25 \times 10^{52} * M^{\frac{5}{3}} P^{\frac{1}{3}} q (1 + q)^{-2} \quad (2.26)$$

where $q = \frac{M_1}{M_2}$ is the mass ratio of the components.

2.2.8 Surface Brightness

In this subsection, we will be introduced to Von Zeipel's theorem. Von Zeipel's theorem relates the flux being emitted from a certain location on the star to the local gravity at the location. This is useful because it allows for light-curves to be created from physical models (see §4.1).

Von Zeipel's theorem states that the radiative flux F in a uniformly rotating star is proportional to the local effective gravity g_{eff} :

$$F = -\frac{L(P)}{4\pi GM_*(P)} g_{\text{eff}} \quad (2.27)$$

$$T_{\text{eff}}(\theta) \approx g_{\text{eff}}^{0.25}(\theta) \quad (2.28)$$

[Von Zeipel, 1924]

[Gazeas and Niarchos, 2006]

2.3 Interior Structure

In this section, we will learn what types of interior structures that contact binaries can have. We will discuss the different energy transport mechanisms which operate inside contact binary systems.

In stars, there are two primary mechanisms of energy transport: In Radiative Transport, energy is able to leave the star through the dispersion of photons (electromagnetic energy)

through the stellar medium (which is mostly Hydrogen gas). Convective Transport occurs when Radiative Transport is not efficient enough to transport the energy out of the star. In convection, energy is transferred through the physical motion of the stellar medium.

Convection has several important effects. It causes the *radial mixing* of elements in the stellar interior. The motion generated by convection can cause strong magnetic fields.

The fractional extent of radiative regions is larger in the secondary than in the primary [Kähler, 2004].

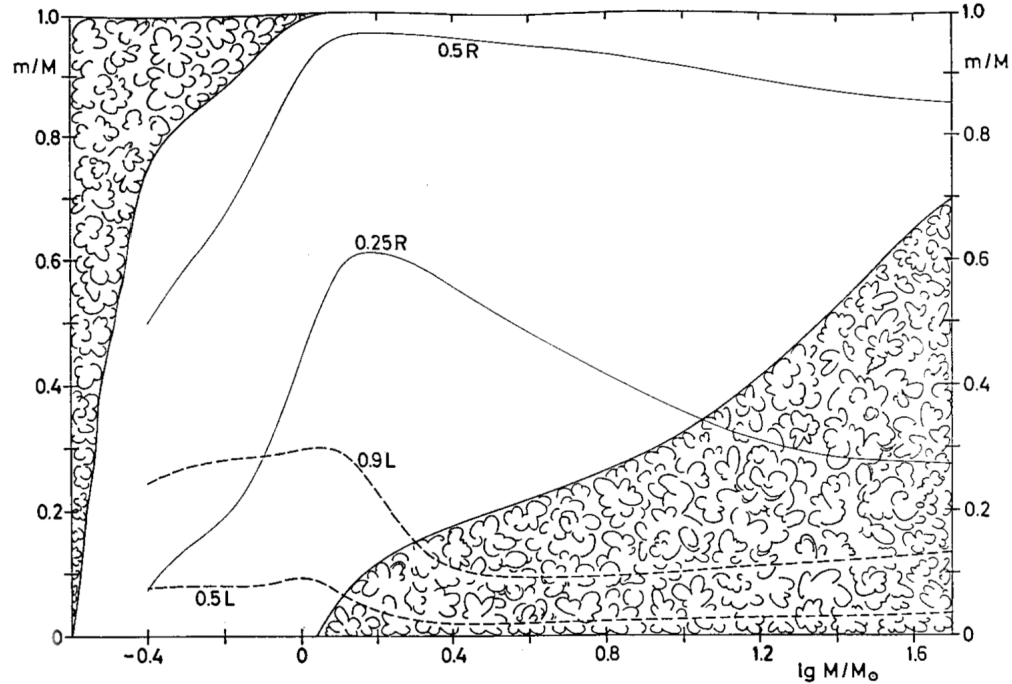


Figure 11: The mass values m from centre to surface are plotted against the stellar mass M for zero-age main-sequence models. “Cloudy” areas indicate the extent of the convective zones inside the models. Two solid lines give the m values at which r is $1/4$ and $1/2$ of the total radius R . The dashed lines show the mass elements inside which 50% and 90% of the total luminosity L are produced. Figure 22.7 from (pp. 212) of Kippenhahn et al. [1990].

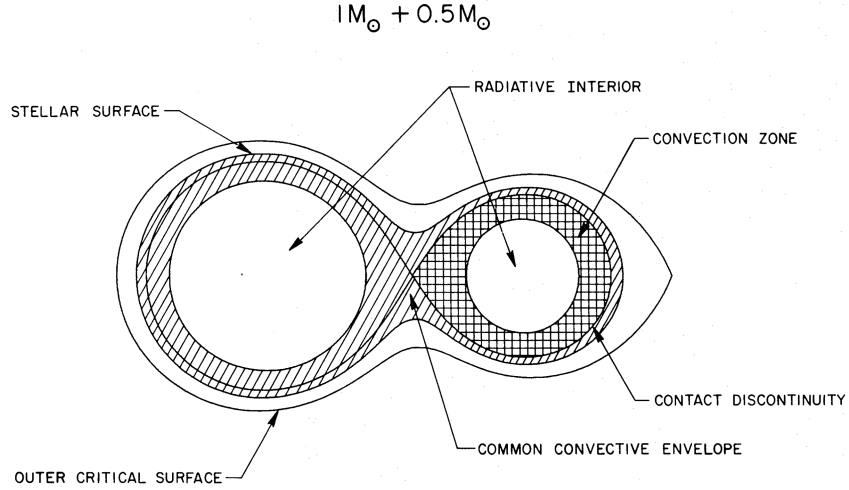


Figure 12: An equatorial cross-section of a $1 M_{\odot} + 0.5 M_{\odot}$ zero-age contact binary of solar composition. The filling factor of this model is $f = 0.41$, and the binary period is $P_d = 0.228$ days. Fig. 2 from Lubow and Shu [1977]

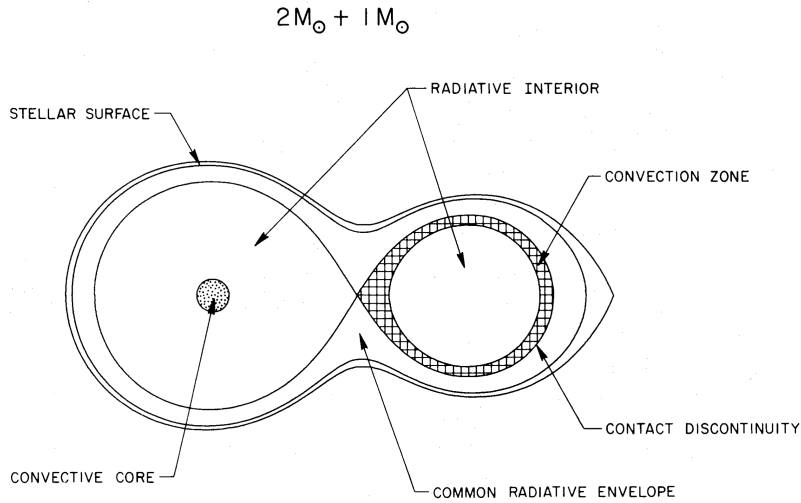


Figure 13: An equatorial cross-section of a $2 M_{\odot} + 1 M_{\odot}$ zero-age contact binary of solar composition. The filling factor of this model is $f = 0.84$, and the binary period is $P_d = 0.314$ days. Fig. 3 from Lubow and Shu [1977]

2.3.1 The Criterion for Stellar Convection

Carroll and Ostlie [325, 2006] gives the criterion for stellar convection. For convection to occur,

$$\frac{d \ln P}{d \ln T} < \frac{\gamma}{\gamma - 1} \quad (2.29)$$

In words, this equations states that when the pressure gradient is smaller than the temperature gradient, convection is likely to occur. Convection occurs when the stellar opacity κ is large.

The two primary methods of energy transport in main-sequence stars are convection, and radiation. In radiation, the stellar material is in hydrostatic equilibrium, and energy is transported through it via electromagnetic waves. If conditions are such that radiation cannot transport energy away from the core efficiently enough, the stellar material itself will have to move to transport this energy, disrupting hydrostatic equilibrium. We call this disruption convection.

[Ivanova et al., 2013]

2.4 The Period-Color Relation

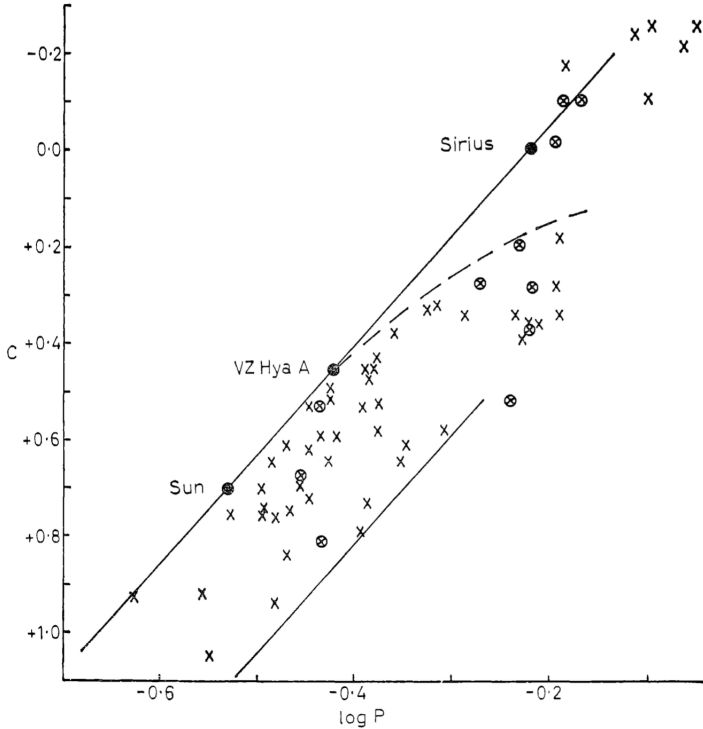


Figure 14: Fig. 6 from Eggen [1967].

Two of the parameters that are the easiest to observe for contact binaries are the orbital period (P) and effective temperature (T). In the 1960's, a correlation between these two physical parameters was discovered [Eggen, 1967]. Because the color of a star is indicative of its temperature, this relationship is most commonly called the period-color relation.

In this section, we will perform a derivation of this relation to understand why there is a relation between the orbital period (P) and effective temperature (T) of a contact binary system. We start with the fact that contact binaries are composed of two main-sequence stars. Remember that main-sequence stars have well defined relationships between mass and radius:

$$\frac{R_{\text{ZAMS}}}{R_{\odot}} \approx 0.89 \left(\frac{M}{M_{\odot}} \right)^{0.89} \quad \text{for } M < 1.66M_{\odot} \quad (2.30)$$

We can relate the combined masses of the two stars to their periods using the generalized form of Kepler's Third Law. We will assume that two components of our contact binary have equal mass.

$$P^2 = \frac{4\pi^2}{G(M_1 + M_2)} a^3 \Rightarrow P^2 = \frac{4\pi^2}{G(2M)} a^3 \quad (2.31)$$

In order for the binaries to be in contact, their photospheres must touch physically. This allows us to introduce the contact criterion, in which the separation between the centers of the components are equal to the sum of the two radii. We will assume that two components of our contact binary have equal radius:

$$a = R_1 + R_2 = 2R \quad (2.32)$$

We can then substitute Eqn. 2.32 into Eqn. 2.31

$$P^2 = \frac{4\pi^2}{G(2M)} (2R)^3 \quad (2.33)$$

Because we know that both of the components of the contact binary are on the main-sequence, we express the radius of the star at ZAMS in terms of its mass using Eqn. 2.30. When we substitute Eqn. 2.30 into Eqn. 2.33 (converting Eqn. 2.30 into SI units), we can express the orbital period P as a function of $\frac{M}{M_{\odot}}$.

$$P^2 = \frac{4\pi^2}{2G(\frac{M}{M_{\odot}})M_{\odot}} 8 \left(\frac{R}{R_{\odot}} \right)^3 R_{\odot}^3 \Rightarrow P^2 = \frac{16\pi^2}{G(\frac{M}{M_{\odot}})M_{\odot}} \left(0.89 \left(\frac{M}{M_{\odot}} \right)^{0.89} \right)^3 R_{\odot}^3 \quad (2.34)$$

We can simplify Eqn. 2.34, in order to be prepared for the next step.

$$P^2 = \frac{(11.2)\pi^2 R_{\odot}^3}{GM_{\odot}} \left(\frac{M}{M_{\odot}} \right)^{1.67} \quad (2.35)$$

Now that we have the period described strictly in terms of stellar-mass, we can use the mass-temperature homology relation to express the period strictly in terms of temperature. Starting from Eqn. 2.7:

$$\frac{T_{ZAMS}}{T_\odot} \approx 1.07 \left(\frac{M}{M_\odot} \right)^{0.41} \Rightarrow \left(\frac{M}{M_\odot} \right) = 0.84 \left(\frac{T}{T_\odot} \right)^{2.44} \quad (2.36)$$

We can substitute Eqn. 2.36 into Eqn. 2.35, and simplify to find the period-temperature relationship:

$$P^2 = \frac{(11.2)\pi^2 R_\odot^3}{GM_\odot} \left[0.84 \left(\frac{T}{T_\odot} \right)^{2.44} \right]^{1.67} \Rightarrow \quad (2.37)$$

$$P = \left(\frac{8.4\pi^2}{G} \frac{R_\odot^3}{M_\odot} \left(\frac{T}{T_\odot} \right)^{4.07} \right)^{\frac{1}{2}} \quad P \propto \left(\frac{T}{T_\odot} \right)^{2.03} \quad (2.38)$$

In Table 2, we plug in a few typical values for stellar temperature into Eqn. 2.38 and see what happens to the period of the contact binary.

Table 2: ZAMS Period-Temperature Relation

Stellar Classification	Stellar Temperature (K)	Orbital Period (days)
F	6500K	0.2138
G	5800K	0.1695
K	5000K	0.1253
M	3700K	0.0691

As we can see, as the temperature of a contact binary increases, so does the period, which matches what we observe in Fig. 14. The values for the periods presented in Table 2 are actually shorter than typically observed values by a factor of 2-3. This is because we used the ZAMS homology relations in the derivation. Contact binaries do not form at ZAMS, and, (as we learned in §2.2.3) ZAMS stars have a much smaller radius than TAMS stars (or, for that matter, any stars further along their main-sequence lifetimes).

There is considerable scatter in the observed period-temperature diagram because a contact binary's position in period-temperature space is affected by the mass of each component (M_1, M_2), the metallicity of each component (Z_1, Z_2), the age of each component (A_1, A_2), the degree of contact (f), and other factors. All of these characteristics vary considerably from binary to binary, resulting in considerable spread in the period-temperature diagram. Fortunately, researchers have made use of age-dependent and metallicity-dependent models to produce a variety of period-color relationships for stars of various ages and metallicities (Fig. 15).

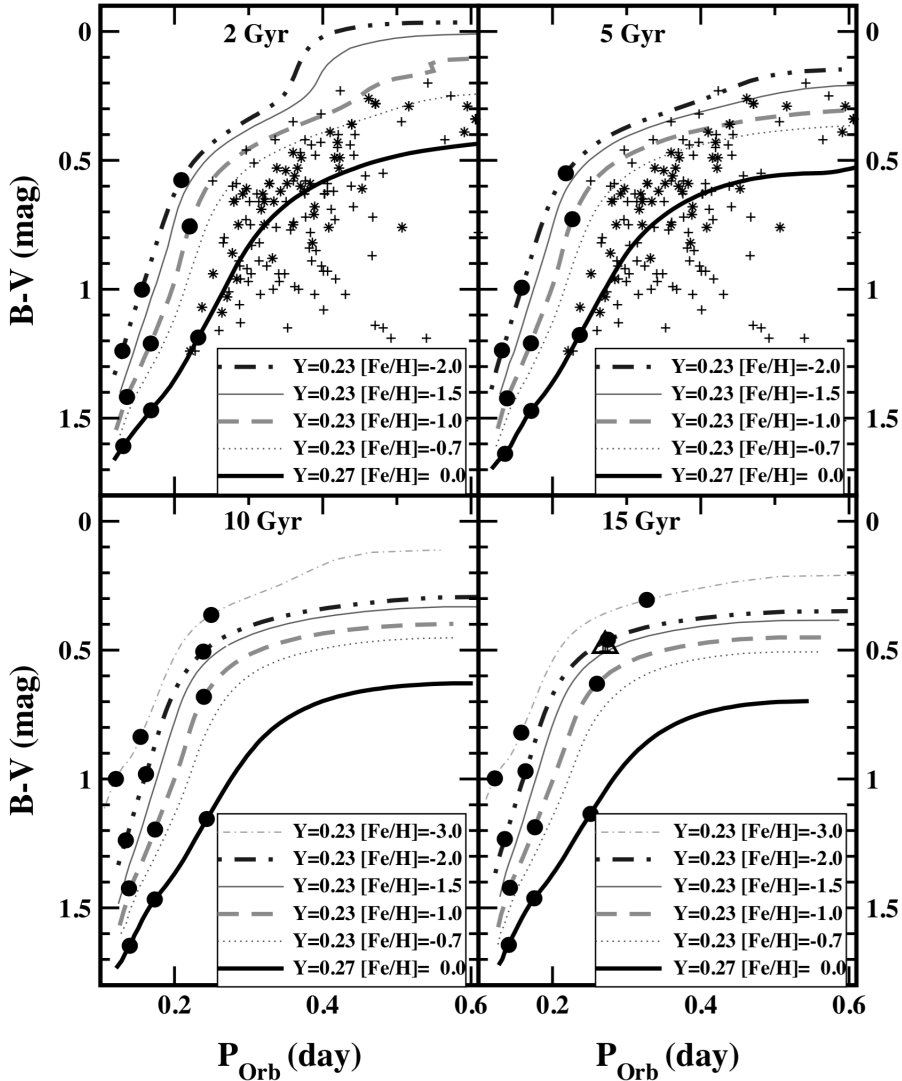


Figure 15: Metallicity and Age-Dependent period-color relations for contact binary stars. Period-color relationships for individual models are plotted as lines, while observed systems are plotted as points. Figure 1 from Rubenstein [2001].

2.5 Frequency and Density

[Rucinski, 1998a] Studies using OGLE data on the galactic bulge (Baade's Window) indicates that the frequency of contact binaries relative to main sequence stars (or spatial frequency) is approximately $\frac{1}{130} = 0.7\%$, in the absolute magnitude range of $2.5 < M_v < 7.5$. A later study using ASAS data shows that the spatial frequency is 0.2% in the solar neighborhood [Rucinski, 2006] in the absolute magnitude range of $3.5 < M_v < 5.5$.

A catalog of 1022 contact binary systems in ROTSE - 1 data placed the the space density of contact binaries at $1.7 \pm 10^{-5} \text{ pc}^{-3}$ [Gettel et al., 2006]

Contact binaries are the most frequently observed type of eclipsing binary star, because their eclipses can be detected at a wide range of orbital inclinations. In recent searches for eclipsing binary stars in survey data [Drake et al., 2014b] contact binary stars comprised 50% of the new variable stars discovered.

Existing catalog of contact binaries in the field [Pribulla et al., 2003]

Absolute magnitudes [Rucinski and Duerbeck, 1997]

2.6 Mechanisms of Formation

Like any astronomical object made up of stars, the starting point in the life of contact binaries is a cold cloud of interstellar gas (which is primarily hydrogen). The gas cloud would like to contract upon itself because of its own gravity, but cannot, because it is supported by its own gas pressure. As the cloud cools (by radiating its energy into the surrounding space), its internal gas pressure decreases and the cloud is allowed to contract. Eventually, the cloud collapses into a small enough space that the temperature and pressure start to increase at the cloud's center. When temperatures get high enough for nuclear fusion to occur, the protostar can support itself against further collapse. At the onset of nuclear fusion, we say that the protostar has become a star, at Zero Age Main Sequence or (ZAMS).

Early theories of contact binary formation posited that contact systems could form in contact Lucy [1968b]. However, the symmetry and precise amount of required angular momentum rendered this formation path unlikely. Instead, it is much more likely that contact binaries start as two separate main-sequence stars which gradually fall into a contact configuration.

Indeed, binary stars are abundant in our galaxy, with over half of all stars being part of a binary or multiple system [Carroll and Ostlie, 2006]. What causes a binary star to become a contact binary? The answer is always angular momentum loss, or AML. The system of two stars in orbit loses angular momentum, resulting in an orbit with a decreasing semi-major axis. When the orbit of the binary gets small enough, tidal interactions between the two components will force them into a contact configuration.

A binary star can lose angular momentum through two mechanisms:

1) All stars slowly lose mass by shedding charged particles in a *solar wind*. For examplee, the mass loss rate for the sun is $\dot{M}_\odot \approx 3 \times 10^{-14} M_\odot \text{yr}^{-1}$ [p.374: Carroll and Ostlie, 2006], which is very small compared to the sun's mass. However, significant amounts of angular momentum can be lost to this wind. As a star rotates, its magnetic field rotates along with it. This rotating magnetic fields accelerates the charged solar wind particles that are moving away from the sun, thereby transferring angular momentum from the sun to the magnetized solar wind. In this way, the rotation of the sun slows, and it loses angular momentum. A interaction between rotating stars and stellar wind occurs in binary systems, causing them

to lose angular momentum. This interaction between a rotating star and a magnetized solar wind creates a pattern in the stellar magnetic field called a Parker spiral [p.380: Carroll and Ostlie, 2006]

2) A binary star system can lose angular momentum through an interaction with a third (or tertiary) star. In recent years, evidence has been amassing for the formation through this pathway. In this pathway, two stars begin in a stable orbit. When a third star is introduced into the system, it steals angular momentum from the first two stars, resulting in a closer orbit. There is evidence that this companion stays in orbit around the contact binary. A study by Pribulla and Rucinski [2006] has established a lower limit on the number of triple systems. Angular Momentum Loss through tertiary components. [Lohr et al., 2015] In a search of 13,927 eclipsing binaries in the SuperWASP catalog, 24% had period-changes indicating a closely orbiting companion. The presence of tertiary components has also been detected via spectral imaging [Hendry and Mochnacki, 1998].

In the Kozai-Lidov mechanism , the orbit of two inner bodies is perturbed by a third body orbiting farther out. The equations of motion for the three-body system, a specific angular momentum is conserved:

$$L_z = \sqrt{1 - e^2} \cos i \quad (2.39)$$

Because the quantity L_z is conserved, orbital eccentricity e can be traded for orbital inclination i . Three body systems with undergo Kozai-Lidov cycles, with a certain period:

$$T_{\text{Kozai}} = 2\pi \frac{\sqrt{GM}}{Gm_2} \frac{a_2^3}{a^{\frac{3}{2}}} (1 - e_2^2)^{\frac{3}{2}} \quad (2.40)$$

[Yıldız and Doğan, 2013]

[Bilir et al., 2005]

[Li et al., 2007]

2.7 Evolution in the Contact State

As we learned in §2.2.3, the characteristics of a main-sequence star change as it progresses through its main-sequence lifetime.

As a star fuses the hydrogen in its core via the pp-chain, the resulting helium builds up at the center of the star. This causes the hydrogen burning to occur in a “shell” of increasing radius around the helium core. Thus, as a main-sequence star progresses from ZAMS to TAMS, its radius increases slightly, and its photosphere becomes slightly cooler. Thus, the age of the two components of a contact binary affects the radius and density of the star.

Thermal Relaxation Oscillations [Wang, 1994]. May cause orbital period changes observed in Qian [2001].

Kahler's first paper on the structure of contact binaries [Kähler, 2002]
The structure of contact binaries [Kähler, 2004]
In the course of evolution the period increases and the mass-ratio decreases [Kähler, 2004].

the surface of the contact system does not obey a simple gravity brightening law [Kähler, 2004], [Hilditch et al., 1988].

[Rubenstein, 2001]

Angular momentum and mass evolution. Some of the most recent modeling work indicates that the typical duration of the contact state is 1 to 1.5 Gyr [Gazeas and Stępień, 2008].

masses and angular momenta [Gazeas and Niarchos, 2006] angular momentum loss [Vilhu and Rahunen, 1981]

contact binaries occupy a very narrow range of parameter space [Gazeas, 2009] [Awadalla and Hanna, 2005]

Overall evolution [Stepien and Gazeas, 2008], 2016 review of close binary evolution [Tutukov and Cherepashchuk, 2016]

Short period limit [Rucinski, 2007] [Drake et al., 2014a] Lohr et al. [2012] [Rucinski, 1992]

2.8 Evolution out of the Contact State

It is generally accepted that the contact state of binary evolution ends with the inspiral and merger of the two components. The merger event is where the contact system becomes dynamically unstable, and rapidly coalesces into a single, rapidly rotating star.

The merger of a contact binary star was observed in 2008 Tylenda et al. [2011]. A “red nova” event was observed in the constellation of Scorpius in late 2008. When archival data was examined, it was revealed that a contact binary system had existed at the nova’s precise location.

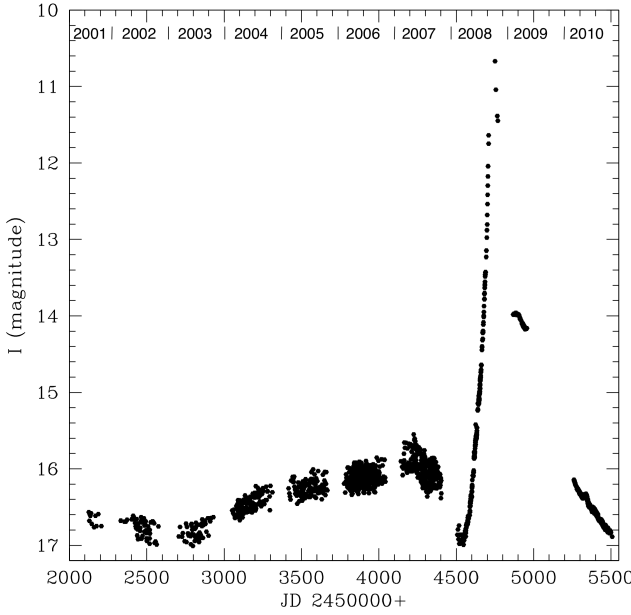


Fig. 1. Light curve of V1309 Sco from the OGLE-III and OGLE-IV projects: I magnitude versus time of observations in Julian Dates. Time in years is marked on top of the figure. At maximum the object attained $I \approx 6.8$.

Figure 16: Light curve of V1309 Sco from the OGLE-III and OGLE-IV projects: I magnitude versus time of observations in Julian Dates. Time in years is marked on top of the figure. At maximum the object attained $I \approx 6.8$. Figure 1 from Tylenda et al. [2011]

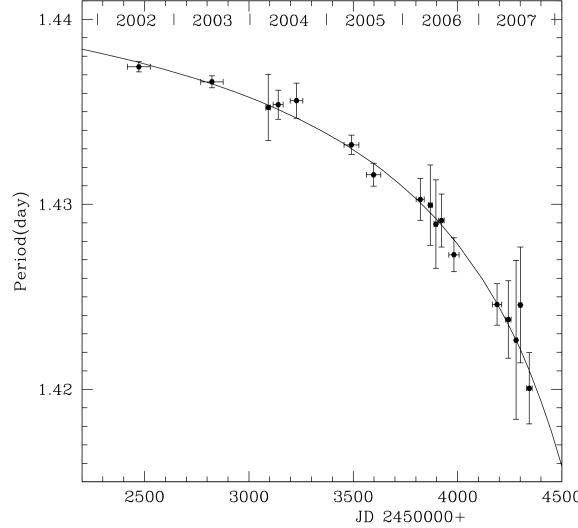


Figure 17: The evolution of the period .Figure 2 from Tylenda et al. [2011]

The contact binary in the OGLE merger had a period of approximately 1.4 days. Long-period contact binaries [Rucinski, 1998b]

Blue straggler Andronov et al. [2006]

stability of the contact configuration [Rasio, 1995]

minimum mass ratio [Arbutina, 2009]

One of the ways that a contact binary system can merge is called the Darwin instability.

In a Darwin instability, the ...

In the early 1990s, large numbers of new contact binaries were discovered among blue stragglers, in open and globular clusters

[Kaluzny and Shara, 1988] no discovery in six open clusters.

In the globular cluster M71, four contact binaries discovered by Yan and Mateo [1994], placing a lower limit of 1.3% on the frequency of primordial binaries in M71 with initial orbital periods in the range of 2.5 to 5 days.

Short period eclipsing binaries have been found among blue stragglers in the globular cluster NGC5466 [Mateo et al., 1990].

Review of binaries in globular clusters [Hut et al., 1992]

modern work on six binaries in NGC188 [Chen et al., 2016]

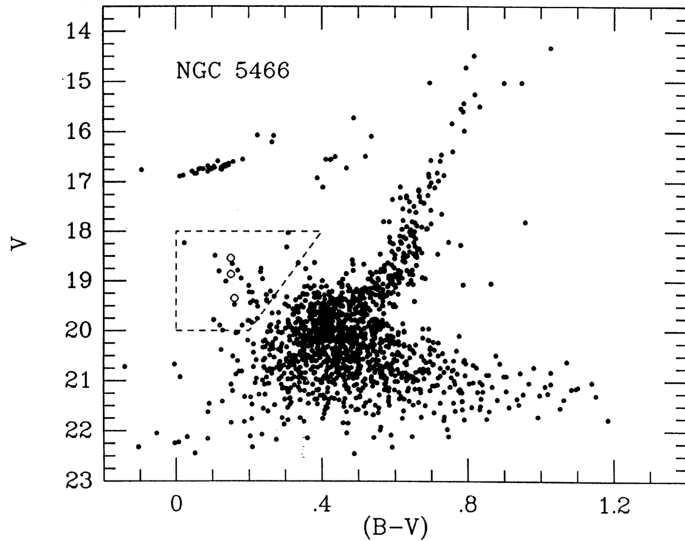


Figure 18: A color-magnitude diagram of globular cluster NGC 5466. The blue stragglers are defined to be all stars located within the region bounded by the dashed lines. The mean V magnitudes and $(B - V)$ colors of the eclipsing binaries discovered by Mateo et al. [1990] are shown as open circles. Figure 1 from Mateo et al. [1990].

2.9 Early-Type Contact Binaries

There is a type of contact binary that is so special that it merits its own section. The contact binaries that we have been talking about in the previous section have been low-mass, meaning that each of the components has a mass of less than $10M_{\odot}$. However, astronomers

have recently found several massive O-type contact binaries, with component masses of close to $40M_{\odot}$.

When astronomers say that a star is “Early-Type”, they mean that it is “early” on the spectral classification sequence (OBAFGKM). O and B stars are more massive, more luminous and hotter than our sun. Early-Type contact binaries deserve a special section due to their extreme mass, luminosity, rarity, and short lifetime. There are only a handful of O and B Type contact binary systems known. The four best studied systems are TU Muscae [Penny et al., 2008], MY Cam [Lorenzo et al., 2014], UW CMa [Antokhina et al., 2011], V382 Cygni [Popper, 1978].

These massive O and B type contact binaries are very different from less massive (F,G,K,M) type contact binaries. Because O and B type stars have such short life-times, O and B type contact binaries are especially short-lived. Also, very few O and B type contact binaries are formed, because the stellar initial mass function (IMF), is heavily skewed towards low-mass M stars. The combination of these two effects makes massive O and B type contact binaries exceedingly rare. In fact, less than 10 systems have been discovered so far.

Early-Type Contact binaries are some of the most luminous stellar objects. This means that they can be seen at extragalactic distances. Over forty intermediate mass systemshave been found in the Small Magellanic Cloud [Hilditch et al., 2005, Priya et al., 2013]. Even at the distance of M31, some eclipsing binaries can be seen. [Lee et al., 2014, Vilardell et al., 2006]

2.10 Magnetic Activity

In the solar atmosphere, the movement of plasma in the convective region creates magnetic fields, which in turn affect the motion of that same plasma. Contact binaries are rapidly rotating systems, with orbital periods of 0.2 to 0.8 days (compare this rate with the approximately 30 day solar rotational period), so they have the potential to form much stronger magnetic fields.

There is a lot of evidence that contact binary stars have strong magnetic fields. Astronomers observe changes in their light-curves, indicating that starspots may be appearing and disappearing on their photospheres. Doppler imaging of contact binaries can reveal the shapes and locations of the starspots on the photosphere (Fig. 20)

Because late-type contact binaries have Common Convective Envelopes (or CCEs),

Some scientists believe that the existence of the CCE buries the very strong surface magnetic field, which could prevent the production of flares [Qian et al., 2014].

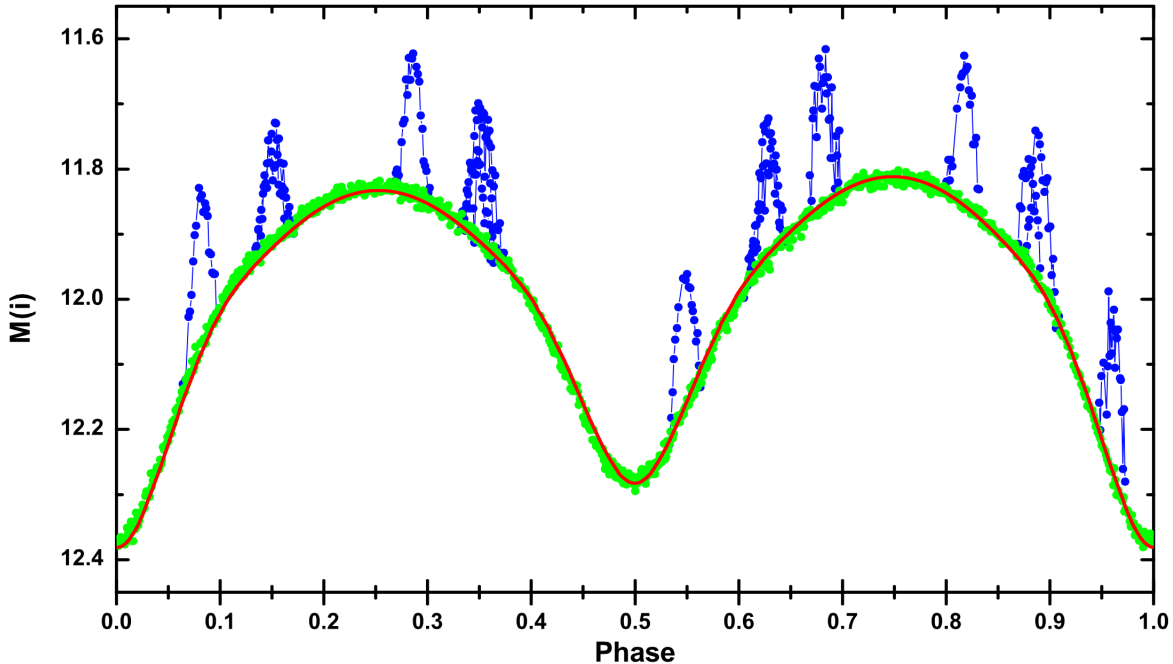


Figure 19: Fig. 15 from Qian et al. [2014]

[Balogh et al., 2015] book review of solar magnetic activity cycles.

The applegate mechanism [Applegate, 1992] [Lanza, 2006]

W UMa as X-ray sources [Stepien et al., 2001]

[Rucinski, 1998c] EUV results.

Observational starspots and magnetic activity cycles. [Borkovits et al., 2005, Shengbang and Qingyao, 2000, Kaszás et al., 1998, Qian et al., 2007, Lee et al., 2004, Yang et al., 2012, Zhang and Zhang, 2004].

It is possible that starspots are responsible for the variation in brightness observed by CRTS. Doppler imaging techniques have confirmed the presence of large starspots on the surface of some contact binaries [Barnes et al., 2004]. An example of a well observed change in the contact binary light-curve [Gazeas et al., 2006].

Barnes et al. [2004] has used an Echelle spectrograph on the 3.9-meter Anglo-Australian Telescope to perform doppler imaging of the AE Phe system ($P = 0.362$ d), revealing that the photosphere of the system is heavily spotted (Fig. 20).

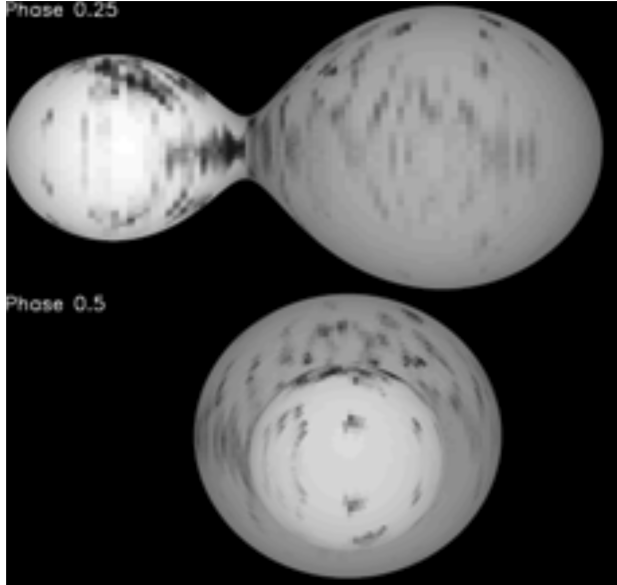


Figure 20: Fig. 5 from Barnes et al. [2004]

Contact binaries are known X-ray sources [Chen et al., 2006]. Flares have been observed in X-ray bands using ROSAT [McGale et al., 1996]. EXOSAT has been used to observe a flare in X-ray and Microwave data on VW Cephei ($P = 0.28$ days, $T_1, T_2 = 5500\text{K}, 5000\text{K}$) [Vilhu et al., 1988]. Extreme UV observations have identified coronal characteristics [Brickhouse and Dupree, 1998]. Long time series observations of single m-dwarfs [Lacy et al., 1976]

During a continuous monitoring campaign in the winters of 2008 and 2010, Qian et al. [2014] observed a contact binary system CSTAR 038663 ($P = 0.27$ days, $T_1, T_2 = 4616\text{K}, 4352\text{K}$) for a total of 4167 hours (174 days) in the SDSS i band using the CSTAR telescope array in the Antarctic. In this time, Qian et al. [2014] discovered 15 i band flares, revealing a flare rate of 0.0036 flares per hour. These 15 flares had durations ranging from 0.006 to 0.014 days (9 to 20 minutes), and amplitudes ranging from 0.14 - 0.27 magnitudes above the quiescent magnitude.

In 1049 close binaries observed by Kepler, Gao et al. [2016] have identified 234 “flare binaries”, on which a total of 6818 flares were detected. Kepler’s continuous monitoring capability and precise photometry make it extremely well suited to the detection of white-light flares [Walkowicz et al., 2011]. While CRTS does not match Kepler’s observing cadence, photometric precision, or ability to observe a given target continuously, it observes 33,000 square degrees a much larger area of the sky than Kepler does (100 square degrees) [Drake et al., 2009, Basri et al., 2005].

The evolution and migration of starspots on contact binaries has been tracked with doppler imaging [Hendry and Mochnacki, 2000] and more recently, in Kepler data [Tran et al., 2013, Balaji et al., 2015]. Starspots are magnetic phenomenon, and so their occurrence

is related to the magnetic activity of their host star [Berdyugina, 2005].

3 Observations

Astronomy is unique as a science because (almost, thanks LIGO) all the information that can be obtained from an object in the sky comes to us as electromagnetic waves. Perhaps *THE* question in observational astronomy is: “What can we learn from these electromagnetic waves?”. The study of contact binary stars is no different. In this section, we will learn the ways that researchers study electromagnetic waves from contact binary stars.

3.1 Images of Contact Binaries

The oldest type of astronomical information is image data: “What do I see when I look through the telescope?”. To put this question in more formal language: “What is the distribution of the intensity of visible light as a function of position?”. When we look at the moon, for example, we can learn a lot about it: we might see some crater “over here”, with a given size, shape, color, etc. We might see a dark lunar mare (or “sea”), “over there”, with another size, shape, color, etc. The moon is what we call a “resolved source”, meaning that features on it are distinguishable: we can separate “over here” from “over there”. In other words, the distance between “over here” and “over there” is larger than the resolution limit of our telescope.

Let’s see if we can reasonably obtain image data from a contact binary:

On a still, clear night at the Las Campanas observatory in Chile, the atmospheric resolution limit (or “seeing”) is 0.5 arcseconds. This is the best resolution that can be expected from a telescope on earth: Chile’s Atacama desert is known for some of the best seeing on earth.

$$0.5 \text{ arcseconds} * \frac{1}{3600} \frac{\text{arcseconds}}{\text{degrees}} = 1.4 \times 10^{-4} \text{ degrees} * \frac{\pi}{180} \frac{\text{radians}}{\text{degrees}} = 2.4 \times 10^{-6} \text{ radians} \quad (3.1)$$

In order to distinguish between the two components of a contact binary, the resolution limit of our telescope must be smaller than the distance between the centers of the two components.

For a contact binary star of solar type, this is about one solar radius: $1R_{\odot} = 6.957 \times 10^5 \text{ km}$. Let us place this hypothetical contact binary at the same distance as the nearest star, *Proxima Centauri*, which is 4.243 light years = 1.301 parsecs = $4.014 \times 10^{13} \text{ km}$.

To calculate the angle that a solar type-contact binary at the distance of *Proxima Centauri* would subtend, we will use the small angle approximation:

$$\sin(\theta) \approx \theta, \quad \cos(\theta) \approx 1 - \frac{\theta^2}{2}, \quad \tan(\theta) = \frac{\sin(\theta)}{\cos(\theta)} = \frac{\theta}{1 - \frac{\theta^2}{2}} \Rightarrow \tan(\theta) \approx \theta \quad (3.2)$$

If we set up a right triangle (as in Fig. 21), we see than the tangent of the angle θ is equal to the radius of the sun divided by the distance to *Proxima Centauri*.

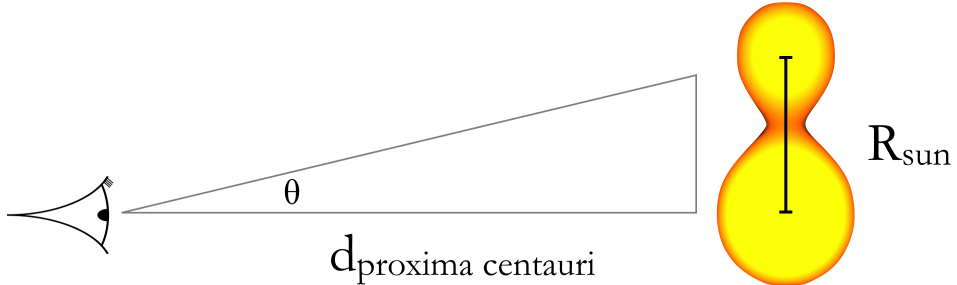


Figure 21: Calculating the angle θ subtended by a solar-type contact binary at the distance of the nearest star.

$$\frac{R_{\text{sun}}}{d_{\text{proxima centauri}}} = \frac{6.957 \times 10^5 \text{ km}}{4.014 \times 10^{13} \text{ km}} = \tan(\theta) \approx \theta = 1.733 \times 10^{-8} \text{ radians} \quad (3.3)$$

When comparing the resolution necessary to distinguish the components of a contact binary to the best resolution possible on earth:

$$\frac{1.733 \times 10^{-8} \text{ radians}}{2.4 \times 10^{-6} \text{ radians}} \approx 0.01 \quad (3.4)$$

To summarize: we would need 100 times the resolving power achievable from the earth to obtain image data from a large contact binary at the distance of the nearest star. In actuality, the situation is worse. 44 Bootis is the nearest contact binary system to earth, at a distance of 13 parsecs (42 light years) it is 10 times further away than *Proxima Centauri* [Eker et al., 2008]. For this reason, we cannot obtain usable image data from contact binaries¹.

3.2 Photometry of Contact Binaries

In images, contact binaries appear as an unresolved point source. At first glance, it may appear that astronomers are stuck: they cannot “see” the contact binary and so must remain

¹it is possible to achieve this resolution (as good as 0.0005") through long-baseline interferometry. Using the CHARA array on Mount Wilson, researchers have constructed a resolved image of the eclipsing binary system β *Lyræ* [Zhao et al., 2008]. However, interferometric imaging is only possible for the brightest stars, so is not useful for contact binaries.

uncertain about its characteristics. However, as Kempf and Müller learned in 1903, the amount of light received from a contact binary varies as a function of time. This function is called the light-curve:

$$f(\text{Time}) = \text{Flux Received at Telescope} \quad (3.5)$$

A light curve is constructed from observations: by repeatedly measuring the brightness of a source over a certain time span, an astronomer can sample the light-curve and approximate its true shape.

Kempf and Müller knew that they could use the light-curve to learn about the shape of the contact binary system. First, they noted that the light-curve was periodic: after a certain amount of time, the trend in flux *exactly repeated* itself. Thus they knew that the process that was responsible for the variation in the flux was cyclical in nature.

They knew that the period of the light variation in W UMa was very stable (“The error of the period can hardly be more than 0.5s...”). They assumed that a rotational or orbital mechanism was responsible for the light variation. They thought that the presence of a large dark spot on a rapidly rotating single star, which was hypothesized to be “in an advanced stage of cooling”. However, W UMa was a white star, not a cool red star, leading Kempf and Müller to discredit this model. They also considered a single star in the shape of an ellipsoid - a large, however they calculated that this model did not describe the shape of the light-curve very well. In 1903, the eclipsing binary model was already proposed as a mechanism for the light-curves of certain stars (most notably Algol). To construct their model, they looked at existing eclipsing binary light curves and imagined what would happen if they brought the two stars close together. If they brought the two stars close enough together so that the stars were almost touching, there was always variation in the light-curve, just like they observed.

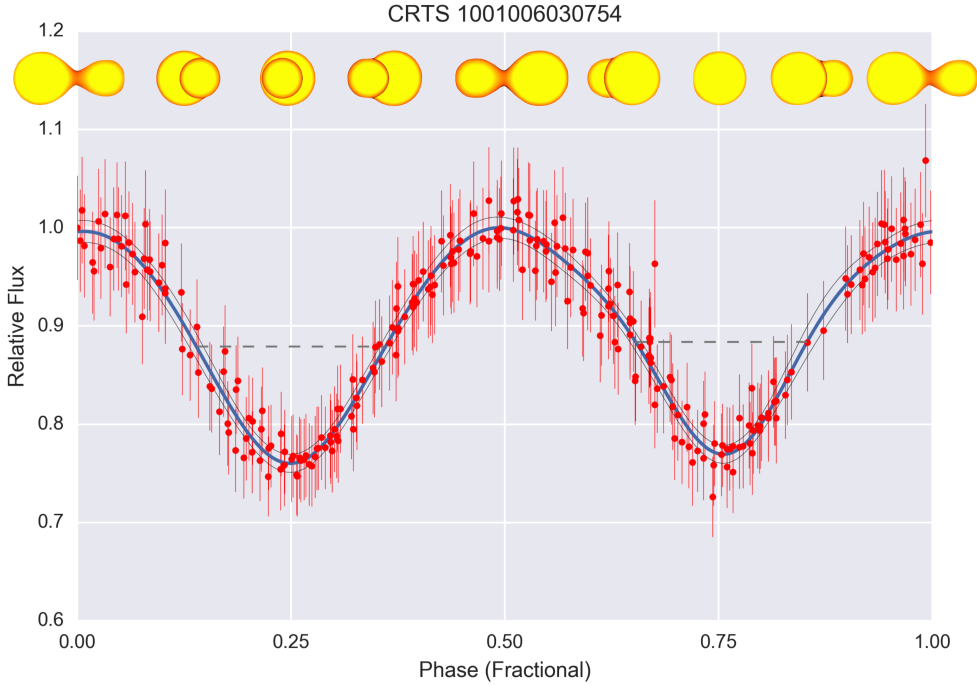


Figure 22: Light-curve is from CRTS data [Drake et al., 2014b]. Illustration of contact binary phase from an animation at: <http://cronodon.com/SpaceTech/BinaryStar.html>

The shape of a contact binary’s light-curve can tell us a lot about it. Indeed, the aim of much of the original work in this thesis is to determine how the shape of the contact binary light-curve correlates with physical parameters. I’ll now go through a few light-curve features

Not all contact binary light-curves look the same, so why is that? What information does can be learned about a contact binary system based only on it’s light-curve?

This means that the light-curve of a system with two (relatively) small and cool M type components should be qualitatively and quantitatively identical to the light-curve of a system with two massive and hot G type components, given the systems have the same geometry $[f, q, i]$.

3.3 Spectra of Contact Binaries

Time-series spectra are some of the most complete observations of contact binaries. By fitting a blackbody curve to the spectrum of a star, we can calculate its temperature to greater precision than we can by using color filters. In addition, spectral features of a known wavelength can be used to measure the velocity of the source. Contact binaries are rapidly rotating systems, which causes spectral lines to be broadened. The analysis of the rotational velocities of contact binaries is especially challenging because unlike some binary systems,

the two components are of approximately equal brightness.

[Hrivnak, 1989] radial velocities and IR data of OO Aql.

Analyzing spectra of contact binaries is challenging. Abundances of elements cannot be determined precisely due to the broadening and blending of spectral lines caused by the fast rotation [Gazeas and Niarchos, 2006].

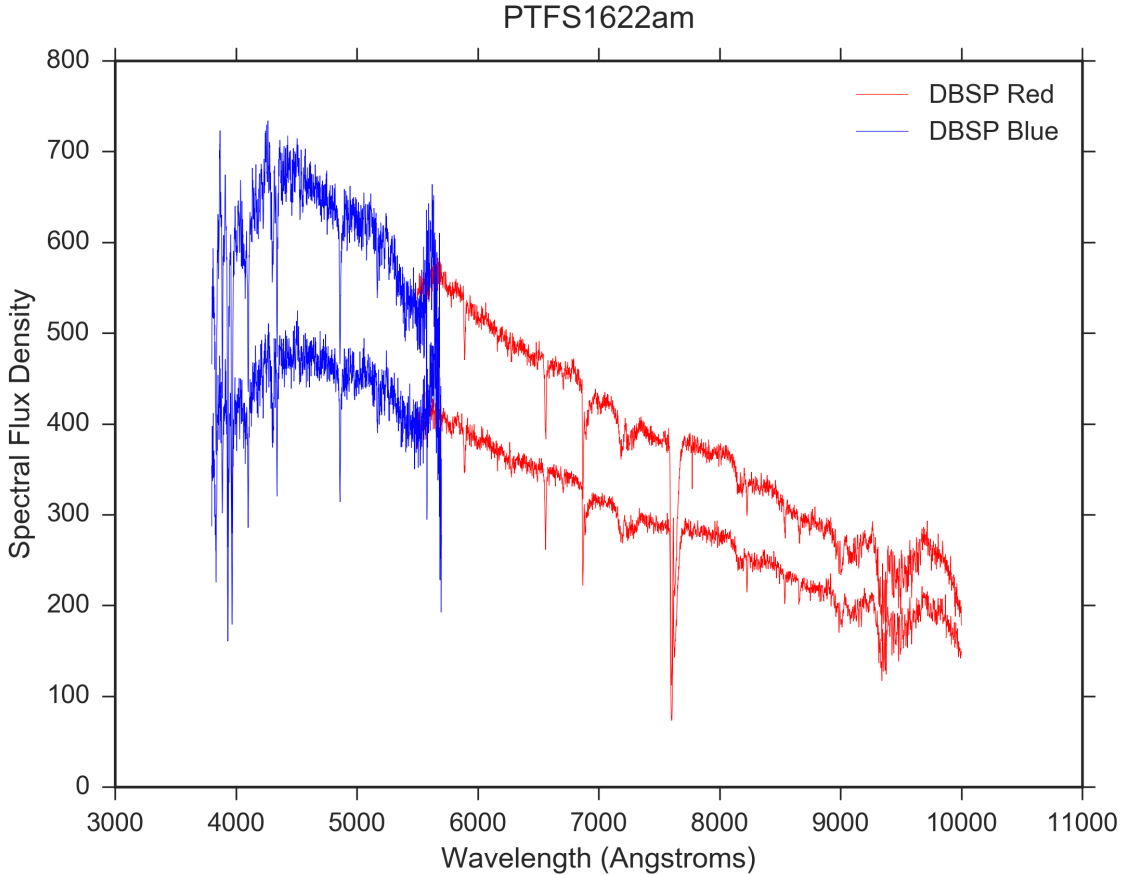


Figure 23: Two spectra of the contact binary star PTFS1622am, as observed with the Double-Beam Spectrograph at the 200'' Hale Telescope. The two colors indicate the separate chips that the spectra was observed on. The Spectral Flux Density is in arbitrary units, what is more important is to observe the relative flux.

3.4 X-ray and Ultraviolet Data on Contact Binaries

Contact binaries are much brighter than main-sequence stars in the ultraviolet, owing to their strong magnetic fields cause by rapid rotation. Earth's atmosphere is opaque to X-ray and ultraviolet (UV) light, but the advent of space-based observatories has made observations of the sky possible in these passbands.

[Cruddace and Dupree, 1984] first *Einstein* survey of 17 contact binaries. Fig 2 has the X-ray luminosity- period relation. [Vilhu and Walter, 1987] “the two components of a contact binary have identical chromospheres and transition regions” F_x/F_{bol} remains roughly constant with $(B - V)$ color. [Stepien et al., 2001] supersaturation in contact binaries.

4 Analysis Techniques

Observational tests of theories of contact binaries Lucy and Wilson [1979]

4.1 Physical Light-Curve Modeling

In §3.2, we learned about how contact binary light-curves contain information about the physical nature of the system. Since the majority of data on contact binaries is in the form of photometric light-curve measurements, there has been much effort spent on refining the process of light-curve analysis.

In this section, we will learn how light-curves can be synthesized from physical models like those of Lucy [1968a]. We also will learn how these synthesized light-curves can be fit to observations. It is important to know about the degeneracies present in this type of analysis.

A large number of papers

The Wilson-Devinney Code (hereafter WD code) was the first code that could produce contact binary light-curves in large quantities.

Fully automated approaches [Prsa et al., 2009] [Prsa et al., 2008]

recent advances in modeling code [Prša et al., 2013]

useful review [Giménez et al., 2006]

`phoebe` is a user friendly implementation of the WD code in `python` developed by an international team of researchers. A researcher can feed a light-curve into `phoebe`. Assumptions about the model atmospheres and other aspects of stellar physics allow for a physical model to be fit to the data.

Almost always, `phoebe` models based on observational data are underdetermined. There are so many free parameters in the models (which allow the user to fit for starspots of various shapes and sizes, and include the light of an unresolved tertiary component), many degenerate perfect fits to observed data can always be found. Unfortunately, the WD code is frequently treated as a black box, and single-band photometry is used, parameters for spots and third light are fit. The degeneracy of these solutions is rarely if ever mentioned.

However, radial velocity data can be used to break degeneracies by providing an independent measurement of the system’s total mass and mass-ratio

Alternatives include `ROCHE` [Pribulla, 2011]

Simultaneous fitting of physical models of the contact binary light-curve and radial velocity data can provide almost totally determined solutions.

4.2 Nomographic Light-Curve Solutions

As larger and larger numbers of contact binaries were discovered, astronomers saw the motivation for providing a less computationally-intensive way of determining a system's geometrical elements from light-curve data.

Mochnacki and Doughty [1972] First nomographic solution, inspired work by Rucinski. [Rucinski, 1973]

In this method, the physical model of the contact binary is used in reverse (as compared to §4.1). A grid of models is produced, covering the parameter space of system geometry [f, q, i]. Then, light-curves are generated for each model. The observed light-curve is then compared with a whole catalog of computed light-curves.

The main advantage of this method is that the model degeneracy can be estimated. Often, (especially for systems with a low orbital inclination) many models will be supported by the observed data.

OGLE work has determined a criterion for overcontact based on Fourier coefficients [Rucinski, 1997]. [Rucinski, 1993b]

Rucinski has used eclipse half-widths and Fourier components to estimate geometrical properties of the system:

the reliability of the mass-ratio determination from light-curve only data [Hambálek and Pribulla, 2013]

ROTSE study using fourier methods [Coker et al., 2013]

phenomenological study [Andronov, 2012]

employing neural networks to find true binary parameters [Zeraatgari et al., 2015]

Difference between q_{sp} and q_{ph} [Van Hamme and Wilson, 1985]

[Rucinski, 1973] [Rucinski, 1993b] [Terrell and Wilson, 2005]

4.3 O-C Analysis

O - C Analysis is one of the oldest analysis techniques for analyzing eclipsing binary stars. Historically, great effort has been spent on compiling “times of periastron”, for the bright eclipsing binary stars. Simply, the time when the eclipsing binary is at its minimum brightness is noted, over a large number of orbital periods.

O-C Analysis is short for “observed minus computed”, referring to the fact that a measurement is the observed time of minimum light as compared to the computed time of minimum light. The process can be described as follows:

1. A full light curve is obtained for the system in question.
2. Based on this light curve, the period is calculated, and an ephemeris is computed, listing all of the future times of minimum light.
3. Then, light curves are obtained at future epochs. The observed times of minimum light (O) are compared to previous times of minimum light as computed by the ephemeris (C). The difference ($O - C$) is plotted as a function of epoch.

On an O-C diagram, a linear change in period (of the form $P = a \times t + b$, for $c \neq 0$) appears as a parabola.

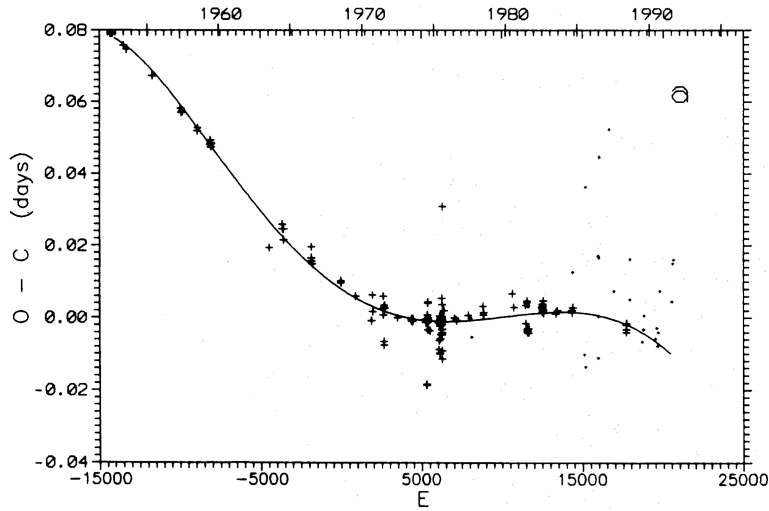


Figure 24: The O - C diagram of V566 Oph, fit by a least squares polynomial. Fig. 4a from Kalimeris et al. [1994]

The orbital period of a contact binary can change for a variety of reasons, but an observed period change always implies underlying geometrical and structural changes [Kalimeris et al., 1994].

In contact systems, orbital period changes can generally be divided into (1) short-term variations, which happen on decadal (10 year) timescales, and (2) long-term variations, which happen on a thermal timescale.

The long-term variations are caused by

- 1) Angular momentum loss due to magnetic braking. 2) mass loss through the L_2 point
- 3) chemical evolution of the primary.

The short-term variations are caused by 1) The orbit of a third body 2) Redistribution of the angular momentum due to magnetic activity. 3) Is O-C Analysis stable against the appearance and disappearance of starspots and photometric noise? [Kalimeris et al., 2002]

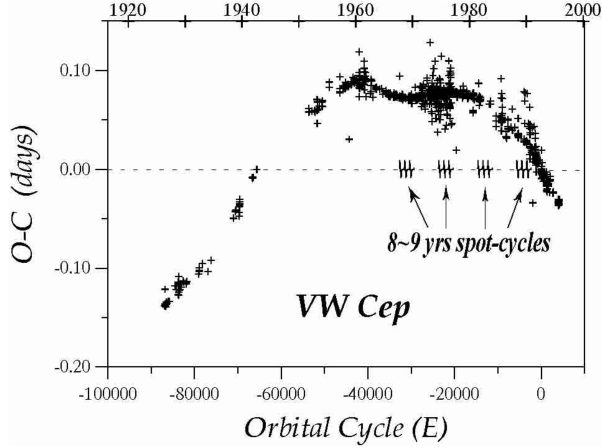


Figure 25: Fig. 7 from Kalimeris et al. [2002]

automated approach with SuperWASP [Lohr et al., 2015]

In data from surveys, the data may be too sparse to estimate times of minimum light from multiple epochs within the survey. A Lomb-Scargle (or LS) [Scargle, 1982] [Horne and Baliunas, 1986]

$$|\delta P| = (0.01728 \text{ s}) \times \left(\frac{N_0}{100}\right)^{-\frac{1}{2}} \times \left(\frac{T_{eff}}{5\text{yr}}\right)^{-1} \times \left(\frac{A/\sigma_N}{10}\right)^{-1} \times \left(\frac{P}{0.2\text{d}}\right)^2 \quad (4.1)$$

Qian [2001] has observed orbital period changes which indicate TRO.

5 Working with Survey Data

Data from large All-Sky surveys is very different in nature compared with data taken on a single night with a single telescope. Working with all-sky surveys presents huge advantages to working with traditional light-curve data, but it also has major drawbacks.

In “traditional” variable star observing, an observer slews the telescope to the target at the beginning of the night, and then takes a continuous sequence of images (from which she will make photometric measurements) at regularly spaced time intervals, until the star has rotated one full period, or until morning twilight. The observer can only look at one target at once, but the selected target is observed many times in one night.

In All-Sky surveys, the observing mode is different. All throughout the night, the telescope pans to a field, taking a few images, and then rapidly moving on to the next field. A given source might only be observed one or two times in a given night. The survey operates night after night, and after several years, it has amassed hundreds of observations of any point on the sky.

When we look in a survey database for photometric measurements of a known contact binary we often see data that looks like the data in Figure 26.

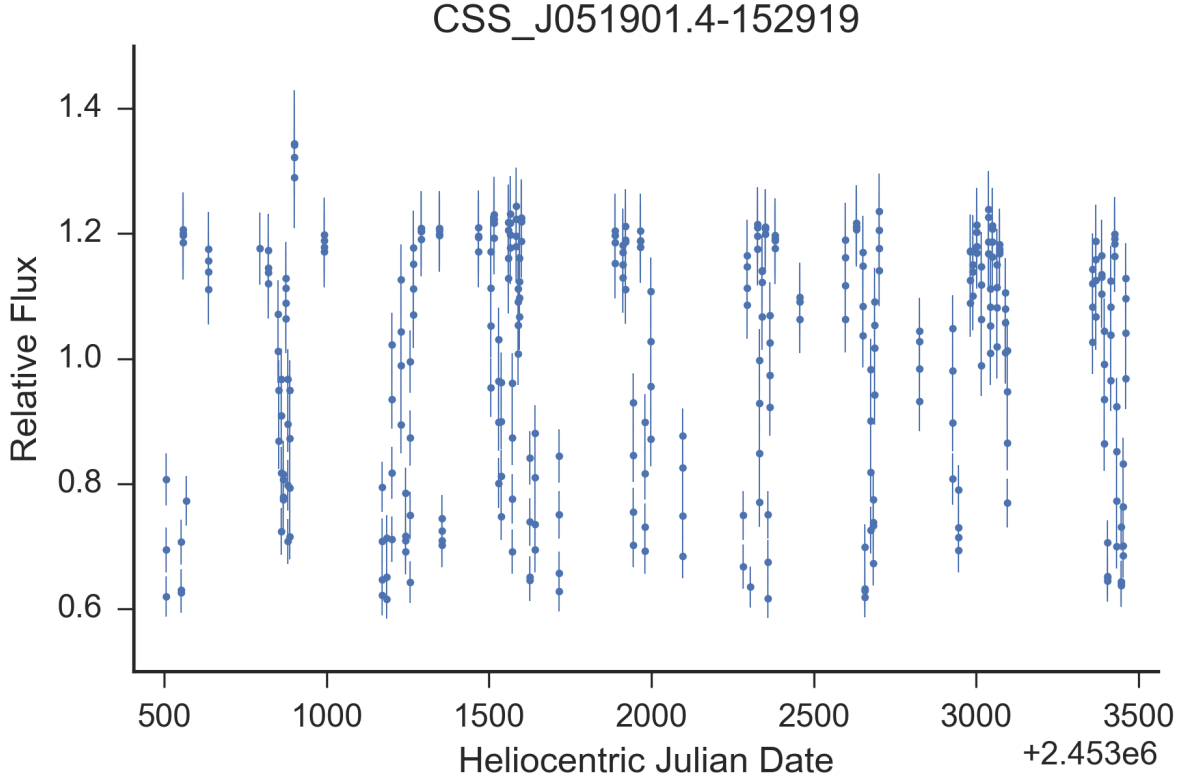


Figure 26: Observations of a contact binary, as returned by CRTS. The x-axis is the time of observation (in days), and the y-axis is the relative flux of the observation. Vertical bars about each point denote the uncertainty in the relative flux measurement. Note that the observed flux varies significantly from observation to observation, but we cannot see the periodic nature of the variability with our eyes

We know that the data in Figure 26 is not data from a source with constant brightness. Look at the size of the error bar on each point. The error bar on each point is much smaller than the scatter in the distribution. We would call this source a variable source.

Hidden in this data is an underlying periodic function - the light-curve caused by the rotation of the contact binary. The period is hidden in this data, we just need to find it.

The data that we have here is a *time-series*: a number of measurements of the flux of a source at many different times. The problem of finding a period in time-series data is usually handled with a *Fourier Transform*.

In the Fourier Transform,

The CRTS telescope does not return to this source at regular times.

The algorithm that is most widely used to find periods in unevenly sampled time-series Scargle [1982]

We calculate the phase of each observation, by dividing by the period found in the signal.

$$\theta = \frac{(\text{Time \% Period})}{\text{Period}} \quad (5.1)$$

where (%) is the “modulo” (or remainder operator)

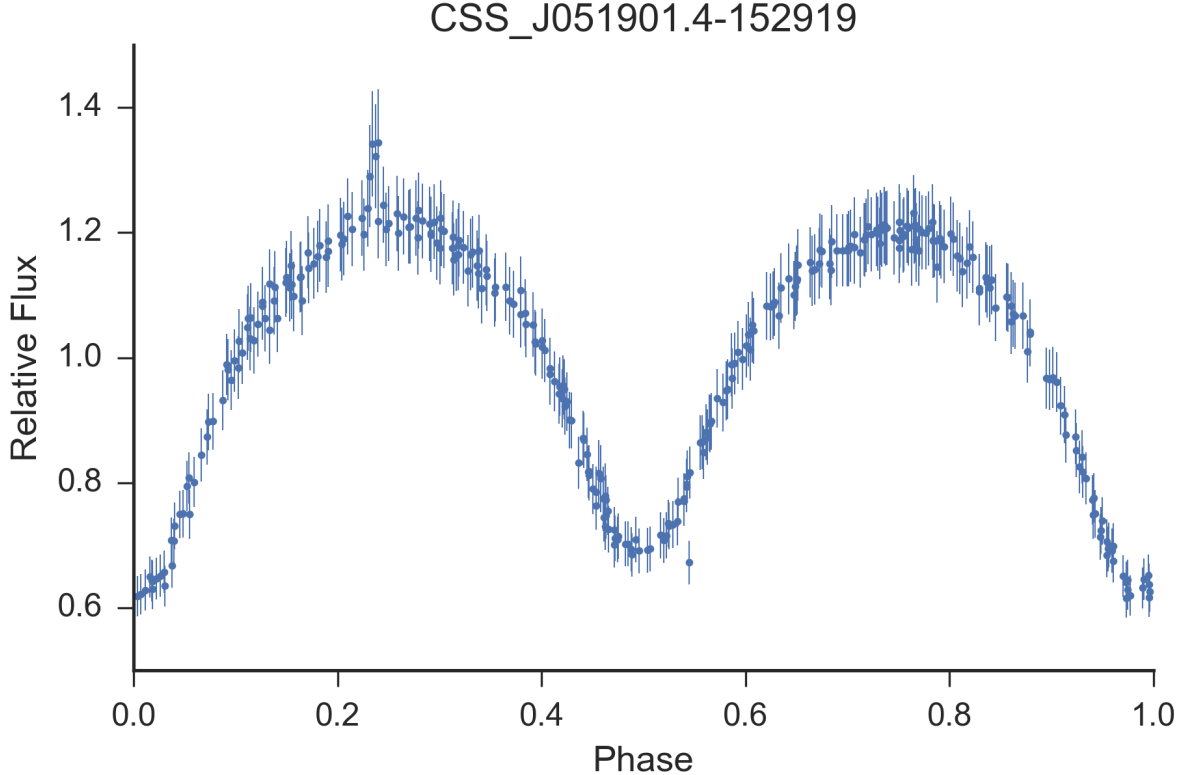


Figure 27: Observations of a contact binary by CRTS, folded by the period as detected by the lomb-scargle algorithm.

In Figure 27, we see survey data of a contact binary, after it has been folded by the orbital period. We see a coherent light-curve with a beautiful shape. This phase-folded light-curve is similar to what would be obtained in a night of observation by a single observer. A phase-folded light-curve constructed in way can be analyzed in the same manner as a light-curve taken in a single night of continuous observing.

Examples of such surveys are the All-Sky Automated Survey [ASAS, Pojmanski, 2000], Robotic Optical Transient Search Experiment [ROTSE, Akerlof et al., 2000], Trans-Atlantic Exoplanet Survey [TrES, Devor et al., 2008], Lincoln Near-Earth Asteroid Research program

[LINEAR, Palaversa et al., 2013], and Catalina Real-Time Transient Survey [CRTS, Drake et al., 2014b]. Researchers have also selected pure samples of contact binary systems from large survey data sets for study. Researchers have previously used data from the Optical Gravitational Lensing Experiment [OGLE, Rucinski, 1996], Super Wide Angle Search for Planets [SuperWASP, Norton et al., 2011], and CRTS [Drake et al., 2014a] to construct pure contact binary samples for study. Lee [2015] have used this approach to study a pure sample detached eclipsing binaries from the CRTS variable catalog.



Figure 28: Images of the instruments used in six modern surveys. In the top left, SuperWASP [SuperWASP, Norton et al., 2011], ASAS [ASAS, Pojmanski, 2000], [ROTSE, Akerlof et al., 2000],

5.1 Modern Sources of Survey Data

5.1.1 The Kepler Spacecraft

5.1.2 The Sloan Digital Sky Survey

York et al. [2000]

[Ivezić et al., 2007]

calibrations allow for stellar temperatures to be derived Fukugita et al. [2011]

SEGUE is a program that collects stellar spectra.

5.1.3 The SuperWASP Survey

follow-up on 1-meter telescopes in South Africa [Koen et al., 2016].

more follow up [Darwish et al., 2016]

6 Paper I: Characterization of 9,380 Contact Binaries from the CRTS Variable Sources Catalogue

This work was submitted to the Monthly Notices of the Royal Astronomical Society (MNRAS) on June 20th, 2016, and was accepted on August 19th, 2016.

Characterization of 9,380 Contact Binaries from the CRTS Variable Sources Catalogue

F. M. Marsh¹ , T. A. Prince,² A. A. Mahabal,² E. C. Bellm,² A. J. Drake,²
and S. G. Djorgovski²

¹ Department of Physics and Astronomy, Pomona College, Claremont, CA 91711, United States

² Astronomy Department, California Institute of Technology, Pasadena, CA 91126, United States

Accepted 2016 August 19. Received 2016 August 18. In original form 2016 June 20.

ABSTRACT

We construct a sample of 9,380 contact binaries (W UMa systems) by using the Catalina Real-Time Transient Survey Variables Sources Catalogue. By measuring brightness change rates, light-curve statistics, and temperatures for this sample, we improve the understanding of contact binary light-curve characteristics, and luminosity variability on decadal timescales. We show that binaries with convective outer envelopes have a different distribution of light curve amplitudes and magnitude differences between eclipse minima than binaries with radiative outer envelopes. We find that more than 2000 binaries exhibit a linear change in mean brightness over the eight-year timespan of observations with at least 3-sigma significance. We note that 25.9% of binaries with convective outer envelopes exhibit a significant change in brightness, while only 10.5% of radiative binaries exhibit a significant change in brightness. In 205 binaries (2.2%), we find that a sinusoid model better describes the luminosity trend within the 8-year observation timespan. For these binaries, we report the amplitudes and periods (as estimated using observed half-periods) of this sinusoidal brightness variation and discuss possible mechanisms driving the variation.

Key words: binaries: eclipsing – stars: magnetic field – surveys

1 INTRODUCTION

Since their first physical characterization in the late 1960’s ([Lucy 1968a,b](#)), great advancements have been made in the understanding of contact binary (or W UMa) systems. W UMa systems consist of two main-sequence stars that are so close to each other that they exchange mass and energy through a region of physical contact. Analysis of contact binary light-curves reveals that the systems exhibit Roche geometry, where a combination of gravitational and rotational forces combine to give contact systems their characteristic “peanut-like” shapes. These systems are interesting because they provide a unique opportunity to study phenomena such as stellar magnetic activity ([Applegate 1992](#)), angular momentum loss (AML, [Vilhu & Rahunen 1981](#)), and thermal relaxation oscillations (TRO, [Wang 1994](#)). A merger of a contact binary system has been observed in time-series photometric data ([Tylenda et al. 2011](#)), indicating that these systems can rapidly destabilize. Connections of stellar merger events to red novae and blue stragglers have been brought to light in recent literature ([Andronov](#)

[et al. 2006](#)). Studies of large numbers of contact systems can provide information about the mechanisms that cause brightness fluctuations and orbital period changes.

Before the 1990s, studies were limited to small numbers of contact systems because of technological constraints. The light-curves necessary for the comparison of different contact systems were time consuming to obtain by using single system photoelectric and CCD photometry, because it took an entire night of observing to obtain a light-curve of just one contact system. Still, carefully assembled samples of tens of contact systems with common characteristics allowed for comparative studies to be performed ([Davidge & Milone 1984](#); [O’Connell 1951](#); [Qian 2001](#)).

Since the late 1990s, photometric surveys that frequently observe large areas of the sky have come online. Through the careful classification of periodic variable sources in survey datasets, larger and larger samples of contact binary systems have been assembled, making studies of contact binaries as a population possible. Previous surveys have compiled variable star Catalogues which include many contact binary systems. Examples of such surveys are the All-Sky Automated Survey (ASAS, [Pojmanski 2000](#)),

* fmars@caltech.edu

Robotic Optical Transient Search Experiment (ROTSE, [Akerlof et al. 2000](#)), Trans-Atlantic Exoplanet Survey (TrES, [Devor et al. 2008](#)), Lincoln Near-Earth Asteroid Research program (LINEAR, [Palaversa et al. 2013](#)), and Catalina Real-Time Transient Survey (CRTS, [Drake et al. 2014a](#)). Researchers have also selected pure samples of contact binary systems from large survey data sets for study. Researchers have previously used data from the Optical Gravitational Lensing Experiment (OGLE, [Rucinski 1996](#)), Super Wide Angle Search for Planets (SuperWASP, [Norton et al. 2011](#)), and CRTS ([Drake et al. 2014b](#)) to construct pure contact binary samples for study. [Lee \(2015\)](#) have used this approach to study a pure sample detached eclipsing binaries from the CRTS Variable Sources Catalogue.

In this work, we perform photometric analysis on a large sample of contact binaries from the CRTS Variable Sources Catalogue, by using both Catalina Sky Survey and Sloan Digital Sky Survey data. Our aim is to learn how contact binary light-curve morphology changes with photospheric temperature, and to assess the luminosity variability of contact binaries on decadal timescales. We do not apply physical models to the contact binaries under study, but instead take a phenomenological approach.

In Section 2, we describe the SDSS and CRTS data that we use. In Section 3, we describe how we constructed our sample set from 30,743 contact binaries published in [Drake et al. \(2014a\)](#). In Section 4, we describe light-curve statistics calculated for the 13,551 binaries that were observed in both SDSS and CRTS data. We describe how the temperature was derived from SDSS colours, including de-reddening. We also describe how some systems were removed from our sample based on SDSS colour and harmonic fit characteristics. In Section 5, we search for variability in the luminosity of the candidates on a decadal timescale, and apply linear and sinusoidal fits to their mean brightness as a function of time. We also describe how some systems were removed from our sample to remove systematic errors in CRTS photometry. In Section 6, we discuss possible mechanisms responsible for the variability of the candidate systems on a decadal timescale. In Section 7, we summarize our findings and mention the types of future observations that can be used to learn more about contact binary systems.

2 OBSERVATIONS

In this study, we use data from two separate surveys: (1) We use CRTS data spanning eight years, which allows for the variation in the luminosity of each system on a decadal timescale to be measured, and (2) We use SDSS data which provides multiband photometric measurements taken within the timespan of a few minutes, allowing the temperature of each binary to be measured.

2.1 CRTS Photometry

The Catalina Sky Survey (CSS) uses three telescopes to survey the sky between declinations of -75 and +65 degrees. Although the CSS was originally designed for the detection of Near Earth Asteroids, the CRTS project aggregates time-series photometry for over 500 million stationary “background” sources ([Drake et al. 2009; Mahabal et al. 2011;](#)

[Djorgovski et al. 2011](#)). CRTS observations are taken in “white light”, i.e. without filters, to maximize survey depth. CRTS can perform photometric measurements on sources with visual magnitudes in the range of ~ 13 to 20. Though we only used eight years of data, CRTS continues collecting data to this day.

The CRTS photometry used in this work is publicly accessible through the Catalina Surveys Data Release 2 at [crtss.caltech.edu](#).

The number of observations that CSS has collected for the candidate systems that we study ranges from 90 (for the least observed systems) to 540 (for the most observed systems). The median number of CSS observations per candidate system is 336, with a standard deviation of 86 observations. The mean photometric error varies from 0.05 magnitudes to 0.10 magnitudes for most systems, increasing as a function of CRTS magnitude.

2.2 SDSS Photometry

The Sloan Digital Sky Survey provides multiband photometry in the u, g, r, i , and z bands. Because of its drift-scanning configuration, SDSS is well suited to performing photometry on short-period variable stars ($P < 1$ day), because all of the bands are exposed within a short time of each other: there is a delay of roughly 5 minutes between the exposure of the g and r images. ([York et al. 2000](#)). We use the SDSS DR10 ($g - r$) colour to calculate the temperature of the binary systems in this study ([Ahn et al. 2014](#)).

3 CANDIDATE SELECTION

The initial set of contact binaries from which we derived our sample was selected as described in [Drake et al. \(2014a\)](#). The CRTS photometry for this sample can be accessed publicly at <http://nesssi.cacr.caltech.edu/DataRelease/Varcat.html>.

The [Drake et al. \(2014a\)](#) sample was created by selecting data from the Catalina Surveys Data Release 1 (CSDR1), based on the criteria of high Stetson variability index (J_{WS}) and large standard deviation of brightness measurements (σ). Drake performed Lomb-Scargle periodogram analysis (LS, [Scargle 1982](#)) on these variables, testing for significant periods. Candidates that passed a LS significance cutoff along with additional data quality cuts were further processed to determine the best period and were then visually inspected. Approximately half of the inspected candidates passed selection and were classified by type (e.g. EW: contact binary, EA: Algol type, RRab: RR Lyrae, etc.) based on period, light-curve morphology, and colour information.

In the [Drake et al. \(2014a\)](#) sample there are 30,743 binaries classified as EW, corresponding to W UMa (contact) binaries. The SDSS photometry was crossmatched to the CRTS photometry by using the Large Survey Database framework (LSD, [Juric 2012](#)). We searched for SDSS point sources within 3" of the coordinates of the CRTS candidates, and when a one-to-one match existed, we correlated the photometry and added the candidate to our sample. When a unique match did not exist between the SDSS and CRTS photometry, we did not add the candidate to our sample. We chose the 3" search radius because CSS pixels subtend

2.5". Out of the 30,743 sources queried, there were 13,551 sources with matching CRTS and SDSS photometry. We will describe the parameters derived for each of these 13,551 binary candidates in Sections 4 and 5.

Drake et al. (2014a) have shown that 98.3% of the sources classified as contact binaries in CRTS data are also classified as contact binaries in the analysis of LINEAR data in Palaversa et al. (2013). They have also shown that many of the candidates have SDSS DR10 spectra consistent with known spectral characteristics of contact binaries. Because our contact binary sample is selected from the Drake subset, we expect that it will also have greater than 98% purity.

4 CALCULATION OF TEMPERATURE AND LIGHT CURVE STATISTICS

In this section, we describe the light-curve statistics for the sample. We also describe how the photospheric temperature was calculated from SDSS colours for the sample. Our aim is to discover how light-curves vary as a function of photospheric temperature.

4.1 Light-Curve Harmonic Fit

We used the period derived in Drake et al. (2014a) to phase-fold the photometry of every system. For every system, we performed a six harmonic (six sine terms, six cosine terms) fit of the phase-folded photometry, by using `gatspy` (Vanderplas 2015; VanderPlas & Ivezić 2015). We chose to use six terms in our model because it provides a balance between flexibility to fit complex light-curve shapes and robustness with sparse data. A model with more than six terms performed better at characterizing well sampled light-curves than models with fewer terms. A six-term model, however, was more likely than a model with fewer terms to produce a non-physical shape when the input light-curve was sparsely sampled, or sampled unevenly in phase. At best, the harmonic fit is a good approximation of the true continuous light-curve shape, but sometimes this was not the case. When the range of phases is sparsely or unevenly sampled, the fit is poorly constrained, and often exhibits more than two local maxima and more than two local minima, which is not expected in a physical system with Roche geometry (Lucy 1968b). This also occurs if the variation due to an eclipse has an amplitude comparable to the photometric error.

4.1.1 Harmonic Fit Filters

If the six-term harmonic fit had more than two local maxima and two local minima, we eliminated the system from the sample, because physical eclipsing binary light-curves should only have two maxima and two minima (like the light-curve in Fig. 2). Other than this criterion, we did not place any constraints on the goodness of fit. This filter eliminated 3,062 of the 13,551 systems in the original sample (22.6%), thereby reducing the sample to 10,488 systems.

We compared the distributions of variability amplitude, and mean CSS magnitude (V_{CSS}) for the 3,062 systems rejected by the harmonic fit filters to the distributions for the 10,488 systems that passed through the filter. In the top

panel of Figure 1, we see that systems with low variability amplitude (< 0.3 magnitudes) are more common among the 3,062 rejected systems. The harmonic fit filter preferentially rejects bright systems, ($V_{CSS} < 13.5$), and faint systems ($V_{CSS} > 17.0$).

A system is likely to be rejected when the variability amplitude is comparable to the photometric errors on individual measurements. Thus, low amplitude systems, and faint systems (which have large photometric errors) are preferentially rejected by the filter. The preferential rejection of the brightest systems is due to additional light-curve scatter introduced by saturation effects in the CRTS photometry.

It is known that the system geometrical element that most strongly affects contact binary light-curve amplitude is the orbital inclination (Ruciński 1993). It has been shown that orbital inclination can be predicted with a precision of $\pm 3^\circ$ based on light-curve data alone (Zeraatgar et al. 2015). Therefore, preferentially rejecting low-amplitude systems will preferentially reject highly inclined systems which only partially eclipse. Since inclination is not a property that is intrinsic to the contact binary system, this is not expected to introduce a physical bias into our sample.

The rejection of faint systems preferentially rejects systems that are intrinsically dim, and distant. The rejection of bright systems preferentially rejects systems that are intrinsically more luminous and close. In the bottom panel of Figure 1, we see that systems at both extremes in brightness are rejected by the filter, but more faint systems are rejected than bright systems. This is expected to bias our sample towards more luminous, hotter, more massive contact binaries with longer orbital periods. We note that the initial sample (like all magnitude-limited samples) is biased towards more luminous contact binaries.

We have not attempted to characterize an unbiased population of contact binaries in this work. A complete and unbiased sample of contact binaries is not a requirement for the analysis performed in this work.

4.2 Derived Light-Curve Parameters

For each system in the sample of 10,488, we performed 1,000 harmonic fits on Monte Carlo simulated datasets. Each new simulated photometric measurement was drawn from a normal distribution generated by using the original value of the measurement as the mean, and the reported error as the standard deviation. We sampled these 1000 new harmonic fits at 10,000 uniformly spaced points across their phase, and computed the standard deviation of the fits for each point in phase. This was taken to be the standard error at each point in phase on the harmonic fit (Fig. 3). We then retrieved the magnitude and phase of the relative extrema on the harmonic fits, corresponding to the minima and maxima of the eclipses.

The three light-curve parameters (Fig. 2) that we derive in this analysis are amplitude (Amp), magnitude difference between eclipse minima (ΔMin), and magnitude difference between out-of-eclipse maxima (ΔMax). We define these three parameters to be positive.

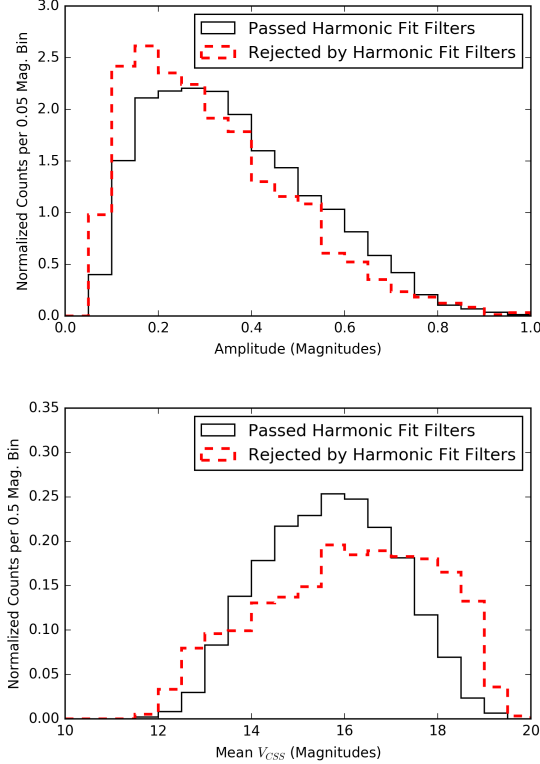


Figure 1. Normalized histograms of variability amplitude (top panel), and mean CSS magnitude V_{CSS} (bottom panel), for systems retained (black, solid line), and rejected (red, dashed line) by the harmonic fit filters. Systems with low variability amplitude are preferentially rejected by the filters. Systems with mean V_{CSS} magnitudes of less than 13.5 (the brightest systems) and mean V_{CSS} of greater than 17 (the faintest systems) are preferentially rejected by the filter.

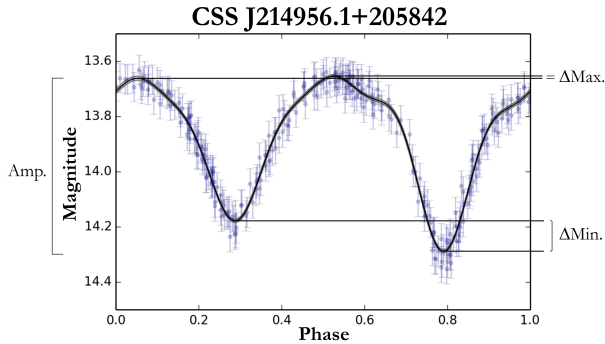


Figure 2. A graphical depiction of the light-curve parameters. Note that $\Delta_{\text{Max.}}$ is the very small difference between out-of-eclipse maxima.

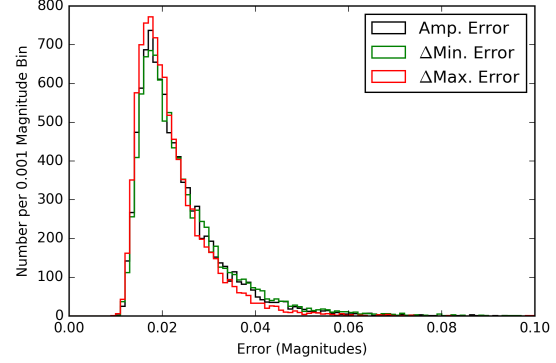


Figure 3. The distribution of errors for the parameters derived from the six-term harmonic fit. A characteristic error for Amp, $\Delta_{\text{Min.}}$, and $\Delta_{\text{Max.}}$ is 0.02 magnitudes.

4.3 Effective Temperature

The contact binaries in our sample tended to be further away than those in previous surveys because the contact binaries in our sample were fainter on average than those in previous surveys ($\sim 13 < V_{CSS} < 20$) and have a limited range ($2 \lesssim M_V \lesssim 7$) of absolute magnitudes (Rucinski & Duerbeck 1997). Consequently, extra care had to be taken with the de-reddening of the SDSS colours.

The recently released 3D dust map derived from Pan-STARRS1 data by Green et al. (2015) has increased the accuracy with which extinction can be calculated, because the extinction is estimated as a function of direction *and* distance. If a way exists to roughly determine the distance to a contact binary system by using a method not affected by extinction, we can use the 3D dust map to compute the extinction along the line of sight to the estimated distance, and thereby retrieve a more accurate temperature measurement than is possible with a 2D dust map and galactic latitude correction.

There is a well-known relationship between the period, colour, and absolute magnitude of contact binary systems. Even without colour information, the absolute magnitude of a contact binary system can be calculated based solely upon its period, with a standard error of 0.3 magnitudes. Rucinski (2006) performed a calibration by using the maximum brightness of 21 contact binary systems with $P < 0.56$ days using Hipparcos data and obtained:

$$M_V = -1.5 - 12 \log P \quad (1)$$

where P is the period in days. This relationship tends to underestimate the absolute magnitude (overestimate the brightness) of systems with $P > 0.56$ days, by about 0.75 absolute magnitudes. As a result, temperatures will be overestimated for hotter systems. Even with this calibration inaccuracy, the 3D dust map method affords better accuracy than the 2D dust map method, which doesn't take distance into account at all.

To calculate $(V - M_V)$, we used Eqn. 1 and the visual magnitude (V) computed from SDSS g and r magnitudes via the empirical relationship $V = g - 0.59 * (g - r) - 0.01$

(Jester et al. 2005). The SDSS g and r measurements used to initially estimate the V band magnitude are not corrected for extinction. The difference $(V - M_V)$ is caused by the dimming due to distance, and the extinction due to reddening. Adopting a ratio of total-to-selective extinction of 3.1, the extinction in the V band A_V can be expressed as:

$$A_V = 3.1 * E(B - V) \quad (2)$$

where $E(B - V)$ is the $(B - V)$ reddening. The Green et al. (2015) dust map allows $E(B - V)$ to be calculated as a function of distance modulus, i.e. $E(B - V) = f(D)$. For each system, we can find a distance modulus such that the sum of the distance modulus and V band extinction A_V at that distance modulus is equal to $(V - M_V)$, because A_V is known as a function of distance modulus. In this way, we can find both the extinction and the distance to the system. We find that 90% of the systems had a B-V reddening, $E(B - V)$, of less than 0.20 magnitudes. The median error in $E(B - V)$ was 0.03 magnitudes.

After the best fit of the distance modulus and $E(B - V)$ was calculated, we were able to calculate the extinction in each of the SDSS $ugriz$ bands using the relationships published in Schlafly & Finkbeiner (2011). We converted $E(B - V)$ to extinctions in each SDSS band. The median extinction in the SDSS g band was 0.11 magnitudes and the median extinction in the SDSS r band was 0.08 magnitudes. Approximately 90% of the candidates had a SDSS g band extinction of less than 0.5 magnitudes. Approximately 90% of the candidates had a SDSS r band extinction of less than 0.3 magnitudes. The median error in the g extinction was 0.10 magnitudes and the median error in the r extinction was 0.07 magnitudes.

We then used an empirical relation (calibrated for main sequence stars) from Fukugita et al. (2011) to calculate the photospheric temperature of the contact binaries.

$$T_{\text{eff}}/10^4 K = \frac{1.09}{(g - r) + 1.47} \quad (3)$$

Temperature calculated from $(g - r)$ colour in this manner carries an uncertainty of 93K in the empirically verified range of 3850 to 8000K, which was added in quadrature to the effects of SDSS photometric error and reddening uncertainties. Over 99% of the systems in the sample lie within the empirically verified range.

We note that SDSS provides a temperature measurement at only one phase of the contact binary rotation. The two component stars of a binary system in true contact have temperatures that are within ~ 100 K of each other. However, this assumption breaks down for semi-detached systems with longer orbital periods.

The uncertainty in the SDSS temperature measurement was computed by adding the provided photometric uncertainties, the reddening uncertainties, and the Fukugita et al. (2011) temperature calibration in quadrature. The resulting mean error in the temperature determination was 324K, with a standard deviation of 153K. Systems with lower mean magnitudes tended to have a slightly higher error in the SDSS temperature determination. This is because brighter contact binaries are hotter, and hotter binaries tend to have larger temperature errors (because a component of the error is proportional to the temperature).

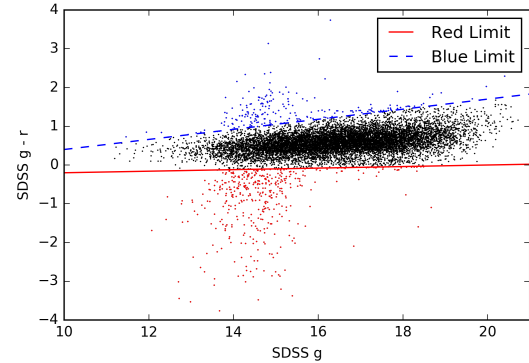


Figure 4. The distribution of the sample in SDSS $(g - r)$ vs. g colour space, dashed lines show the red and blue limits imposed upon the data. These limits were imposed to eliminate systems with evidence of saturated SDSS photometry. Points in red and blue show the systems rejected by the respective limits. 661 out of the 10,488 systems plotted were eliminated.

4.3.1 Colour Limits

Some of the 10,488 system remaining after the harmonic fit filters (Section 4.1.1) exhibited colours that are outside the range expected for contact binary systems. The likely cause of this discrepancy is that much of the SDSS g band photometry is saturated for $g < 15$. Systems with saturated photometry were eliminated by choosing a colour cutoff (Fig. 4). We selected both blue and red limits in SDSS $(g - r)$ as a function of SDSS g . Candidates were selected such that

$$\begin{aligned} (g - r) &> 0.02 * g - 0.4 \quad (\text{Red Limit}) \\ (g - r) &< 0.13 * g - 0.9 \quad (\text{Blue Limit}) \end{aligned} \quad (4)$$

The $(g - r)$ colour derived from SDSS photometry has the largest standard deviation in the SDSS g magnitude range of $\approx 13 - 15$. Outside of this magnitude range, the systems exhibited a sharp cutoff in $(g - r)$ colour as a function of temperature. On each end of the distribution, a line was fit by eye to the cutoff in the magnitude ranges of 16 to 20, which was the source of the red and blue limits. Of the 10,488 binaries in the sample remaining after the first filter, this eliminated 661, for a new total of 9,827 systems.

4.4 Light-Curve Shape and Temperature

For each of the 9,827 light curves that passed the colour filters (as described in Section 4.3.1), we calculate the amplitude (Amp), difference between eclipse minima (ΔMin) and the difference between out-of-eclipse maxima (ΔMax). To generate the plots in this section, we have also filtered out 447 systems that do not pass a criterion described in Section 5.1.1. This is so that the results presented in this section can be compared with those presented in Section 5, (Fig. 5).

The distributions of each of these derived light-curve parameters changes with the effective temperature of the binary system. We find that at certain critical temperatures, many of the characteristics of the systems change.

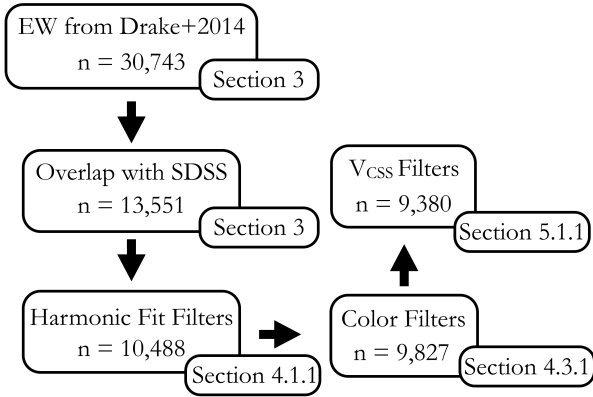


Figure 5. A flowchart describing each of the filters applied to the sample. The type of filter is at the top of each box, while the sample size after applying that filter is at the bottom. The section where each filter is described is at the bottom right of each box.

We discover that the photospheric temperature of 6200K divides the binaries in multiple parameter distributions (e.g. Figs. 6, 7, and 9), and this temperature is important physically. The mode of energy transport at the photosphere changes at the temperature of 6200K (pp. 212, Kippenhahn et al. 1990). Main sequence stars with temperatures cooler than 6200K have a convective outer envelope, while stars hotter than 6200K are radiative at the surface. We will refer to the binary systems hotter than 6200K as “radiative” and systems cooler than 6200K as “convective”, for short. In our final sample there are 1,381 radiative systems and 7,999 convective systems.

Both the system geometry and the inclination of the orbit relative to the earth’s line of sight affect the amplitude of a contact binary light-curve. We find that the amplitude distribution of the binaries changes dramatically as a function of temperature, convective systems having larger amplitudes (Fig. 6).

The temperatures of the two component stars in a contact binary system affect the magnitude difference between eclipse minima in a contact binary light-curve. A temperature difference between the primary and secondary components is the cause of a non-zero ΔMin . We find that the ΔMin distribution changes significantly as a function of temperature (Fig. 7). Radiative systems typically have larger ΔMin than convective systems.

Our data show the well known period-colour relation (Fig. 9) for contact binaries (Rubenstein 2001). We note that the binaries that are cooler than most other binaries with the same orbital period tend to have larger ΔMin / Amp than binaries that are in the middle of the period-colour relation. The component stars of a system with a longer orbital period than that of the majority of binaries with similar temperatures are separated by a larger distance, in accordance with Kepler’s Laws. A larger physical separation between the component stars reduces the likelihood that they are in thermal equilibrium. We expect to see a significant ΔMin in systems where the two components are not in thermal equilibrium.

The difference in out-of-eclipse maxima is affected by

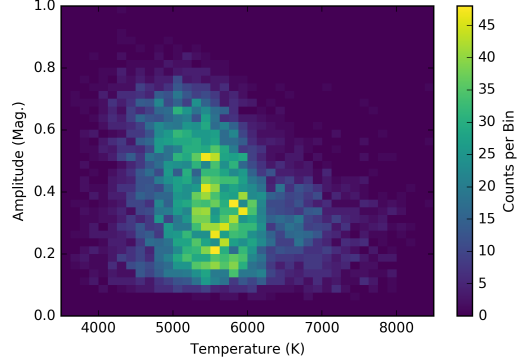


Figure 6. A 2D histogram of amplitude and temperature for the sample. Systems with effective temperatures greater than 6200K generally do not have amplitudes greater than ≈ 0.5 magnitudes, while systems with effective temperatures lower than 6200K do not have amplitudes greater than ≈ 0.8 magnitudes. The mean amplitude of the systems cooler than 6200K is 0.40, with a standard deviation of 0.18. The mean amplitude of the systems hotter than 6200K is 0.30, with a standard deviation of 0.12.

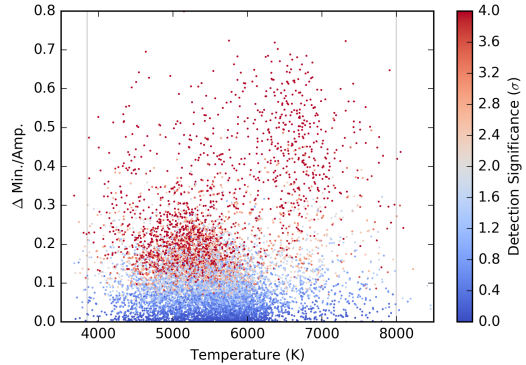


Figure 7. The amplitude-normalized ΔMin plotted against temperature. We normalize by amplitude to control for inclination effects. The color axis describes the significance of the ΔMin measurement. ΔMin measurements that are significant at the greater than 2σ level are plotted as red points. Systems with effective temperatures greater than 6200K can have much larger ΔMin than systems cooler than 6200K.

an asymmetry in the contact binary system (Fig. 8). A contact binary system exhibiting a significant ΔMax is said to exhibit the O’Connell Effect (O’Connell 1951). This effect is theorized to be caused by starspots, asymmetric gas impact (Kallrath & Milone 1999), asymmetric distribution of circumbinary matter (Liu & Yang 2003), or Coriolis heating (Zhou & Leung 1990) of the binary’s photosphere. We find that 8,862 systems in the sample (94.5% of the sample) do not have ΔMax detectable at greater than 2σ significance. We observe that 107 systems (1.1% of the sample) exhibit a ΔMax significant at 3σ . Drake et al. (2014a) have observed the stability of the O’Connell effect over the 8-year times-

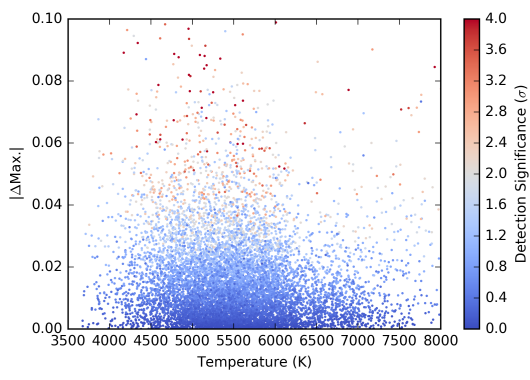


Figure 8. The magnitude difference between eclipse maxima plotted against temperature. The color axis describes the significance of the Δ_{Max} measurement. The vast majority of the systems in the sample do not have a Δ_{Max} detectable at greater than 2σ . For light-curve parameters, the typical 2σ error is 0.04 magnitudes.

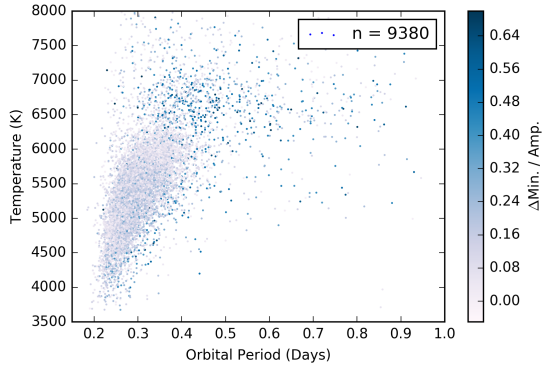


Figure 9. The orbital period and temperature of each contact binary system. Δ_{Min} normalized to the eclipse amplitude (Amp.) is on the colour axis. We have normalized Δ_{Min} to Amp. to control for inclination effects. Note that radiative binaries ($T > 6200\text{K}$) tend to have larger differences between eclipse minima.

pan of CRTS observations in this same sample, providing evidence against the theory that starspots are the cause of the effect. This is because starspots can be observed to appear and disappear during the 8-year timespan of CRTS observations (Fig. 14). It is likely that the cause of O’Connell effect varies from binary to binary. Wilsey & Beaky (2009) is a review of the possible causes of the O’Connell effect.

5 SEARCH FOR LUMINOSITY CHANGES ON A DECADAL TIMESCALE

5.1 Linear Brightness Parameter

Changes in the mean magnitude of contact binary systems over timescales of years have previously been attributed to changes in the mean photospheric temperature or mean

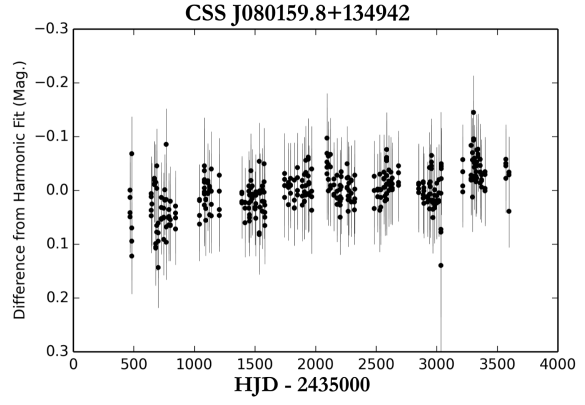


Figure 10. The harmonic fit residuals (and 1σ error bars) plotted as a function of time for a system with increasing brightness (top), and for a system with decreasing brightness (bottom) over the 8-year time baseline of CRTS observations. Top panel: CSS_J080159.8+134942, orbital period = 0.35 days. Bottom panel: CSS_J012302.7+253713, orbital period = 0.28 days.

starspot coverage fraction (Kaszás et al. 1998). To detect luminosity variability on a decadal timescale, we subtracted the harmonic fit from all of the observations and performed a linear fit on the residuals as a function of time. The six-term harmonic fit effectively eliminated the short term variability due to the eclipses. When a single harmonic fit is performed on observations with changing mean brightness over the 8-year timespan of observations, the residuals are minimized for observations in the middle of the time baseline, but the fit is poor for observations at the beginning and end of the time baseline (Fig. 10). We re-fit 1000 Monte Carlo resamplings of the harmonic fit residuals to perform the linear fit error computation (Fig. 11).

5.1.1 Mean Magnitude Filters

In CRTS data we find that a systematic error is present in the magnitude derivative calculation. In 2005 and 2006 (the first two years of data in CSDR2), the mean magnitude derivative (\dot{V}_{CSS}) is positive, instead of being close to zero. In the first two years of photometry, a larger photometric aperture was used for the brighter stars in the sample. Light

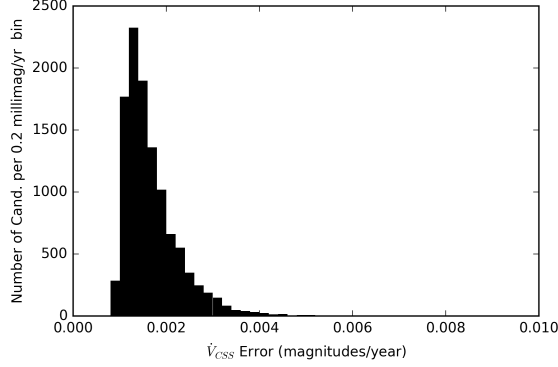


Figure 11. Histogram of the estimated error in the magnitude derivative \dot{V}_{CSS} , if a linear model is assumed. A characteristic error in (\dot{V}_{CSS}) is 0.018 magnitudes per year.

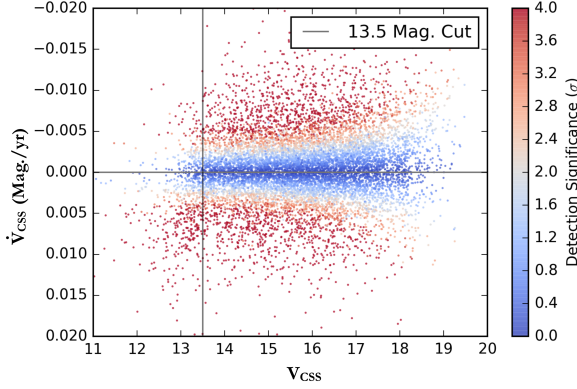


Figure 12. The magnitude derivative (\dot{V}_{CSS}) of the systems in the sample during the 8-year observation time period, plotted as a function of CRTS mean magnitude V_{CSS} . The color axis describes the significance of the \dot{V}_{CSS} measurement. For systems brighter than magnitude ≈ 13.5 , the distribution of magnitude derivatives is not symmetric around zero, due to changes in the photometric aperture for bright systems. A vertical line is plotted at magnitude 13.5 illustrating the cutoff that we imposed on the data.

from additional stars within the aperture added to the calculated flux. When the aperture size was changed in 2006, the light from the additional stars was lost, resulting in an apparent decrease in brightness. This introduces a systematic error when calculating the trend in brightness over time (Fig. 12).

To eliminate this systematic error, we rejected all candidates with a mean V_{CSS} of less than 13.5. This ensures that the distribution of magnitude derivatives is symmetric around zero. This filter eliminated 447 systems from the sample of 9,827 remaining after the first two filters, to produce the final number of 9,380 systems. All of the analysis in Sections 4, and 5 is based on this final sample of 9,380. As was previously mentioned, all of the plots in Section 4.4 were generated using the final sample of 9,380.

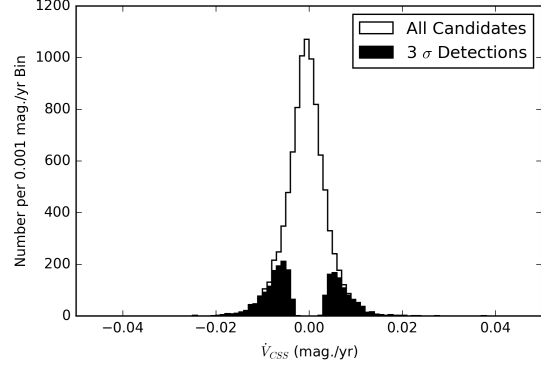


Figure 13. Histogram of the magnitude derivative (\dot{V}_{CSS}) in CRTS data. The histogram 3σ detections are plotted in black. Of the 9,380 systems in the sample, 2,219 (23.7%) had linear magnitude changes that were significant at 3σ .

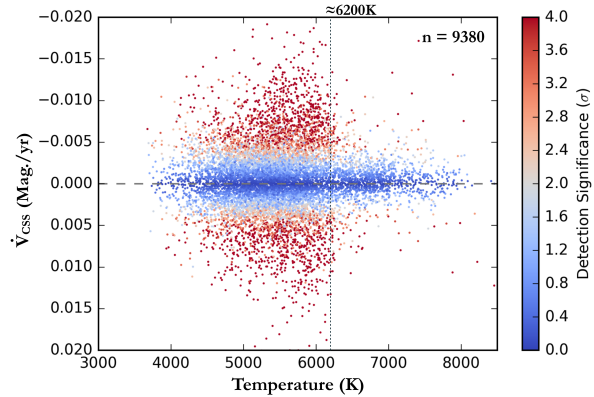


Figure 14. The magnitude derivative (\dot{V}_{CSS}) of the systems plotted against their effective temperatures. The color axis describes the significance of the \dot{V}_{CSS} measurement. Systems with effective temperatures greater than ≈ 6200 K do not generally exhibit significant changes in their magnitude. A dashed vertical line indicates the temperature of 6200K

5.2 Linear Brightness Parameter and Temperature

As described in Section 5.1, we fit a line to the residuals of the six term harmonic fit as a function of time, and assessed the significance of the measured slope (the magnitude derivative). For a 3σ detection, the probability of the observed data given the null hypothesis of constant magnitude has to be less than $1 - 0.997 = 0.003$. We detected 3σ significant magnitude derivatives in 2,219 systems (23.7% of the sample). The distribution of magnitude derivatives is symmetric about zero, as ensured by the mean magnitude filter described in Section 5.1.1. We discover that some systems have magnitude derivatives as large as 0.02 magnitudes per year.

The photospheric temperature of 6200K separates two distributions of magnitude derivatives. Only 10.5% of the

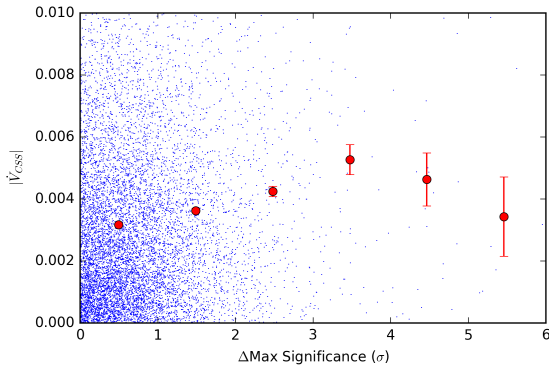


Figure 15. The absolute value of the magnitude derivative $|\dot{V}_{CSS}|$ plotted against the significance of the O’Connell effect. The mean and standard error of the mean are computed in 1σ wide bins, and graphically represented as red points with error-bars. The mean of $|\dot{V}_{CSS}|$ in the $\Delta\text{Max}(\sigma) = 3$ to 4 bin is ≈ 0.0053 mag/yr, while the mean in the $\Delta\text{Max}(\sigma) = 0$ to 1 bin is ≈ 0.0032 mag/yr. This difference suggests that systems with a large O’Connell effect are more likely to have a variable luminosity on decadal timescales.

1,381 systems with effective temperatures of greater than 6200K exhibit brightness changes significant at 3σ , while 25.9% of the 7,999 systems with effective temperatures of less than 6200K exhibit 3σ significant brightness changes.

To determine if the luminosity of systems with a large ΔMax (equivalently, systems with a large O’Connell effect) are more likely to vary on a decadal timescale, we calculated the mean the $|\dot{V}_{CSS}|$ distribution as a function of ΔMax detection significance (σ) in six discrete bins (Fig. 15). Since the distribution of \dot{V}_{CSS} is symmetric about zero, the mean of the absolute value of the distribution is a good way to measure the level of variability. We find that the mean of the $|\dot{V}_{CSS}|$ distribution increases smoothly with ΔMax significance (σ), until the number of systems in each bin is too small to produce reliable statistics. The mean of the $|\dot{V}_{CSS}|$ distribution in the $\Delta\text{Max}(\sigma) = 3$ to 4 bin is 1.7 times the mean in the $\Delta\text{Max}(\sigma) = 0$ to 1 bin.

We made an effort to see if the brightness of the systems varied at some orbital phases more than at others. By visually examining the phase-folded light-curves of about 20 binaries that exhibited brightness changes significant at 3σ , it appears that variable binaries vary at all orbital phases. We observed that some of these light-curves varied more on one half of the orbital phase than the other. In this work, we will not comment further on the phase variance of the brightness fluctuations.

5.3 Sinusoidal Brightness Parameters

We find that for some candidates, the trend in harmonic fit residuals as a function of time is not well described by a linear model. While many systems (like those in Fig. 10) exhibit a monotonic increase or decrease in brightness over the 8-year CRTS time baseline, many others exhibit one or two points of inflection, where the brightness trend reverses in direction (Fig. 16).

In some cases, the trend in the harmonic fit residuals as a function of time appear to be well described by a sinusoid model. This was especially true for systems whose trends have two points of inflection. In order to quantify the number of systems that exhibited sinusoidal trends in brightness over a decadal timescale, we performed LS periodogram analysis on all of the harmonic fit residuals as a function of time.

We cannot say definitively if the luminosity variation of these systems is truly periodic, because in each case, our observations do not capture multiple “cycles” of the variation. If the variation proves to be truly periodic, we can estimate the period and amplitude of this variation based on observed half-periods. The following analysis assumes that a sinusoid model describes the luminosity variation over time periods longer than the time period of observation. While there are physical reasons to expect that this should be the case (discussed in Section 6), we cannot prove that the luminosity variation is periodic by using CRTS data alone.

The sampling of the CRTS survey and its limited time baseline place limits on the range of luminosity variation periods that we can search. All of the systems are randomly, but uniformly sampled in time, except for gaps that occur every year when the system is only above the horizon in the day and is therefore unobservable by the CSS. This leaves a strong signature in the periodogram of any CSS source (with peaks corresponding to periods of 1 and 2 years), and thus periodic signals shorter than roughly two years (we chose the cutoff of 800 days) were unable to be measured. The total time baseline of the CRTS survey up to Catalina Surveys Data Release 2 is about 8 years. Because at least half of a period must be observed to see an inflection point, the 8-year time baseline sets an upper limit on the longest periods detectable. We chose to filter out all systems with periods of brightness variation that were longer than 11 years.

A system had to pass several tests to be marked as sinusoidally variable:

1. The period of the long term luminosity variation as determined by a LS periodogram must be greater than 800 days but less than 4000 days.
2. The sinusoid model must have a Bayesian information criterion (BIC) of greater than 15, indicating strong evidence for the sinusoid model as compared to the null hypothesis of constant system brightness (Schwarz et al. 1978).
3. The peak LS power must be 5 times the 3-sigma power as predicted by 1000 Monte Carlo resamplings - this ensures that only systems with amplitudes large compared to the variation caused by photometric errors alone are considered (VanderPlas et al. 2014).

If a system passed these three tests, a sinusoid model with a period (in years) and an amplitude (in magnitudes) was fit to the harmonic fit residuals as a function of time (Fig. 16).

205 systems in the 9,380 binary sample exhibited oscillating brightness variations as discovered by the LS analysis described in Section 5.3. A sinusoid model was fit to the brightness variations with two parameters: (1) period (in years) and (2) amplitude (in magnitudes). We did not compute errors for the parameters of the sinusoid model. From a visual inspection of the LS periodograms, the lower limit

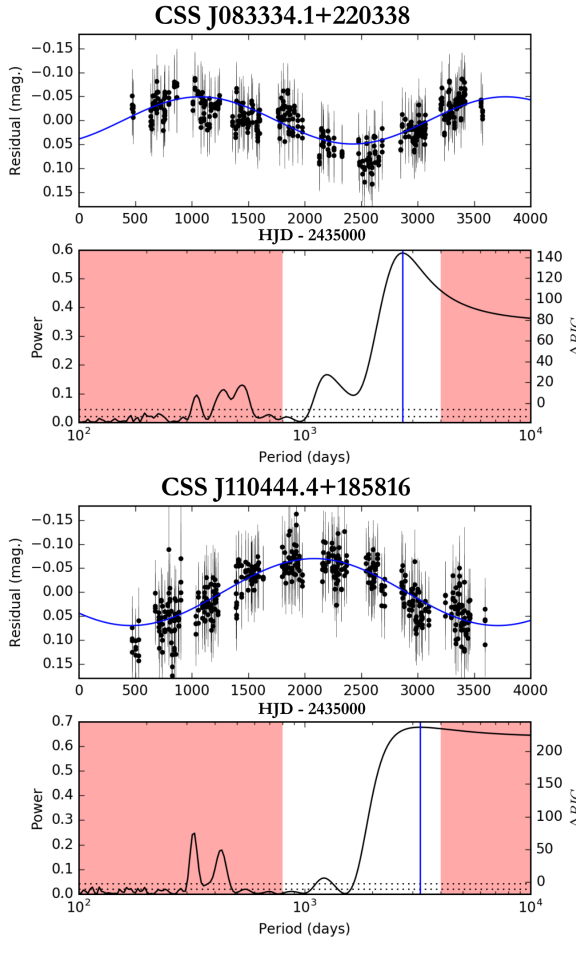


Figure 16. Examples of binaries with evidence of sinusoidal variation in luminosity. This figure shows the luminosity trend of the system after the variation due to eclipsing has been subtracted. The harmonic fit residuals are plotted in the top panel of each plot. One-sigma error bars are plotted for each harmonic fit residual. A Lomb-Scargle periodogram of the residuals is shown in the bottom panel of each plot. The red regions are periods for which the periodogram is influenced by aliases caused by the sampling pattern of the survey. The two dashed lines near the bottom of the Lomb-Scargle plots are the 1σ and 3σ significance levels for the periodogram, as computed by Monte Carlo resampling. Top panel: CSS_J110444.4+185816, orbital period = 0.32 days. Bottom panel: CSS_J083334.1+220338, orbital period = 0.31 days.

on the error in the period determination can be estimated to be 2 to 3 years. From a visual inspection of the residuals, we can say that the amplitude is only known to a 30% to 40% level, at best. These errors, though large, will not affect the very broad conclusions that we are able to draw from this analysis.

From the difference in magnitude between the system at maximum brightness and the system at minimum brightness, we were able to calculate the difference between the maximum and minimum luminosities (Fig. 17). By assum-

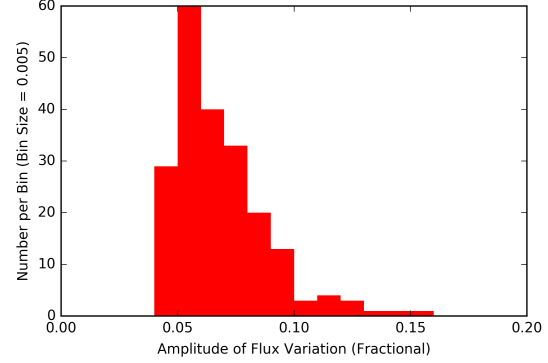


Figure 17. A histogram of the fractional flux (equivalently, the fractional luminosity) variation for the 205 binaries in the sinusoid sample. For a given source, the amplitude errors are at least 30%, as discussed in Section 5.3.

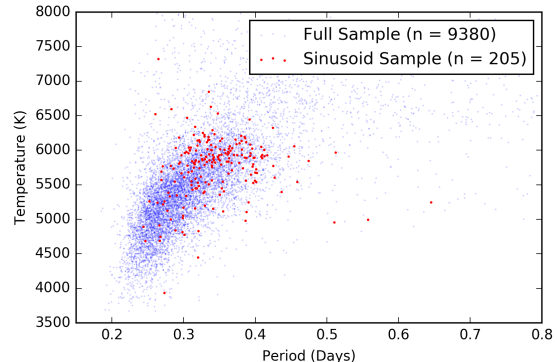


Figure 18. The orbital period and temperature of the 9,380 systems in the total sample, and the period and temperature of the 205 systems that exhibit significant sinusoidal variation in their brightness detectable on a decadal timescale. Systems in the sinusoid sample tend to have higher temperatures and longer periods than systems in the remaining sample.

ing that the binaries radiate isotropically, we can calculate the fractional luminosity variance:

$$\frac{|\Delta L|}{L} = \frac{|\Delta F|}{F} = \frac{F_{\max} - F_{\min}}{\bar{F}} \quad (5)$$

In general, we observe luminosity variability at the 4% level (the lower limit of detection) to the 16% level. We can state that 2.2% of the contact binaries in the whole sample have luminosities that vary by more than 4% on a decadal timescale, making this a rare phenomenon. If the variable binaries are assumed to be isotropically radiating perfect blackbodies of constant shape and size, then a fluctuation of the mean photospheric temperature with peak to trough amplitudes ranging from 50K to 150K can explain the observed flux variations.

We note that binaries with temperatures ranging from 5600K to 6300K are more likely to exhibit periodic lumi-

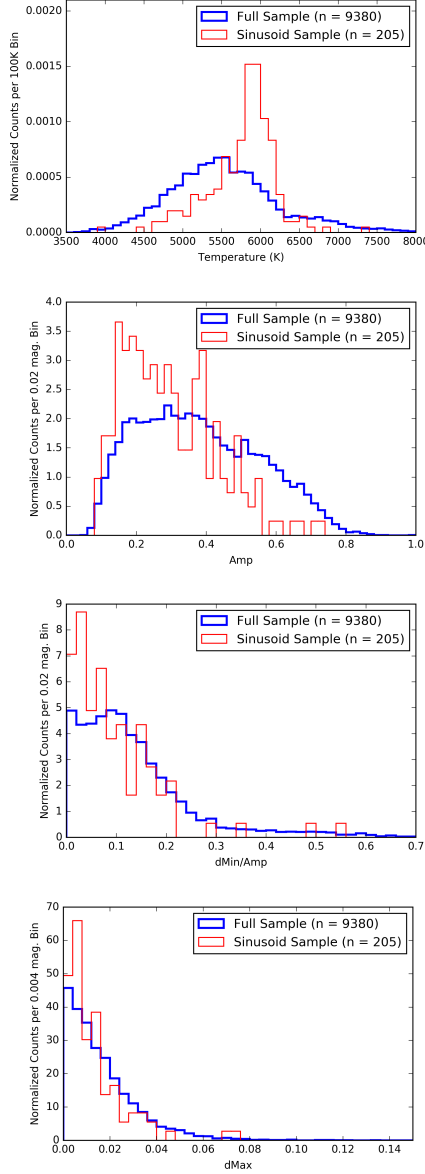


Figure 19. Normalized histograms of the temperature, Amp, dMin, dMax, distribution of systems in the whole sample, and systems in the sinusoid sample showing the overabundance of variable systems in the 5600K to 6300K temperature range. Systems in the sinusoid sample have a lower mean Amp, and lower dMin/Amp as compared to systems in the full sample of 9,380.

nosity variation (above the 4% level, with a period of less than 11 years) than binaries outside that temperature range. Very few binaries hotter than 6300K exhibit this luminosity variation, leading us to speculate that convective activity is responsible for driving the luminosity variation (Figs. 18, 19).

In general, systems with photospheric temperatures of less than $\approx 4500\text{K}$ did not exhibit significant luminosity variation with periods of less than 11 years. There are two possible explanations: (1) Binaries with temperatures of less

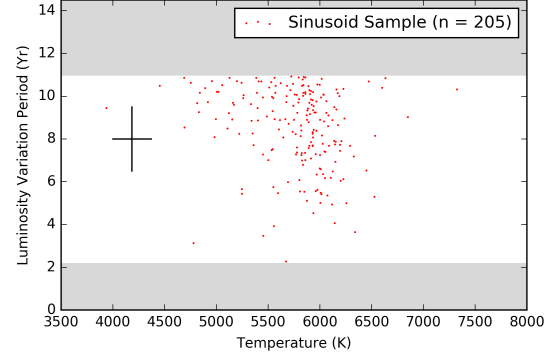


Figure 20. The temperature and luminosity variation period of the 205 systems in the sinusoidal sample. In grey are periods that are not detectable in our analysis. Periods shorter than two years are not detectable due to the annual gaps in sampling due to solar conjunction. A representative error bar is included in black.

than $\approx 4500\text{K}$ could have luminosity variation periods that are longer than 11 year window or, (2) binaries with temperatures of less than $\approx 4500\text{K}$ could luminosity variation with amplitudes of less than 4%.

Binaries in the sinusoid sample have a lower mean light-curve amplitude (Amp.) than binaries in the full sample of 9,380 (Fig. 19). This could be a selection effect: Binaries with low amplitudes were better fit by the six-term sinusoid model, resulting in smaller errors in the fit residuals. This allowed systems with smaller decadal luminosity variations to pass through the filters as described earlier in Section 5.3. The light-curve amplitude of a contact binary is affected strongly by its orbital inclination with respect to the observer, a property not intrinsic to the binary. Thus, it is unlikely that the difference in the light-curve amplitude distribution has a physical cause.

We searched for a relationship between the photospheric temperature of the binary and the period of the luminosity variation for the 205 binaries in the sinusoid sample (Fig. 20). Given the large errors, there is no clear relationship in the data, except for the slight suggestion that hotter convective binaries (with temperatures closer to 6200K) exhibit a wide range of luminosity variation periods and are capable of having shorter luminosity variation periods than cooler convective binaries.

We found that four binaries in the sinusoid sample had photospheric temperatures greater than 6200K at greater than 1σ significance. We examined the SDSS imagery manually for these four binaries. Three out of these four binaries had another star of similar brightness within 5''. It is possible that the varying brightness of the nearby source is causing the binary to be marked as sinusoidally variable. Another explanation is that an error in the de-reddening procedure could have caused a large error in the temperature measurement - causing an overestimate of the temperature of the star. If the variation is intrinsic to the star and our temperature estimate is accurate, a non-convective mechanism must be causing the luminosity variation in these cases.

6 DISCUSSION

In this section we discuss two possible theories that can explain the decadal luminosity changes observed in 2,219 binary systems (23.7% of the 9,380), with a particular focus on explaining the sinusoidal luminosity variation detected in 205 binary systems (2.2% of the 9,380).

6.1 The Applegate Mechanism

[Applegate \(1992\)](#) has suggested that orbital period modulations of amplitude $\Delta P/P \approx 10^{-5}$ can be explained by the gravitational coupling of the orbit to variations in the shape of a magnetically active star in the system. Applegate has predicted that the active star be variable at the $\Delta L/L \approx 0.1$ level, the period of this variability matching the period of the orbital period modulation. This luminosity variation should be entirely caused by a temperature variation since large changes in the radius of the star are ruled out by energetics. Under Applegate's model, the period of the luminosity variation is the same as the period of the magnetic activity cycle of the magnetically active star in the system. A detailed discussion of magnetically driven period changes can be found in [Lanza \(2006\)](#).

We detected luminosity variation at the $0.04 \leq (\Delta L/L) \leq 0.16$ level in 205 contact binaries. While the period of the luminosity variation is poorly constrained in our data, based on observed half periods we can speculate that these 205 binaries have luminosity variation periods ranging from 4 to 11 years, similar to the solar magnetic activity cycle period of 11 years. We estimate that fluctuations of the mean photospheric temperature with amplitudes in the range of 50 to 150K can explain the observed flux variations for the binaries in our sample. The vast majority of the variable binaries have photospheric temperatures of less than $\approx 6200\text{K}$, indicating that the mode of energy transport near their surfaces is convective. We do not detect decadal variability above the $(\Delta L/L) > 0.04$ level in binaries cooler than $\approx 4500\text{K}$.

The observed behaviour in these 205 contact binaries matches the predictions made by Applegate's theory. If the Applegate mechanism is indeed responsible for the luminosity variation, this study would add to the evidence for short period magnetic activity cycles on W UMa stars ([Borkovits et al. 2005](#); [Shengbang & Qingyao 2000](#); [Kaszás et al. 1998](#); [Qian et al. 2007](#); [Lee et al. 2004](#); [Yang et al. 2012](#); [Zhang & Zhang 2004](#)).

6.2 Variable Starspot Coverage

It is possible that starspots are responsible for the variation in brightness observed by CRTS. Doppler imaging techniques have confirmed the presence of large starspots on the surface of some contact binaries ([Barnes et al. 2004](#)). The evolution and migration of starspots on contact binaries has been tracked with doppler imaging ([Hendry & Mochnacki 2000](#)) and more recently, in Kepler data ([Tran et al. 2013](#); [Balaji et al. 2015](#)). Starspots are magnetic phenomenon, and so their occurrence is related to the magnetic activity of their host star ([Berdyugina 2005](#)). On the sun, the sunspot count varies with the magnetic field strength at the solar surface, which is expected to be true of main sequence stars

in general. As one of the component stars of the contact binary progresses through its magnetic activity cycle, the mean starspot coverage fraction varies, changing the luminosity of the whole system. At this point, we are unsure if the mean photospheric temperature fluctuation of 50K to 150K is caused by spots, or is truly a uniform global variation. The fact that luminosity variation can be seen to some extent at all the orbital phases of the 20 phase-folded light curves that we examined by eye leads us to believe that the temperature variation cannot be caused by a localized, large spot, but instead must be caused by many smaller spots distributed evenly on the contact binary surface.

Under either the Applegate model, or the variable spot coverage model, the luminosity variation has a period that is the same as the magnetic activity cycle of one of the stars in the system. If the luminosity variation is caused by either model, we can measure the magnetic activity cycle period of large numbers of contact binaries by measuring their luminosity variation period. In contrast, magnetic activity cycle periods are challenging to measure ([Vaughan 1983](#)) in single stars.

7 CONCLUSIONS

The photospheric temperature of 6200K separates binaries into two classes: binaries with convective envelopes ($T < 6200\text{K}$), and binaries with radiative envelopes ($T > 6200\text{K}$). We find that radiative binaries generally have larger brightness differences between eclipse minima, indicative of temperature and/or mass differences between the primary and secondary component stars. We find that convective binaries have a larger range of eclipse amplitudes than radiative binaries. We discover 3σ significant brightness changes on a decadal timescale in roughly 20% of the sample. We find that 23.7% of binaries with convective outer envelopes exhibited a significant change in brightness, while only 10.5% of radiative binaries exhibited a significant change in brightness, leading us to believe that the outer convective envelope of the binary is primarily responsible for driving brightness changes. We have detected luminosity variation at the $0.04 \leq (\Delta L/L) \leq 0.16$ level in 205 contact binaries (2.2% of the sample). If this luminosity variation proves to be cyclic, we estimate luminosity variation periods ranging from 4 to 11 years. The characteristics of the observed luminosity variation agree well with the predictions of the Applegate Mechanism, in which a luminosity change at the $\Delta L/L \approx 0.1$ level can be explained by the gravitational coupling of the orbit to variations in the shape of a magnetically active star in the system. Alternatively, the luminosity variation can be explained by a variation in the mean starspot coverage fraction of the binary photosphere with the same period as the magnetic activity cycle of the primary. Under either model, the luminosity variation period has the same period as the magnetic activity cycle of one of the stars in the system. If the magnetic interpretation of the brightness variation is correct, measuring the period of decadal luminosity variation will also yield the period of its magnetic activity cycle.

Observations of the 205 sinusoidally variable stars over a time baseline of longer than 8 years will allow for a more accurate measurement of the period and amplitude of the luminosity variation on a decadal timescale. Measurements

of the temperature history of variable contact binaries over a multiyear time period will help determine if the Applegate Mechanism is a viable explanation of this phenomenon.

We have included the data used in this study in an online table named `Marshtetal2016Data.csv`, accessible via the online version of this work. This table includes the following for each binary: celestial coordinates, the measured orbital period, the light-curve shape parameters described in Section 4.4 and associated errors, the linear brightness parameter described in Section 5.1 and associated errors, the sinusoidal brightness parameters described in Section 5.3 and associated significance levels, the computed photospheric temperature, and the computed levels of extinction in each SDSS band.

8 ACKNOWLEDGEMENTS

This work made use of data products from the CSS survey. The CSS survey is funded by the National Aeronautics and Space Administration under Grant No. NNG05GF22G issued through the Science Mission Directorate Near-Earth Objects Observations Program. The CRTS survey is supported by the U.S. National Science Foundation under grants AST-0909182, AST-1313422, AST-1413600, and AST-1518308.

This work made use of data products from the SDSS-III survey. Funding for SDSS-III has been provided by the Alfred P. Sloan Foundation, the Participating Institutions, the National Science Foundation, and the U.S. Department of Energy Office of Science. The SDSS-III web site is <http://www.sdss3.org/>.

SDSS-III is managed by the Astrophysical Research Consortium for the Participating Institutions of the SDSS-III Collaboration including the University of Arizona, the Brazilian Participation Group, Brookhaven National Laboratory, Carnegie Mellon University, University of Florida, the French Participation Group, the German Participation Group, Harvard University, the Instituto de Astrofísica de Canarias, the Michigan State/Notre Dame/JINA Participation Group, Johns Hopkins University, Lawrence Berkeley National Laboratory, Max Planck Institute for Astrophysics, Max Planck Institute for Extraterrestrial Physics, New Mexico State University, New York University, Ohio State University, Pennsylvania State University, University of Portsmouth, Princeton University, the Spanish Participation Group, University of Tokyo, University of Utah, Vanderbilt University, University of Virginia, University of Washington, and Yale University.

I would like to acknowledge the California Institute of Technology Summer Undergraduate Research Fellowship program for their financial support. I thank an anonymous reviewer for providing comments which greatly improved the paper. I thank James Davenport and Lynne Hillenbrand for their helpful comments, Jake VanderPlas for his help with `gatspy`, and John McBride for his help preparing the manuscript.

REFERENCES

- Ahn C. P., et al., 2014, The Astrophysical Journal Supplement Series, 211, 17
- Akerlof C., et al., 2000, The Astronomical Journal, 119, 1901
- Andronov N., Pinsonneault M., Terndrup D., 2006, The Astrophysical Journal, 646, 1160
- Applegate J. H., 1992, The Astrophysical Journal, 385, 621
- Balaji B., Croll B., Levine A. M., Rappaport S., 2015, Monthly Notices of the Royal Astronomical Society, 448, 429
- Barnes J., Lister T., Hilditch R., Cameron A. C., 2004, Monthly Notices of the Royal Astronomical Society, 348, 1321
- Berdugina S. V., 2005, Living Rev. Solar Phys., 2, 8
- Borkovits T., Elkhatib M., Csizmadia S., Nuspl J., Biró I., Hegedüs T., Csorvási R., 2005, Astronomy & Astrophysics, 441, 1087
- Davidge T., Milone E., 1984, The Astrophysical Journal Supplement Series, 55, 571
- Devor J., Charbonneau D., O'Donovan F. T., Mandushev G., Torres G., 2008, The Astronomical Journal, 135, 850
- Djorgovski S., et al., 2011, The First Year of MAXI: Monitoring Variable X-ray Sources, eds. T. Mihara & M. Serino, Special Publ. IPCR-127, p. 263
- Drake A., et al., 2009, The Astrophysical Journal, 696, 870
- Drake A., et al., 2014a, The Astrophysical Journal Supplement Series, 213, 9
- Drake A., et al., 2014b, The Astrophysical Journal, 790, 157
- Fukugita M., Yasuda N., Doi M., Gunn J. E., York D. G., 2011, The Astronomical Journal, 141, 47
- Green G. M., et al., 2015, The Astrophysical Journal, 810, 25
- Hendry P. D., Mochnacki S. W., 2000, The Astrophysical Journal, 531, 467
- Jester S., et al., 2005, The Astronomical Journal, 130, 873
- Juric M., 2012, Astrophysics Source Code Library, 1, 09003
- Kallrath J., Milone E., 1999, New Your: Springer-Velag
- Kaszás G., Vinkó J., Szatmáry K., Hegedus T., Gal J., Kiss L., Borkovits T., 1998, Astronomy and Astrophysics, 331, 231
- Kippenhahn R., Weigert A., Weiss A., 1990, Stellar structure and evolution. Vol. 44, Springer
- Lanza A. F., 2006, Monthly Notices of the Royal Astronomical Society, 369, 1773
- Lee C.-H., 2015, Monthly Notices of the Royal Astronomical Society, 454, 2946
- Lee J. W., Kim C.-H., Han W., Kim H.-I., Koch R. H., 2004, Monthly Notices of the Royal Astronomical Society, 352, 1041
- Liu Q.-Y., Yang Y.-L., 2003, Chinese Journal of Astronomy and Astrophysics, 3, 142
- Lucy L., 1968a, The Astrophysical Journal, 151, 1123
- Lucy L., 1968b, The Astrophysical Journal, 153, 877
- Mahabal A., et al., 2011, Bull. Astr. Soc. India, 39, 387
- Norton A. J., et al., 2011, Astronomy & Astrophysics, 528, A90
- O'Connell D., 1951, Publications of the Riverview College Observatory, 2, 85
- Palaversa L., et al., 2013, The Astronomical Journal, 146, 101
- Pojmanski G., 2000, Acta Astronomica, 50, 177
- Qian S., 2001, Monthly Notices of the Royal Astronomical Society, 328, 635
- Qian S.-B., Yuan J.-Z., Soonthornthum B., Zhu L.-Y., He J.-J., Yang Y.-G., 2007, The Astrophysical Journal, 671, 811
- Rubenstein E. P., 2001, The Astronomical Journal, 121, 3219
- Rucinski S., 1993, Publications of the Astronomical Society of the Pacific, pp 1433–1440
- Rucinski S. M., 1996, arXiv preprint astro-ph/9611158
- Rucinski S. M., 2006, Monthly Notices of the Royal Astronomical Society, 368, 1319
- Rucinski S. M., Duerbeck H. W., 1997, in Hipparchos-Venice'97. pp 457–460
- Scargle J. D., 1982, The Astrophysical Journal, 263, 835
- Schlafly E. F., Finkbeiner D. P., 2011, The Astrophysical Journal, 737, 103
- Schwarz G., et al., 1978, The annals of statistics, 6, 461

- Shengbang Q., Qingyao L., 2000, *Astrophysics and Space Science*, 271, 331
- Tran K., Levine A., Rappaport S., Borkovits T., Csizmadia S., Kalomeni B., 2013, *The Astrophysical Journal*, 774, 81
- Tylenda R., et al., 2011, *Astronomy & Astrophysics*, 528, A114
- VanderPlas J. T., Ivezić Ž., 2015, *The Astrophysical Journal*, 812, 18
- VanderPlas J., Fouesneau M., Taylor J., 2014, *Astrophysics Source Code Library*
- Vanderplas J., 2015, gatspy: General tools for Astronomical Time Series in Python, doi:10.5281/zenodo.14833, <http://dx.doi.org/10.5281/zenodo.14833>
- Vaughan A., 1983, in *Solar and Stellar Magnetic Fields: Origins and Coronal Effects*. pp 113–131
- Vilhu O., Rahunen T., 1981, in *Fundamental problems in the theory of stellar evolution*. p. 181
- Wang J.-M., 1994, *The Astrophysical Journal*, 434, 277
- Wilsey N. J., Beaky M. M., 2009, in *Society for Astronomical Sciences Annual Symposium*. p. 107
- Yang Y.-G., Qian S.-B., Soonthornthum B., 2012, *The Astronomical Journal*, 143, 122
- York D. G., et al., 2000, *The Astronomical Journal*, 120, 1579
- Zeraatgari F., et al., 2015, *Contrib. Astron. Obs. Skalnaté Pleso*, 45, 5
- Zhang X., Zhang R., 2004, *Monthly Notices of the Royal Astronomical Society*, 347, 307
- Zhou D.-Q., Leung K.-C., 1990, *The Astrophysical Journal*, 355, 271

This paper has been typeset from a *TeX/LaTeX* file prepared by the author.

7 Paper II: Geometrical Parameters

We hope to detect systems for which the light-curve shape is not explainable by Roche-geometry. We will do this by deriving a set of measurements that describe the shape of a light-curve. We will then measure optical light-curves of contact binaries from the CRTS variable sources catalog, and then we will measure a set of theoretical models published in Rucinski [1993b].

7.1 Light-curve Features

In order to understand how the light-curves change as a function of temperature, we must first figure out a way to describe a light-curve in a way that makes sense, both to humans and computers. In data science, this problem is called “feature selection” . Let’s consider what our light curve data actually is: a set of measurements of the flux of a contact binary. These measurements are taken at a certain time (t), have a certain value, in our case a measurement of flux (f), and this measured value has an associated error (e). From CRTS, we obtain lots of these measurements. Our light curve looks like this:

In §??, we were able to construct a coherent light-curve out of survey data taken at random times by folding the data by the orbital period. Just as before, we can input out data into a Lomb-Scargle , or similar period-finding algorithm, find the best period p and fold the observations by that period. This returns us a new version of the light-curve:

In the eight years between 2005 and 2013, CRTS observes a given source roughly 350 times. In other words, it reports about 350 phases (θ), 350 fluxes (f), and 350 errors (e) on those fluxes. So, the raw data comes to us as $\approx 350 \times 3 = 1050$ individual numbers. These numbers are perfectly valid descriptors of the light-curve, but they are not easily understandable, neither by a human nor a computer.

Thankfully, we can introduce some assumptions that will make the task of succinctly describing our light-curves easier. First, we assume that our light-curve is a *continuous function*. This means that there are not jumps or breaks in the true variation of light. The light-curve has a value at every point in phase, and is differentiable at every point in phase. Second, we assume that *the light-curve is periodic*: that the pattern of light variation will exactly repeat itself after some amount of time. In §??, we learn that this is not exactly true for contact binaries when we observe them over many years. But for now, this assumption will serve us well.

Now, armed with our two new assumptions and light-curve data, we can construct a light-curve function. There are many ways to construct a continuous, periodic function from a set of data.

Table 3: Format of Raw Data from CRTS

time (t)	flux (f)	error (e)
number	number	number
number	number	number
...

Table 4: Format of Phase-folded Data from CRTS

phase (θ)	flux (f)	error (e)
number	number	number
number	number	number
...

1. Polynomial Fit.

$$f(\theta) = a_0 + a_1\theta + a_1\theta^2 + a_2\theta^3 + \dots (0 \leq p < 1)$$

$$f(\theta) = \sum_{i=0}^n a_i \theta^i (0 \leq \theta < 1) \quad (7.1)$$

2. Polynomial - Spline Fit.

$$f(p) = \dots \quad (7.2)$$

[Gettel et al., 2006] a spline fit is employed. [Akerlof et al., 1994] explanation of spline fit.

3. Fourier (Harmonic) Fit.

$$f(p) =$$

$$f(p) = \sum_{i=0}^n a_i \cos(2\pi i p) \quad (7.3)$$

There are many other forms that can be used to represent a continuous periodic function - but these are the most obvious choices. Each has advantages and disadvantages. For example, if the light-curve has large derivatives at some points in the phase (it has “sharp turns”), a polynomial spline fit may be the best choice.

We have elected to use the harmonic fit, because it has a history of use in the description contact binary light-curves. It is easy to implement and can fit the data accurately, provided that there are not sharp turns.

By choosing a fitting function, we have turned our raw data from CRTS (which was 1000 numbers) into a continuous, periodic function which we can use to derive other, physically meaningful features.

Recall (as in Eqn. 3.5)

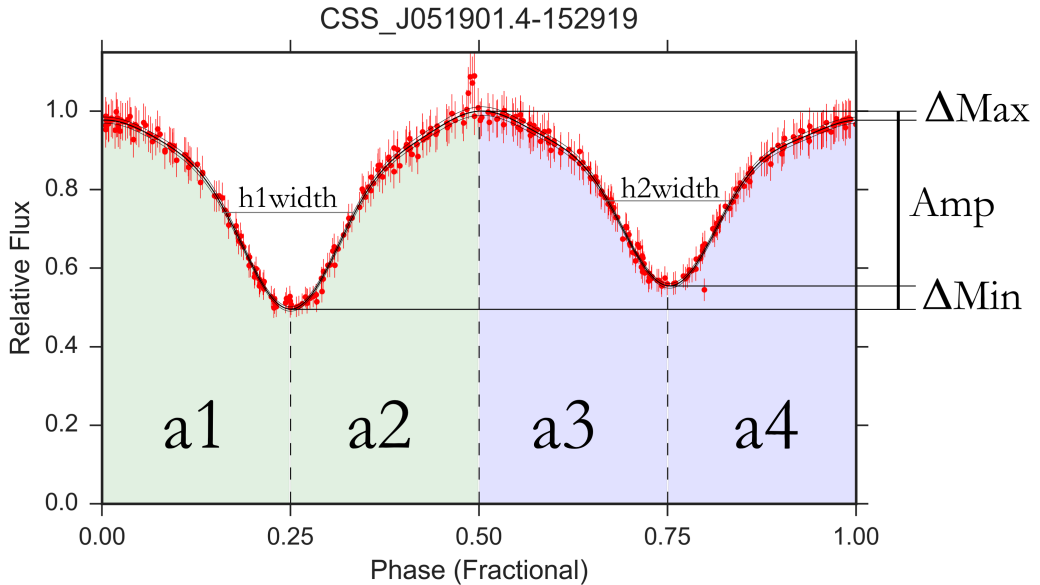


Figure 29: A graphical description of the light-curve features that we derive for contact binaries in our sample.

For each light-curve, we have derived the following geometrical features:

Areas (a_1, a_2, a_3, a_4). The features have units of energy, being products of phase (which is time), and flux (which is rate at which energy is received by the telescope.)

Flux Differences (Amp , ΔMin ΔMax). These features have units of flux, because they are differences of fluxes. Eclipse Width and Half Minimum. ($h_1\text{width}$, $h_2\text{width}$). These features have units of time, because they are differences of phases.

In the following mathematical descriptions of the light-curve features, we will compute the light-curve on a grid of at least 500 points spaced evenly in phase. The relative flux computed from the harmonic fit at a point i is denoted F_i . This is the y -coordinate on the

light-curve graph. The phase of the point i is denoted by P_i . This is the x -coordinate on the light-curve graph.

The area features were computed as Riemann sums on a fixed, evenly spaced, grid of discrete phases:

$$\begin{aligned}
 a1 &= \frac{\sum_i F_i}{\sum_i 1} (0 < P_i \leq 0.25) \\
 a2 &= \frac{\sum_i F_i}{\sum_i 1} (0.25 < P_i \leq 0.50) \\
 a3 &= \frac{\sum_i F_i}{\sum_i 1} (0.50 < P_i \leq 0.75) \\
 a4 &= \frac{\sum_i F_i}{\sum_i 1} (0.75 < P_i \leq 1.00)
 \end{aligned} \tag{7.4}$$

The following light-curve features have units of flux. The light-curve amplitude (Amp) is the total range of the flux variation, ranging from a maximum at 1.0 (by the definition of our flux, see Eqn.??) to the lowest value of the light-curve, $F_{\min 1}$. The flux difference between eclipse minima (ΔMin) is the difference between the flux at the second local minimum in the light curve $F_{\min 2}$, and the flux at the lowest value of the light-curve, $F_{\min 1}$. The flux difference between out-of-eclipse maxima

$$\begin{aligned}
 \text{Amp} &= 1.0 - F_{\min 1} \\
 \Delta\text{Min} &= F_{\min 2} - F_{\min 1} \\
 \Delta\text{Max} &= 1.0 - F_{\max}
 \end{aligned} \tag{7.5}$$

We also compute two intermediate flux features that will help us calculate the eclipse full-width at half-minimum.

$$\begin{aligned}
 F_{h1} &= 0.5 + \frac{F_{\min 1}}{2} \\
 F_{h2} &= 0.5 + \frac{F_{\min 2}}{2}
 \end{aligned} \tag{7.6}$$

The following light-curve features have units of time. P_{h1} and P_{h2} are the closest points in phase.

$$\begin{aligned} \text{h1width} &= P_{\text{h1}} - P_{\text{h1}} \\ \text{h2width} &= P_{\text{h2}} - P_{\text{h2}} \end{aligned} \tag{7.7}$$

8 Paper III: Optical and UV Variability

In our study, we aim to learn how the luminosity of contact binary systems vary on decadal timescales. We hope to learn the relationship between the UV-color of a contact binary, and its optical variability.

In §?? we talked about the light-curve as if it was one single function. In actuality, the shape of contact binary light-curves change over time (Eqn. ??).

$$f(\text{Phase, Time}) = \text{Flux Received at Telescope} \tag{8.1}$$

We can detect light-curve changes with a survey that observes the same set of contact binaries over a timespan of several years (like CRTS). In order to detect changes in the contact binary light-curve in CRTS data, we will re-use much of the machinery that we have developed in §??.

We detect deviations of the light-curve with respect to the harmonic fit performed on all CRTS observations. We can consider the harmonic the “average” light-curve of the contact binary during the eight-year CRTS observation timespan. This is because the CRTS measurements are randomly, (but uniformly) sampled in time, and the harmonic fit assigns equal weight to every measurement.

We can measure the difference between observations and the harmonic fit as a function of time. If this difference becomes too large to attribute to photometric noise, we know that the contact binary is changing its brightness over a timespan of many years.

[Bradstreet and Guinan, 1988]

9 The Future

In this section, I’d like to outline a few projects that are possible with existing datasets. I will also summarize a few future surveys that I believe have great potential to improve our understanding of contact binary systems.

9.1 Coronal Rotation with GALEX

π steradian (quarter of the sky) imaging survey. GALEX also completed a deep imaging survey, where a small portion of the sky was imaged for a long time. The two (FUV, NUV) detectors on GALEX are *photon counting*, meaning that they record the time of arrival (to 5 milliseconds) and location (x,y pixel coordinated) of each incident photon. This means that it is possible construct light-curves from this data.

The python package `gphoton` allows the user to easily access and download GALEX photon-counting data. The user can construct light-curves out of the individual photon counts, to perform a periodicity analysis.

<https://archive.stsci.edu/prepds/gphoton/>

McGale et al. [1996] have shown that the coronal rotation rate of convective contact binaries can be measured by using X-ray light-curves.

9.2 Period Changes with Evryscope

Evryscope is a wide-field, high-entendue survey instrument. It can perform photometry on the entire visible night-sky, down to magnitude $V \approx 16$. This places thousands of known contact binaries within its reach. What makes Evryscope special is its cadence: V -band photometry will be performed every 2-minutes on every star in the visible sky. The cadence of Evryscope enables complete light-curves to be constructed for each night of observing. The cadence of this data means that traditional $O - C$ analysis can be used to analyze period changes of over 1000 bright contact binaries.

9.3 H α Fluxes in PTF

The Palomar Transient Facility

9.4 Future Surveys



Figure 30

10 Conclusion

References

- C Akerlof, S Amrose, R Balsano, J Bloch, D Casperson, S Fletcher, G Gisler, J Hills, R Kehoe, B Lee, et al. Rotse all-sky surveys for variable stars. i. test fields. *The Astronomical Journal*, 119(4):1901, 2000.
- Carl Akerlof, C Alcock, R Allsman, T Axelrod, DP Bennett, KH Cook, K Freeman, K Griest, S Marshall, H-S Park, et al. Application of cubic splines to the spectral analysis of unequally spaced data. *The Astrophysical Journal*, 436:787–794, 1994.
- Ivan L Andronov. Phenomenological modeling of the light curves of algol-type eclipsing binary stars. *Astrophysics*, 55(4):536–550, 2012.
- N Andronov, MH Pinsonneault, and DM Terndrup. Mergers of close primordial binaries. *The Astrophysical Journal*, 646(2):1160, 2006.
- EA Antokhina, M Srinivasa Rao, and M Parthasarathy. Light curve analysis of hipparcos data for the massive o-type eclipsing binary uw cma. *New Astronomy*, 16(3):177–182, 2011.
- James H Applegate. A mechanism for orbital period modulation in close binaries. *The Astrophysical Journal*, 385:621–629, 1992.
- B Arbutina. Possible solution to the problem of the extreme mass ratio w uma-type binaries. *Monthly Notices of the Royal Astronomical Society*, 394(1):501–509, 2009.
- NS Awadalla and MA Hanna. Absolute parameters and mass-radius-luminosity relations for the sub-types of w uma binaries. *Journal of Korean Astronomical Society*, 38:43–57, 2005.
- Bhaskaran Balaji, Bryce Croll, Alan M Levine, and Saul Rappaport. Tracking the stellar longitudes of starspots in short-period kepler binaries. *Monthly Notices of the Royal Astronomical Society*, 448(1):429–444, 2015.
- André Balogh, Hugh Hudson, Kristóf Petrovay, and Rudolf Steiger. *The Solar Activity Cycle: Physical Causes and Consequences*, volume 53. Springer, 2015.
- JR Barnes, TA Lister, RW Hilditch, and A Collier Cameron. High-resolution doppler images of the spotted contact binary ae phe. *Monthly Notices of the Royal Astronomical Society*, 348(4):1321–1331, 2004.
- Gibor Basri, William J Borucki, and David Koch. The kepler mission: A wide-field transit search for terrestrial planets. *New Astronomy Reviews*, 49(7):478–485, 2005.

Svetlana V Berdyugina. Starspots: a key to the stellar dynamo. *Living Rev. Solar Phys.*, 2:8, 2005.

S Bilir, Y Karataş, O Demircan, and Z Eker. Kinematics of w ursae majoris type binaries and evidence of the two types of formation. *Monthly Notices of the Royal Astronomical Society*, 357(2):497–517, 2005.

Marvin Bolt, Thomas Hockey, JoAnn Palmeri, Virginia Trimble, Thomas R Williams, Katherine Bracher, Richard Jarrell, Jordan D Marché, and F Jamil Ragep. *Biographical encyclopedia of astronomers*. Springer Science & Business Media, 2007.

T Borkovits, MM Elkhateeb, Sz Csizmadia, J Nuspl, IB Biró, T Hegedüs, and R Csorvási. Indirect evidence for short period magnetic cycles in w uma stars-period analysis of five overcontact systems. *Astronomy & Astrophysics*, 441(3):1087–1097, 2005.

David H Bradstreet and Edward F Guinan. Mapping of surface activity on the w uma-type system vw cephei. 1988.

NS Brickhouse and AK Dupree. Extreme ultraviolet explorer observations of the w ursae majoris contact binary 44i bootis: Coronal structure and variability. *The Astrophysical Journal*, 502(2):918, 1998.

Bradley W Carroll and Dale A Ostlie. *An introduction to modern astrophysics and cosmology*, volume 1. 2006.

WP Chen, Kaushar Sanchawala, and MC Chiu. W ursae majoris contact binary variables as x-ray sources. *The Astronomical Journal*, 131(2):990, 2006.

Xiaodian Chen, Licai Deng, Richard de Grijs, Xiaobin Zhang, Yu Xin, Kun Wang, Changqing Luo, Zhengzhou Yan, Jianfeng Tian, Jinjiang Sun, et al. Physical parameter study of eight w ursae majoris-type contact binaries in ngc 188. *arXiv preprint arXiv:1607.06152*, 2016.

D Coker, S Özdemir, C Yeşilyaprak, SK Yerli, N Aksaker, and BB Güçsav. A study on w ursae majoris-type systems recognised by the rotse-iiid experiment. *Publications of the Astronomical Society of Australia*, 30:e013, 2013.

RG Cruddace and AK Dupree. Contact binary stars. i-an x-ray survey. *The Astrophysical Journal*, 277:263–273, 1984.

MS Darwish, MM Elkhateeb, MI Nouh, SM Saad, MA Hamdy, MM Beheary, K Gadallah, and I Zaid. Orbital solution and evolutionary state for the eclipsing binary 1swasp j080150. 03+ 471433.8. *arXiv preprint arXiv:1606.07510*, 2016.

Osman Demircan and Göksel Kahraman. Stellar mass-luminosity and mass-radius relations. *Astrophysics and Space Science*, 181(2):313–322, 1991.

Jonathan Devor, David Charbonneau, Francis T O’Donovan, Georgi Mandushev, and Guillermo Torres. Identification, classifications, and absolute properties of 773 eclipsing binaries found in the trans-atlantic exoplanet survey. *The Astronomical Journal*, 135(3):850, 2008.

AJ Drake, SG Djorgovski, A Mahabal, E Beshore, S Larson, MJ Graham, R Williams, E Christensen, M Catelan, A Boattini, et al. First results from the catalina real-time transient survey. *The Astrophysical Journal*, 696(1):870, 2009.

AJ Drake, SG Djorgovski, D García-Álvarez, MJ Graham, M Catelan, AA Mahabal, C Donalek, JL Prieto, G Torrealba, S Abraham, et al. Ultra-short period binaries from the catalina surveys. *The Astrophysical Journal*, 790(2):157, 2014a.

AJ Drake, MJ Graham, SG Djorgovski, M Catelan, AA Mahabal, G Torrealba, D García-Álvarez, C Donalek, JL Prieto, R Williams, et al. The catalina surveys periodic variable star catalog. *The Astrophysical Journal Supplement Series*, 213(1):9, 2014b.

Olin J Eggen. Contact binaries, ii. *Memoirs of the Royal Astronomical Society*, 70:111, 1967.

Peter P Eggleton. Approximations to the radii of roche lobes. *The Astrophysical Journal*, 268:368, 1983.

Z Eker, S Bilir, E Yaz, O Demircan, and M Helvacı. New absolute magnitude calibrations for w ursa majoris type binaries. *arXiv preprint arXiv:0807.4989*, 2008.

Masataka Fukugita, Naoki Yasuda, Mamoru Doi, James E Gunn, and Donald G York. Characterization of Sloan Digital Sky Survey stellar photometry. *The Astronomical Journal*, 141(2):47, 2011.

Qing Gao, Yu Xin, Ji-Feng Liu, Xiao-Bin Zhang, and Shuang Gao. White-light flares on close binaries observed with kepler. *arXiv preprint arXiv:1602.07972*, 2016.

K Gazeas and K Stępień. Angular momentum and mass evolution of contact binaries. *Monthly Notices of the Royal Astronomical Society*, 390(4):1577–1586, 2008.

KD Gazeas. Physical parameters of contact binaries through 2-d and 3-d correlation diagrams. *Communications in Asteroseismology*, 159:129–130, 2009.

KD Gazeas and PG Niarchos. Masses and angular momenta of contact binary stars. *Monthly Notices of the Royal Astronomical Society: Letters*, 370(1):L29–L32, 2006.

KD Gazeas, PG Niarchos, and G-P Gradoula. Modeling the 2004.5 brightening of the contact binary v839 oph. In *Close Binaries in the 21st Century: New Opportunities and Challenges*, pages 123–125. Springer, 2006.

Sara J Gettel, Michael T Geske, and Tim A McKay. A catalog of 1022 bright contact binary stars. *The Astronomical Journal*, 131(1):621, 2006.

Àlvaro Giménez, Edward Guinan, Panagiotis Niarchos, and Slavek Rucinski. Close binaries in the 21 st century: New opportunities and challenges. In *Close Binaries in the 21st Century: New Opportunities and Challenges*, pages 1–2. Springer, 2006.

L Hambálek and T Pribulla. The reliability of mass-ratio determination from light curves of contact binary stars. *Contributions of the Astronomical Observatory Skalnate Pleso*, 43: 27–46, 2013.

Paul D Hendry and Stefan W Mochnacki. Detection of tertiary components in w ursae majoris systems. *The Astrophysical Journal*, 504(2):978, 1998.

Paul D Hendry and Stefan W Mochnacki. Doppler imaging of vw cephei: distribution and evolution of starspots on a contact binary. *The Astrophysical Journal*, 531(1):467, 2000.

RW Hilditch, DJ King, and TM McFarlane. The evolutionary state of contact and near-contact binary stars. *Monthly Notices of the Royal Astronomical Society*, 231(2):341–352, 1988.

RW Hilditch, ID Howarth, and TJ Harries. Forty eclipsing binaries in the small magellanic cloud: fundamental parameters and cloud distance. *Monthly Notices of the Royal Astronomical Society*, 357(1):304–324, 2005.

James H Horne and Sallie L Baliunas. A prescription for period analysis of unevenly sampled time series. *The Astrophysical Journal*, 302:757–763, 1986.

Bruce J Hrivnak. Radial velocity studies and absolute parameters of contact binaries. ii-oo aquilae. *The Astrophysical Journal*, 340:458–467, 1989.

Piet Hut, Steve McMillan, Jeremy Goodman, Mario Mateo, ES Phinney, Carlton Pryor, Harvey B Richer, Frank Verbunt, and Martin Weinberg. Binaries in globular clusters. *Publications of the Astronomical Society of the Pacific*, pages 981–1034, 1992.

N Ivanova, S Justham, X Chen, O De Marco, CL Fryer, E Gaburov, H Ge, E Glebbeek, Z Han, X-D Li, et al. Common envelope evolution: where we stand and how we can move forward. *The Astronomy and Astrophysics Review*, 21(1):1–73, 2013.

Željko Ivezić, J Allyn Smith, Gajus Miknaitis, Huan Lin, Douglas Tucker, Robert H Lupton, James E Gunn, Gillian R Knapp, Michael A Strauss, Branimir Sesar, et al. Sloan digital sky survey standard star catalog for stripe 82: The dawn of industrial 1% optical photometry. *The Astronomical Journal*, 134(3):973, 2007.

H Kähler. On the structure of contact binaries. *Astronomy & Astrophysics*, 395(3):907–913, 2002.

H Kähler. The structure of contact binaries. *Astronomy & Astrophysics*, 414(1):317–333, 2004.

A Kalimeris, H Rovithis-Livaniou, and P Rovithis. On the orbital period changes in contact binaries. *Astronomy and Astrophysics*, 282:775–786, 1994.

A Kalimeris, H Rovithis-Livaniou, and P Rovithis. Starspots and photometric noise on observed minus calculated (o–c) diagrams. *Astronomy & Astrophysics*, 387(3):969–976, 2002.

Josef Kallrath and Eugene F Milone. *Eclipsing binary stars: modeling and analysis*. Springer, 2009.

Janusz Kaluzny and Michael M Shara. A ccd survey for contact binaries in six open clusters. *The Astronomical Journal*, 95:785–793, 1988.

G Kaszás, J Vinkó, K Szatmáry, T Hegedus, J Gal, LL Kiss, and T Borkovits. Period variation and surface activity of the contact binary vw cephei. *Astronomy and Astrophysics*, 331:231–243, 1998.

R Kippenhahn and H-C Thomas. A simple method for the solution of the stellar structure equations including rotation and tidal forces. In *Stellar Rotation*, pages 20–29. Springer, 1970.

Rudolf Kippenhahn, Alfred Weigert, and Achim Weiss. *Stellar structure and evolution*, volume 44. Springer, 1990.

C Koen, T Koen, and RO Gray. Multi-filter light curves of 29 very short period candidate contact binaries. *The Astronomical Journal*, 151(6):168, 2016.

Zdenek Kopal. Close binary systems. *The International Astrophysics Series, London: Chapman & Hall*, 1959, 1959.

Kevin Krisciunas. A brief history of astronomical brightness determination methods at optical wavelengths. *arXiv preprint astro-ph/0106313*, 2001.

CLAUD H Lacy, Th J Moffett, and DAVID S Evans. Uv ceti stars-statistical analysis of observational data. *The Astrophysical Journal Supplement Series*, 30:85–96, 1976.

Antonino F Lanza. Internal stellar rotation and orbital period modulation in close binary systems. *Monthly Notices of the Royal Astronomical Society*, 369(4):1773–1779, 2006.

C-H Lee, J Koppenhoefer, S Seitz, R Bender, A Riffeser, M Kodric, U Hopp, J Snigula, C Gössl, R-P Kudritzki, et al. Properties of m31. v. 298 eclipsing binaries from pandromeda. *The Astrophysical Journal*, 797(1):22, 2014.

Chien-Hsiu Lee. Properties of eclipsing binaries from all-sky surveys–ii. detached eclipsing binaries in catalina sky surveys. *Monthly Notices of the Royal Astronomical Society*, 454(3):2946–2953, 2015.

Jae Woo Lee, Chun-Hwey Kim, Wonyong Han, Ho-Il Kim, and Robert H Koch. Period and light variations for the cool, overcontact binary bx pegasi. *Monthly Notices of the Royal Astronomical Society*, 352(3):1041–1055, 2004.

Lifang Li, Fenghui Zhang, Zhanwen Han, and Dengkai Jiang. Formation and evolution of w ursae majoris contact binaries. *The Astrophysical Journal*, 662(1):596, 2007.

ME Lohr, AJ Norton, UC Kolb, DR Anderson, Francesca Faedi, and Richard G West. Period decrease in three superwasp eclipsing binary candidates near the short-period limit. *Astronomy & Astrophysics*, 542:A124, 2012.

ME Lohr, AJ Norton, SG Payne, RG West, and PJ Wheatley. Orbital period changes and the higher-order multiplicity fraction amongst superwasp eclipsing binaries. *arXiv preprint arXiv:1505.00941*, 2015.

J Lorenzo, I Negueruela, AKF Val Baker, Miriam García, Sergio Simón-Díaz, P Pastor, and M Méndez Majuelos. My camelopardalis, a very massive merger progenitor. *Astronomy & Astrophysics*, 572:A110, 2014.

SH Lubow and FH Shu. On the structure of contact binaries. ii-zero-age models. *The Astrophysical Journal*, 216:517–525, 1977.

LB Lucy. The light curves of w ursae majoris stars. *The Astrophysical Journal*, 153:877, 1968a.

LB Lucy. The structure of contact binaries. *The Astrophysical Journal*, 151:1123, 1968b.

LB Lucy and RE Wilson. Observational tests of theories of contact binaries. *The Astrophysical Journal*, 231:502–513, 1979.

Mario Mateo, Hugh C Harris, James Nemec, and Edward W Olszewski. Blue stragglers as remnants of stellar mergers—the discovery of short-period eclipsing binaries in the globular cluster ngc 5466. *The Astronomical Journal*, 100:469–484, 1990.

PA McGale, JP Pye, and ST Hodgkin. Rosat pspc x-ray spectral survey of w uma systems. *Monthly Notices of the Royal Astronomical Society*, 280:627–637, 1996.

SW Mochnacki. Contact binary stars. *The Astrophysical Journal*, 245:650–670, 1981.

SW Mochnacki. Accurate integrations of the roche model. *The Astrophysical Journal Supplement Series*, 55:551–561, 1984.

SW Mochnacki and NA Doughty. A model for the totally eclipsing w ursae majoris system aw uma. *Monthly Notices of the Royal Astronomical Society*, 156(1):51–65, 1972.

G Muller and P Kempf. A new variable star unusually short period. *The Astrophysical Journal*, 17:201–211, 1903.

Andrew J Norton, SG Payne, T Evans, Richard G West, Peter J Wheatley, DR Anderson, SCC Barros, OW Butters, A Collier Cameron, Damian Joseph Christian, et al. Short period eclipsing binary candidates identified using superwasp. *Astronomy & Astrophysics*, 528:A90, 2011.

B Paczynski. Evolutionary processes in close binary systems. *Annual Review of Astronomy and Astrophysics*, 9:183, 1971.

Lovro Palaversa, Željko Ivezić, Laurent Eyer, Domagoj Ruždjak, Davor Sudar, Mario Galin, Andrea Kroflin, Martina Mesarić, Petra Munk, Dijana Vrbanec, et al. Exploring the variable sky with linear. iii. classification of periodic light curves. *The Astronomical Journal*, 146(4):101, 2013.

Laura R Penny, Cynthia Ouzts, and Douglas R Gies. Tomographic separation of composite spectra. xi. the physical properties of the massive close binary hd 100213 (tu muscae). *The Astrophysical Journal*, 681(1):554, 2008.

G Pojmanski. The all sky automated survey. catalog of about 3800 variable stars. *Acta Astronomica*, 50:177–190, 2000.

DM Popper. Masses of hot main-sequence stars. *The Astrophysical Journal*, 220:L11–L14, 1978.

T Pribulla, JM Kreiner, and J Tremko. Catalogue of the field contact binary stars. *Contributions of the Astronomical Observatory Skalnaté Pleso*, 33:38–70, 2003.

Theodor Pribulla. Roche: Analysis of eclipsing binary multi-dataset observables. *Proceedings of the International Astronomical Union*, 7(S282):279–282, 2011.

Theodor Pribulla and Slavek M Rucinski. Contact binaries with additional components. i. the extant data. *The Astronomical Journal*, 131(6):2986, 2006.

James Edward Pringle and Richard Alan Wade. Interacting binary stars. 1985.

D Shanti Priya, K Sriram, KY Shaju, and P Vivekananda Rao. Photometric study of hot contact binaries in smc. *Bull. Astr. Soc. India*, 41:159–172, 2013.

A Prsa, EF Guinan, EJ Devinney, SG Engle, M DeGeorge, GP McCook, PA Maurone, J Pepper, DJ James, DH Bradstreet, et al. Fully automated approaches to analyze large-scale astronomy survey data. *arXiv preprint arXiv:0904.0739*, 2009.

A Prša, P Degroote, K Conroy, S Bloemen, K Hambleton, J Giamarco, and H Pablo. Physics of eclipsing binaries: Motivation for the new-age modeling suite. *EAS Publications Series*, 64:259–268, 2013.

Andrej Prsa, EF Guinan, EJ Devinney, M DeGeorge, DH Bradstreet, JM Giamarco, CR Alcock, and SG Engle. Artificial intelligence approach to the determination of physical properties of eclipsing binaries. i. the ebai project. *The Astrophysical Journal*, 687(1):542, 2008.

S-B Qian, J-Z Yuan, B Soonthornthum, L-Y Zhu, J-J He, and Y-G Yang. Ad cancri: A shallow contact solar-type eclipsing binary and evidence for a dwarf third component and a 16 year magnetic cycle. *The Astrophysical Journal*, 671(1):811, 2007.

S-B Qian, J-J Wang, L-Y Zhu, B Soonthornthum, L-Z Wang, EG Zhao, X Zhou, W-P Liao, and N-P Liu. Optical flares and a long-lived dark spot on a cool shallow contact binary. *The Astrophysical Journal Supplement Series*, 212(1):4, 2014.

Shengbang Qian. Orbital period changes of contact binary systems: direct evidence for thermal relaxation oscillation theory. *Monthly Notices of the Royal Astronomical Society*, 328(3):914–924, 2001.

Frederic A Rasio. The minimum mass ratio of w ursae majoris binaries. *arXiv preprint astro-ph/9502028*, 1995.

Eric P Rubenstein. The effect of stellar evolution on population ii contact binaries in the period-color relation. i. equal-mass, marginal contact systems. *The Astronomical Journal*, 121(6):3219, 2001.

- Slavek M Rucinski. Eclipsing binaries in the ogle variable star catalog. ii. light curves of the w uma-type systems in baade's window. *arXiv preprint astro-ph/9611158*, 1996.
- Slavek M Rucinski. Eclipsing binaries in the ogle variable star catalog. iw uma-type systems as distance and population tracers in baade's window. *The Astronomical Journal*, 113: 407, 1997.
- Slavek M Rucinski. Contact binaries of the galactic disk: Comparison of the baade's window and open cluster samples. *The Astronomical Journal*, 116(6):2998, 1998a.
- Slavek M Rucinski. Eclipsing binaries in the ogle variable star catalog. iii. long-period contact systems. *The Astronomical Journal*, 115(3):1135, 1998b.
- Slavek M Rucinski. Extreme ultraviolet explorer investigation of three short-period binary stars. *The Astronomical Journal*, 115(1):303, 1998c.
- Slavek M Rucinski. The photometric amplitude and mass ratio distributions of contact binary stars. *The Astronomical Journal*, 122(2):1007, 2001.
- Slavek M Rucinski. Luminosity function of contact binaries based on the all sky automated survey (asas). *Monthly Notices of the Royal Astronomical Society*, 368(3):1319–1322, 2006.
- Slavek M Rucinski. The short-period end of the contact binary period distribution based on the all-sky automated survey. *Monthly Notices of the Royal Astronomical Society*, 382(1): 393–396, 2007.
- Slavek M Rucinski and Hilmar W Duerbeck. Absolute magnitude calibration for the w uma-type contact binary stars. In *Hipparcos-Venice'97*, volume 402, pages 457–460, 1997.
- SM Rucinski. The w uma-type systems as contact binaries. i. two methods of geometrical elements determination. degree of contact. *Acta Astronomica*, 23:79, 1973.
- SM Rucinski. Can full convection explain the observed short-period limit of the w uma-type binaries? *The Astronomical Journal*, 103:960–966, 1992.
- SM Rucinski. The realm of interacting binary stars, 1993a.
- SM Rucinski. A simple description of light curves of w uma systems. *Publications of the Astronomical Society of the Pacific*, pages 1433–1440, 1993b.
- Jeffrey D Scargle. Studies in astronomical time series analysis. ii-statistical aspects of spectral analysis of unevenly spaced data. *The Astrophysical Journal*, 263:835–853, 1982.

Qian Shengbang and Liu Qingyao. A possible connection between the variation of light curve and the change of the orbital period in the contact binary ck bootis. *Astrophysics and Space Science*, 271(4):331–339, 2000.

FH Shu, SH Lubow, and L Anderson. On the structure of contact binaries. i-the contact discontinuity. *The Astrophysical Journal*, 209:536–546, 1976.

Marc Van Der Sluys. Roche potential, 2006. URL <http://hemel.waarnemen.com/Informatie/Sterren/hoofdstuk6.html#h6.2>.

Klaus Staubermann. The trouble with the instrument: Zöllner’s photometer. *Journal for the History of Astronomy*, 31:323, 2000.

K Stepien and K Gazeas. Evolutionary scenario for w uma-type stars. *Proceedings of the International Astronomical Union*, 4(S252):427–428, 2008.

K Stepien, JHMM Schmitt, and W Voges. Rosat all-sky survey of w ursae majoris stars and the problem of supersaturation. *Astronomy & Astrophysics*, 370(1):157–169, 2001.

Dirk Terrell. Eclipsing binary stars: Past, present, and future. *Journal of the American Association of Variable Star Observers (AAVSO)*, 30:1, 2001.

Dirk Terrell and RE Wilson. Photometric mass ratios of eclipsing binary stars. In *Zdeněk Kopal’s Binary Star Legacy*, pages 221–230. Springer, 2005.

K Tran, A Levine, S Rappaport, T Borkovits, Sz Csizmadia, and B Kalomeni. The anti-correlated nature of the primary and secondary eclipse timing variations for the kepler contact binaries. *The Astrophysical Journal*, 774(1):81, 2013.

AV Tutukov and AM Cherepashchuk. The evolution of close binary stars. *Astronomy Reports*, 60(5):461–476, 2016.

R Tylenda, M Hajduk, T Kamiński, A Udalski, I Soszyński, MK Szymański, M Kubiak, G Pietrzyński, R Poleski, K Ulaczyk, et al. V1309 scorpii: merger of a contact binary. *Astronomy & Astrophysics*, 528:A114, 2011.

W Van Hamme and RE Wilson. A contribution on the problem of empirical masses for contact binaries. *Astronomy and Astrophysics*, 152:25–32, 1985.

F Vilardell, I Ribas, and C Jordi. Eclipsing binaries suitable for distance determination in the andromeda galaxy. *Astronomy & Astrophysics*, 459(1):321–331, 2006.

Osmi Vilhu and Frederick M Walter. Chromospheric-coronal activity at saturated levels. *The Astrophysical Journal*, 321:958–966, 1987.

Osmi Vilhu, Jean-Pierre Caillault, and John Heise. Simultaneous exosat and vla observations of the contact binaries vw cephei and xy leonis-quiescent emission and a flare on vw cephei. *The Astrophysical Journal*, 330:922–927, 1988.

Osraij Vilhu and Timo Rahuinen. Contact binary evolution and angular momentum loss. In *Fundamental problems in the theory of stellar evolution*, volume 93, page 181, 1981.

H Von Zeipel. The radiative equilibrium of a rotating system of gaseous masses. *Monthly Notices of the Royal Astronomical Society*, 84:665–683, 1924.

Lucianne M Walkowicz, Gibor Basri, Natalie Batalha, Ronald L Gilliland, Jon Jenkins, William J Borucki, David Koch, Doug Caldwell, Andrea K Dupree, David W Latham, et al. White-light flares on cool stars in the kepler quarter 1 data. *The Astronomical Journal*, 141(2):50, 2011.

J-M Wang. The thermal relaxation oscillation states of contact binaries. *The Astrophysical Journal*, 434:277–282, 1994.

RE Wilson. Binary star morphology and the name overcontact. *Information Bulletin on Variable Stars*, 2001.

Lin Yan and Mario Mateo. Primordial main sequence binary stars in the globular cluster m71. *The Astronomical Journal*, 108:1810–1827, 1994.

Y-G Yang, S-B Qian, and B Soonthornthum. Deep, low-mass ratio overcontact binary systems. xii. ck bootis with possible cyclic magnetic activity and additional companion. *The Astronomical Journal*, 143(5):122, 2012.

Mutlu Yıldız and T Doğan. On the origin of w uma type contact binaries—a new method for computation of initial masses. *Monthly Notices of the Royal Astronomical Society*, page stt028, 2013.

Donald G York, J Adelman, John E Anderson Jr, Scott F Anderson, James Annis, Neta A Bahcall, JA Bakken, Robert Barkhouser, Steven Bastian, Eileen Berman, et al. The Sloan digital sky survey: Technical summary. *The Astronomical Journal*, 120(3):1579, 2000.

FZ Zeraatgari, A Abedi, M Farshad, M Ebadian, N Riazi, J Nedoroščík, M Vaňko, T Pribulla, D Kjurkchieva, V Popov, et al. Neural network analysis of w uma eclipsing binaries. *Contrib. Astron. Obs. Skalnaté Pleso*, 45:5–16, 2015.

XB Zhang and RX Zhang. Long-term photometric study of the w uma binary star v523 cas. *Monthly Notices of the Royal Astronomical Society*, 347(1):307–315, 2004.

M Zhao, D Gies, JD Monnier, N Thureau, E Pedretti, F Baron, A Merand, T Ten Brummelaar, H McAlister, ST Ridgway, et al. First resolved images of the eclipsing and interacting binary β lyrae. *The Astrophysical Journal Letters*, 684(2):L95, 2008.